Self-assembling Peptide-Carbon Nanotube Dispersions and Hydrogels for Tissue Engineering and Biosensor Applications

by

Mohammadali Sheikholeslam

A thesis
presented to the University of Waterloo
in fulfillment of the
thesis requirement for the degree of
Doctor of Philosophy
in
Chemical Engineering - Nanotechnology

Waterloo, Ontario, Canada, 2015

AUTHOR'S DECLARATION

This thesis consists of material all of which I authored or co-authored: see Statement of Contributions included in the thesis. This is a true copy of the thesis, including any required final revisions, as accepted by my examiners.

I understand that my thesis may be made electronically available to the public.

STATEMENT OF CONTRIBUTIONS

Chapter 3 of this thesis is adapted from a paper "Sheikholeslam, M.; Pritzker, M.; Chen, P. Dispersion of multi-walled carbon nanotubes in water using ionic-complementary peptides. *Langmuir,* 2012, 28, 12550–12556".

Chapter 4 of this thesis is adapted from a paper "Sheikholeslam, M.; Pritzker, M.; Chen, P. Hybrid peptide–carbon nanotube dispersions and hydrogels. *Carbon*, 2014, 71, 284–293".

Abstract

Carbon nanotubes (CNTs) are attractive functional materials for use in a broad range of fields due to their unique mechanical and electrical properties. However, their hydrophobic nature is a major problem for some of these applications. Several approaches such as dispersing them in organic solutions and covalently or non-covalently modifying them have been developed to make CNTs usable for desired applications. Since organic solutions can be problematic for bio-applications and covalent modification can introduce defects into the CNT structure (responsible for its unique properties), the approach of making non-covalent modification is more promising. Different types of polymers and surfactants have been used so far in this way. In the past two decades, self-assembling peptides have emerged as promising functional nanomaterials capable of use for different bio-applications. Employing biocompatible self-assembling peptides for CNT dispersion not only removes the first obstacle to use CNTs in solution, but also can result in a new class of hybrid nanomaterials benefitting from the synergistic effects of peptides and CNTs. To the best of our knowledge, this is the first work reporting the dispersion of CNTs using β-sheet-forming self-assembling ionic-complementary peptides. Also this is the first study on the application of peptide-CNT hybrid dispersions and hydrogels for biosensor and tissue engineering applications.

This thesis focuses on the modification of CNTs with self-assembling peptides, characterization of the resulting hybrid dispersions and their application for biosensor development and scaffolding for tissue engineering and cancer spheroid studies. In particular, the study includes the following topics: (i) characterization of the dispersions of multi-walled carbon nanotubes (MWNTs) modified with EFK16-II peptide, (ii) AFM characterization of dispersions of single-walled carbon nanotubes (SWNTs) modified with EFK8 peptide, (iii) formation of hybrid EFK8-SWNT hydrogels, (iv) application of the hybrid EFK8-SWNT dispersion in electrode modification and design of a hemoglobin biosensor, and (v) application of the EFK8 and EFK8-SWNT hydrogels as scaffolds for tissue engineering and 3D cancer cell spheroid formation.

First, we have shown that by non-covalently modifying MWNTs with the ionic-complementary peptide EFK16-II, very stable dispersions of MWNTs can be formed due to the electrostatic repulsion between self-assembled peptides on the MWNTs. Zeta potential and DLS measurements indicated that as the pH diverges from the isoelectric point of ~ 6.7 for EFK16-II, the repulsion between the particles increases and their resulting sizes decrease. AFM, SEM and TEM studies revealed a uniform

distribution of individual modified MWNTs. Finally, tissue culture plates treated with these hybrid dispersions were found to have enough biocompatibility for cell attachment and growth.

In the next step, the peptide EFK8, a shorter version of EFK16-II, was used to disperse SWNTs in water. Scanning probe microscopy (SPM) techniques based on nano-mechanical measurements and electric force microscopy (EFM) were used to more closely examine the structure formed between nanotubes and peptides. The SPM images reveal a structure consistent with EFK8 fibers wrapping around SWNTs and rendering their outer surfaces hydrophilic which enables their dispersion in water. Also it was shown that the hybrid dispersions can form uniform composite EFK8-SWNT hydrogels upon adding solutions containing ≥1mM monovalent salts.

In the third part of the study, EFK8 and EFK8-SWNT hybrid hydrogels were prepared and used to culture NIH-3T3 fibroblast and A549 lung cancer cells. The effect of the presence of SWNTs in the peptide hydrogel on NIH-3T3 cells behavior cultured on hydrogels was first investigated. Inverted light and confocal microscopy images showed that although cells grow they tend to maintain spherical morphology and form colonies on the EFK8 hydrogel. The presence of SWNTs significantly improved cell behavior so that they exhibited a stretched morphology, spread individually and homogeneously over the surface and proliferated faster. In addition, the cells were observed to migrate into the hydrogel after being seeded on top of the hydrogel. Micro-indentation tests showed that increasing EFK8 solution concentration led to an increase in the hydrogel compressive modulus, whereas the presence of SWNTs did not have any effect in this case. So the beneficial effect of SWNTs on cell behavior cannot be attributed to mechanical property modification and is probably due to their providing locations for cell anchorage that facilitate attachment, spreading and migration. The cells encapsulated in both hydrogels showed the same behavior as in 2D environments (i.e., forming colonies on EFK8 and spreading individually on the hybrid hydrogel). In the second part of this study, the potential of EFK8 hydrogels for spheroid formation of cancer cells was explored. These cancer cell spheroids can be used as models for real tumors, to carry out drug screening in 3D cell cultures and to investigate the effect of the microenvironment on tumor progression and metastasis. It was observed that cells formed spheroids on EFK8 hydrogels at normal peptide concentrations, but exhibited a more stretched morphology and migratory phenotype when seeded on the stiffer hydrogel. The cells also adopted a stretched morphology with higher migration when seeded on the EFK8-SWNT hydrogels. Again this behavior can be attributed to the effect of

SWNTs to facilitate cell adhesion and migration. This effect can be used to study another effect of the microenvironment, namely cell-binding motifs, on tumor progression and metastasis.

In the last step of the study, the application of the hybrid EFK8-SWNT dispersion was investigated for immobilization and direct electrochemistry of hemoglobin (Hb) on a glassy carbon electrode (GCE) as well as the efficacy of this platform for making a hydrogen peroxide (H_2O_2) biosensor. Cyclic voltammetry (CV) and electrochemical impedance spectroscopy (EIS) experiments showed that the presence of SWNTs in the modifying peptide layer on GCE significantly enhances the electrochemical response of the electrode. Furthermore, this response was further increased as more layers of the EFK8-SWNT dispersion were applied. The next step was to immobilize hemoglobin on the electrode by a casting method. The effectiveness of this approach was confirmed by CV and EIS experiments which showed that immobilized Hb retained its bio-catalytic activity for Fe ions in Hb chains and could form the basis of a mediatorless H_2O_2 biosensor.

Overall, by expanding the functionalities of both CNTs and self-assembling peptides, this work has introduced a new hybrid nanomaterial for bio-applications, especially biosensors, 3D cell cultures and tissue engineering.

Acknowledgements

First and above all, I praise God, the almighty, for providing me this opportunity and granting me the capability to proceed successfully. Next, I would like to express my sincere gratitude to my supervisors, Dr. Pu Chen and Dr. Mark Pritzker, for their encouragement and guidance during my Ph.D. They have provided me with infinite support through difficulties in the research and helped me to become an independent open-minded critical thinker and creative researcher. I would like to acknowledge my advisory committee members, Dr. Mungo Marsden, Dr. Frank Gu and Dr. Marc Aucoin, for their interest and critical advice during my Ph.D. research program. I also thank my external committee member Dr. Dérick Rousseau for his participation in my defense and valuable comments.

I want to extend my special thanks to the individuals and our research group that supported me by their constructive discussions and helped me in my experiments during my research at the University of Waterloo. I really acknowledge Dr. Boxin Zhao's group especially Hamed Shahsavan for microindentation tests at the Chemical engineering department, Adrienne Boone for her endless assistance for confocal microscopy and Dale Weber for his help with TEM and CPD both at the department of Biology. I am also so thankful to my dear sister, Maryam, for the designing schematic view of peptide-CNT hydrogel.

I have been fortune to work with many brilliant people in the Biomedical Engineering and Energy Storage Group (BEES). My acknowledgements go to all of them for creating an excellent environment for creativity and innovation. A tribute goes to Dr. Madjid Soltani, Dr. Bahram Zargar, Dr. Mousa Jafari, Dr. Parisa Sadatmousavi, Dr. Weiping Sui, Tatiana Sheinin, Nita Modi, Dr. Denise Gosselink, Kaveh Sarikhani, Lei Zhang, Mohammad Mohammadi, Dr. Baoling Chen, Danyang Zhao, Dr. Kazem Jeddi, Ran Pan, Yong Ding, Dr. Wen Xu and Morteza Torabi.

I am so thankful to the co-op students who helped me in my research: Scott Wheeler, Piyush Nanda, Keely Duke and Chad Sweeting. Finally, I would like to thank my friends and family for their continued support and belief in me. A special thanks to my parents, brother and sisters for all their unconditional supports, love and prays. Most importantly, I would like to dedicate this thesis to my darling wife Dr. Samaneh Hosseini Semnani, who never stopped supporting me and believing in my ability to pursue my ambitions. Finally I am thankful to the happiness of our life, my daughter, Zahra, for all her smiles, hugs, kisses and laughs.

Dedication

To my parents, for their never-ending love and support

To my wife, Samaneh, for his remarkable patience and unwavering love

To my daughter, Zahra, for making our life much happier and warmer than ever

Table of Contents

List of Figures

Chapter 1
Introduction

1.1 Overview

In the past two decades, nanotechnology has emerged as a major multidisciplinary field of knowledge that combines different aspects of science and engineering. Nanomaterials play a key role in expanding nanotechnology in our everyday life. Due to the similarity in their sizes to that of biological molecules, nanomaterials have made a significant effect in medicine [12]. Biomedical applications of nanomaterials range from drug delivery and tissue engineering to visualization and biosensors. However, the toxicity of nanomaterials is a major issue that must be faced for each bio-application. Thus, nanomaterials are often functionalized with biomolecules to enable safer interaction in both in vitro and in vivo systems [3].

From their discovery in 1991 [4], carbon nanotubes (CNTs) have been the subject of extensive research in various fields of science and engineering for different types of applications due to their multifunctional nature and unusual properties [5]. These materials have the highest strength and stiffness yet discovered, with a hardness greater than that of diamond, an electrical conductivity more than 1000 times greater than that of copper and thermal conductivity about 10 times better than that of copper. Obviously, these properties make CNTs very attractive for incorporation into many systems [6789]. On the other hand, strong van der Waals forces between individual CNTs cause them to readily aggregate, something which hampers their handling and usage. Consequently, different types of modifications classified as being covalent or non-covalent, have been developed to separate and disperse CNTs in order to more fully realize the benefits of their unique properties [10]. Since covalent modifications tend to introduce defects into the CNT structure and degrade their properties, the approach of introducing non-covalent modifications is usually preferred. Also, since toxicity and biocompatibility are of special concern for biomedical applications of nanomaterials, non-covalent modification using biological molecules would be an attractive option for the use of CNTs in such applications [11]. At the same time, some biological molecules can functionalize CNTs and introduce special properties and

provide a template for conjugating further nanoparticles to CNTs, in addition to facilitating their dispersion [3]. Self-assembling peptides are one of the materials that have been explored for this application [12–17].

Similar to carbon nanotubes, self-assembling peptides are considered to be multifunctional nanomaterials. These biomaterials can form supramolecular structures through self-assembly processes [18]. They have been used as scaffolds for tissue engineering and hydrogels for 3D cell culture and drug delivery [19–22]. The first generation of these materials was ionic-complementary peptides which form β-sheet nanofibers in aqueous media. Their sequences can be modified with functional motifs for specific cell interactions or nanoparticle attachment [2324]. Also, they are amphiphilic which makes them potentially effective dispersants for hydrophobic nanomaterials such as anti-cancer drugs [22]. Thus, these peptides should be able to interact with hydrophobic CNTs if the appropriate sequence is employed. If these ideas are successful, the synergy between these two multifunctional nanomaterials will enhance the action of each species with regard to their original purpose. For example, CNTs have been used widely to modify bio-electrode surfaces and biosensor electrodes [25]. The interaction of these CNTs with self-assembling peptides not only can functionalize them but also can increase their biocompatibility for biomedical applications. Meanwhile, while self-assembling peptides are widely used to form hydrogel scaffolds, the incorporation of CNTs would enhance hydrogel functionality. Consequently, the research presented in this thesis is first aimed at investigating the interaction of a specific sequence of self-assembling peptide with both MWNTs and SWNTs. Based on the results obtained in this first phase, peptide-CNT hybrid dispersions are prepared and used for several applications: composite hydrogels for tissue engineering and 3D cell cultures and modification of a model biosensor electrode.

1.2 Objectives

The objective of this research is to modify and disperse carbon nanotubes using the EFK family of ionic-complementary self-assembling peptides. If successful, the prepared dispersions will be employed first to explore the possibility of making a hybrid hydrogel and its application in tissue

engineering and next to enhance the electrochemical response of a glassy carbon electrode for use as a model hydrogen peroxide biosensor. The detailed objectives are as follows:

1. Dispersion of multi-walled carbon nanotubes in water using EFK16-II peptide and assessing the attachment and growth of normal and cancer cells on plates modified with this dispersion.

2. Dispersion of single-walled carbon nanotubes in water using EFK8 and investigation of the peptide-SWNT interactions. This study is extended to investigate the possibility of forming hybrid EFK8-SWNT hydrogels.

3. Exploration of the possibility of using the hybrid peptide-SWNT hydrogels for tissue engineering and 3D cell cultures.

4. Investigation of the use of the hybrid dispersion to modify glassy carbon electrodes for application as an electrochemical H_2O_2 biosensor.

1.3 Outline of thesis

This thesis includes seven chapters: introduction, literature review, 4 research chapters followed by conclusions and recommendations.

Chapter 1 opens with an introduction of the thesis including a brief review of carbon nanotubes, self-assembling peptide and their applications. Also the research objectives and thesis outline are given.

Chapter 2 includes a literature review of carbon nanotube dispersions, different types of self-assembling peptides and their applications. Also, the use of hydrogels in tissue engineering and 3D cancer tumor research and previous studies on mediatorless electrochemical biosensors are reviewed.

Chapter 3 reports on the dispersion of MWNTs using the self-assembling peptide EFK16-II. Also the resulting dispersions are characterized and the individual dispersion of MWNTs is confirmed. Finally, experiments concerned with the attachment and growth of cells on tissue culture plates modified with the peptide-MWNT dispersion are discussed.

Chapter 4 focuses on the interaction between EFK8 and SWNTs using scanning probe microscopy (SPM) techniques to distinguish peptide fibers from SWNTs. Also, the possibility of forming peptide-SWNT hybrid hydrogels is reported for the first time.

Chapter 5 explores the application of hybrid EFK8-SWNT hydrogels for tissue engineering and the effect of SWNTs on the properties and effectiveness of the hydrogels. Also, the potential of EFK8 hydrogels and hybrid EFK8-SWNT hydrogels for use in studying the effect of microenvironment on tumors is examined.

Chapter 6 considers the application of hybrid EFK8-SWNT dispersions to modify the surface of glassy carbon electrodes and enhance their electrochemical response. Based on these results, the modified electrode is used to immobilize hemoglobin and form the basis of a biosensor for hydrogen peroxide. The sensitivity, linear range and the stability of this biosensor are then evaluated.

The main findings and contributions of this research are summarized in Chapter 7. Also included are recommendations for future work in this area.

Chapter 2
Literature Review

2.1 Carbon nanotubes for biomedical applications

Since the discovery of carbon nanotubes (CNTs) in 1991[4], considerable interest has been shown in incorporating them in chemical sensors, biochemical sensors and nano-scale electronic devices and utilizing them for tissue engineering applications due to their excellent electronic and mechanical properties. CNT-modified electrodes have higher electronic conductivity than graphite-based ones and have been shown to perform better and be more sensitive than those based on single metals such as Au, Pt and carbon-based nanomaterials such as C60 and C70 [25–29]. Their electronic properties give CNT electrodes the ability to mediate electron transfer reactions with electroactive species in solution. To date, CNT-based electrodes have been widely used in electrochemical sensing [11,25,26,29,30]. Furthermore, they are capable of providing suitable interfaces for the signal transfer and neurite outgrowth of neurons as well as supporting the attachment and growth of osteoblast, fibroblast and cardiac cells [28]. They have also shown great promise for applications in tissue engineering by enhancing the properties of biomaterials [27,28,31–42].

2.1.1 Carbon nanotube dispersions

One of the main methods to modify an electrode is to coat its surface with a CNT-containing suspension. Fig. 2.1 shows SEM images of glassy carbon electrodes modified with bilayers of poly(diallyldimethylammonium chloride) and multi-walled carbon nanotubes (MWNT). However, the first obstacle for electrode modification is that the strong van der Waals forces between carbon nanotubes leads to their aggregation and poor dispersion in water and other solvents, which severely limits their usefulness. Although CNT dispersions can be stabilized in organic solvents containing DMF, ethanol and acetone and then used to modify electrodes to enhance their electrochemical response, these organic solvents typically denature biomolecules and so limit their application as biosensors [11]. Thus, the ability to form stable CNT-containing suspensions in aqueous solutions has attracted considerable attention.

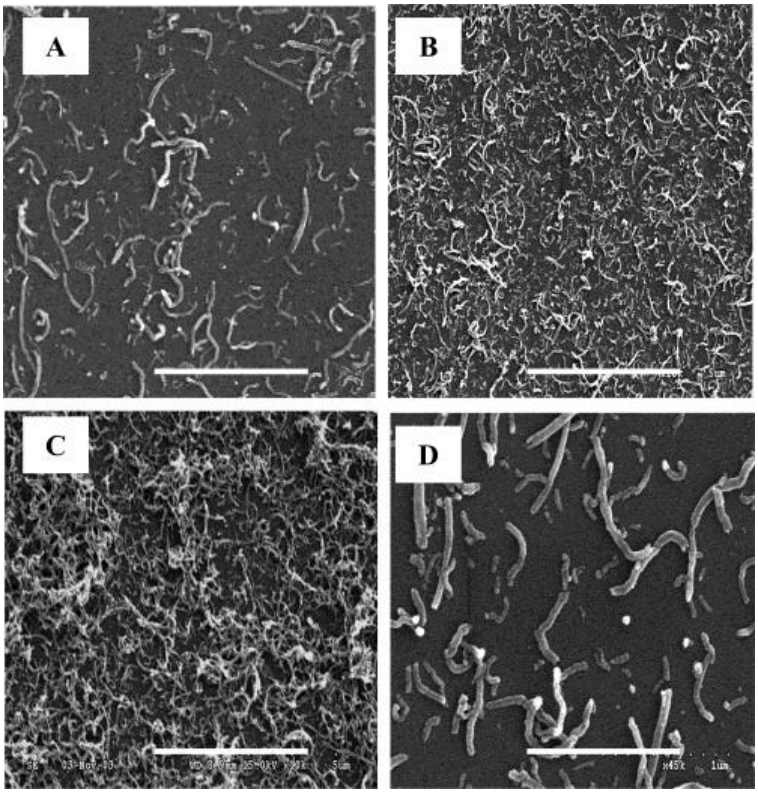

Figure 2.1. SEM images of a (A) single layer, (B) three layers and (C) five layers of {PDDA/MWNT} assembled on a silicon wafer. The scale bars in A-C correspond to a 5 μm length. SEM image of (A) at higher resolution appears in (D) (scale bar corresponds to 1 μm length). "Reprinted (adapted) with permission from [43]. Copyright (2015) American Chemical Society."

Although covalent stabilization of CNTs (using a method such as acid treatment) can successfully produce such suspensions, this approach has its problems since it tends to diminish the excellent optical and electronic character of CNTs and impede their inherent conductivity. Consequently, the formation of suspensions by non-covalent stabilization of CNTs may be a more promising method. For this purpose, the modification of CNTS by polymers and surfactants has been studied [44]. When polymers or non-ionic surfactants are used, a CNT suspension can be successfully dispersed through steric stabilization by an adsorbed surfactant or polymer layer. The hydrophobic part of the surfactant makes contact with the CNTs, while its hydrophilic part is oriented toward the solution. When ionic surfactants adsorb onto CNTs, electrostatic repulsion

between their similarly charged ends is the dominant factor, impeding nanotube aggregation and stabilizing the suspensions [44].

2.1.2 Peptide-based CNT dispersions

The use of peptide-based molecules has been explored as an option for dispersion of CNTs. The association of CNTs with peptides is expected to be useful in biosensor and tissue engineering applications and in the development of new bioactive nanomaterials. The biological potential of carbon nanotubes in immunology was investigated by Pantarotto *et al.* [12] who demonstrated enhanced *in vivo* antibody response from covalently linked nanotube-peptide conjugates. Toward this end, peptide sequences using phage display with specific affinities for carbon nanotubes have been identified [1314]. These peptides contain sequences rich in histidine and tryptophan at specific locations. Also, nanotubes have been successfully dispersed in aqueous solutions by pre-treating with amphiphilic peptide sequences which contain phenylalanine at specific locations (Fig. 2.2) and can fold into α-helixes on nanotube sidewalls [1516]. The main interaction responsible for suspending carbon nanotubes in water is reported to be π-π stacking between the aromatic rings in the amino acids and the nanotubes.

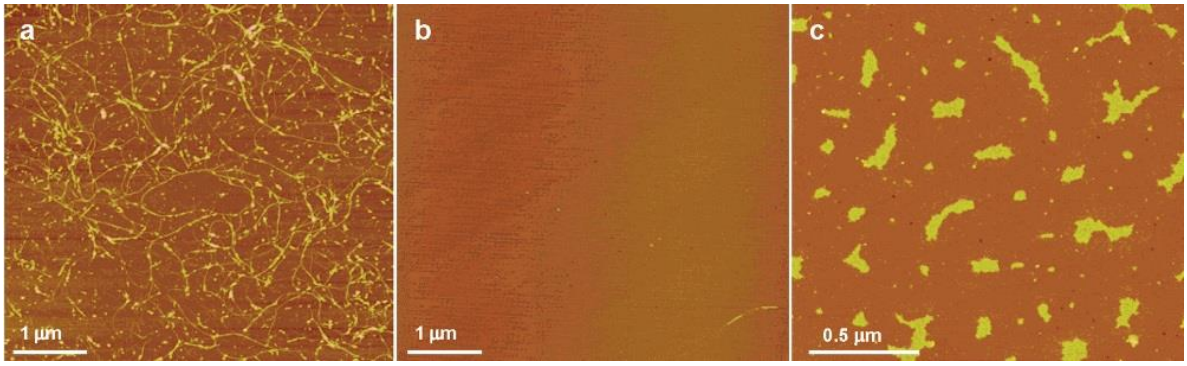

Figure 2.2 AFM images of (a) nano-1/SWNT dispersion revealing many long SWNTs, (b) SDS/SWNT exhibiting minimal dispersion of SWNTs and (c) nano-1 control sample lacking SWNTs (note: nano-1 is a 29-residue peptide). "Reprinted (adapted) with permission from [16]. Copyright (2015) American Chemical Society."

2.1.2.1 Self-assembling peptides for CNT dispersion

Arnold *et al*. [17] investigated an approach utilizing peptide amphiphile (PA) molecules whereby amino acid sequences are covalently coupled to a hydrophobic alkyl tail. Since the surface of carbon nanotubes is non-polar and hydrophobic, peptide amphiphiles in an aqueous solution are expected to self-assemble on this surface and thereby minimize the interfacial energy of the nanotube-water interface through hydrophobic interaction between the tail and the carbon nanotubes and as a result expose the hydrophilic sequence to the water (Fig. 2.3). This approach has several potential benefits. First, due to the non-covalent assembly of peptide amphiphiles, the nanotube sidewalls should not be chemically modified and so should maintain their outstanding electrical, mechanical and optical properties. Second, the hydrophobic tail of the peptide amphiphile is expected to interact with the hydrophobic nanotube surface and leave the peptide sequence exposed on the exterior for sensing or other biological applications. Furthermore, the water solubility of nanotubes biofunctionalized with peptide amphiphiles should be controllable by adjusting the pH since this affects the net charge of peptide segments and the resulting ionic repulsion among nanotubes in solution. Finally, this approach is expected to be generally useful for either positively or negatively charged peptide sequences without the need to incorporate sequences that specifically bind to nanotube surfaces.

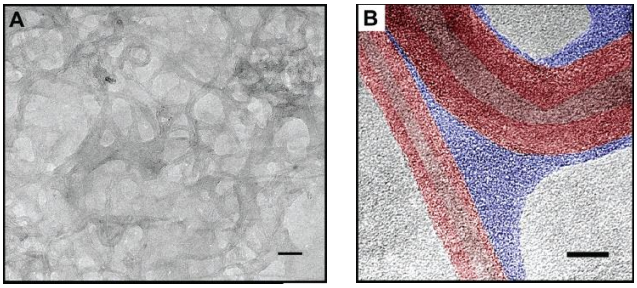

Figure 2.3 TEM micrographs of MWNTs with anionic PA at (A) low magnification (scale bar corresponds to 50 nm) and (B) high magnification (scale bar corresponds to 10 nm length). MWNTs are highlighted in red and the surrounding coating is indicated in blue. "Reprinted (adapted) with permission from [17]. Copyright (2015) American Chemical Society."

2.2 Self-assembling peptides

The thermodynamically driven spontaneous arrangement of molecules to form stable ordered structures via non-covalent interactions is called molecular self-assembly [45]. From the discovery of the first self-assembling peptide EAK16-II by Zhang et al. in 1993, a considerable amount of attention has been focused on this type of nano-biomaterial as a promising option for a wide range of biomedical applications such as anti-cancer drug delivery, biocompatible hydrogels as scaffolds for 3D cell cultures, tissue engineering and wound healing (hemostasis) [19,22,46–52]. EAK16-II consists of a 16-amino acid sequence including negative and positive residues (corresponding to glutamic acid and lysine, respectively) lying on one side of the peptide backbone and the hydrophobic residues (i.e. alanine) lying on the other side. With such a structure, EAK16-II spontaneously adopts a β-sheet secondary structure due to its ionic-complementary character as well as through hydrogen and hydrophobic bonding [5053]. Since the resulting β-sheet has a hydrophobic side and a hydrophilic side, two β-sheets can attach to each other in water so as to hide the hydrophobic side from water and orient the hydrophilic sides toward the water (Fig. 2.4). This secondary structure enables the formation of nanofibers in water that remain very stable over a wide temperature range (25-90°C), at extreme pHs (1.5 and 11) and in the presence of denaturation agents such as SDS, urea, HCl and enzymes such as trypsin, α-chymotrypsin and pronase [54]. EAK16-II has been reported not to induce an immune response when injected in mice, rabbits and goats [5055]. In addition, EAK16-II nanofibers can form hydrogels with a water content of 99.5-99.9% at peptide concentrations between 1 and 5 mg ml^{-1} H_2O [19]. Due to its amphiphilic property, it can disperse hydrophobic compounds in aqueous solutions [56].

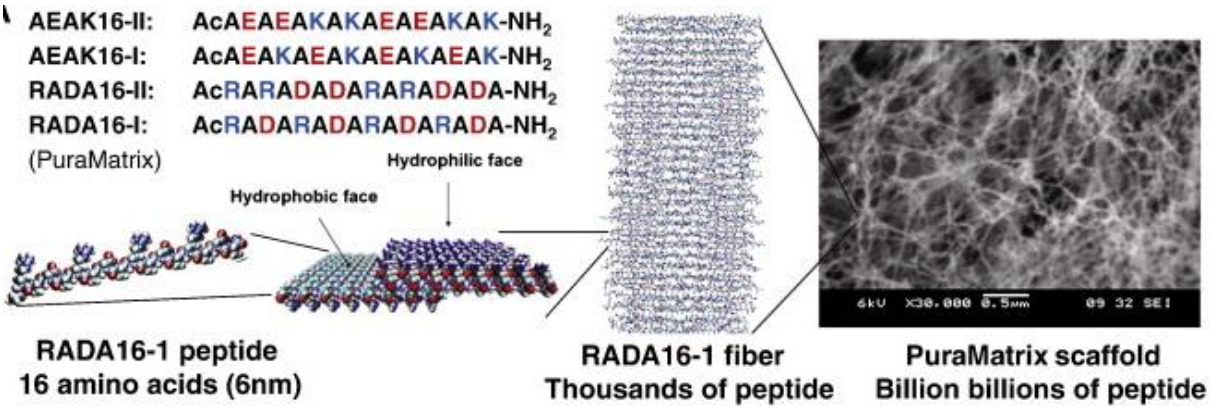

Figure 2.4 Amino acid sequences of four peptides containing EAK16-II, β-sheets and the resulting nanofibrous hydrogels of RADA16-II. "Reprinted from [20], Copyright (2015), with permission from Elsevier".

Several types of self-assembling peptides exist. The structure and characteristics of these peptides are described in the following subsections.

2.2.1 β-sheet forming self-assembling peptides

EAK16-II is the first member of this peptide family. As described previously, due to electrostatic interactions (ionic-complementarity), hydrogen bonding and hydrophobic interactions, these peptides assume a β-sheet secondary structure and form ordered nanofibers. Several other peptides similar to EFK16-II have been designed in order to form 3D scaffolds. Among these, RADA16-I with the commercial name of Puramatrix™ is the most popular one. RADA16-I hydrogels with a fiber size of 10-20 nm in diameter have been shown to support neurite outgrowth similar to the level on Matrigel and exhibit no toxicity to rats after 5 weeks of exposure. Due to these promising results, RADA16-based hydrogels have been used for a diverse range of cells and tissues including osteoblasts, neurons and keratinocytes [23]. They have been shown to be effective as 3D cell culture platforms for anti-cancer drug screening. Cells seeded in such 3D systems show higher drug resistance compared to 2D cultures [21]. Interestingly, the introduction of cell-interactive motifs to the RADA16 sequence does not impede its self-assembly while enhancing cell behavior [57–60]. The introduction of matrix metalloproteinase cleavage sites has also been observed to speed up hydrogel biodegradation without interrupting

the RADA16 self-assembly [61–63]. By replacing the hydrophobic amino acids in the sequences of these peptides (i.e. alanine) with more hydrophobic ones, the hydrophobic interactions become stronger and the critical concentration for β-sheet formation is reduced. Reduction of the number of amino acids from 16 to 8 is also shown to decrease the critical gelation concentration [6465]. KLD12 is another β-sheet forming peptide which has been used as a scaffold for chondrocyte encapsulation that is biocompatible with rabbit mesenchymal stem cells and nucleus pulposus cells [23].

2.2.2 β-hairpin forming peptides

β-hairpin peptides consist of two β-strands connected to each other via a kink and can form nanofibers. For example, MAX1 ($VKVKVKVKV^{D}PPTKVKVKVKV\text{-}NH_2$) and MAX8 ($VKVKVKVKV^{D}PPTKVEVKVKV\text{-}NH_2$) are two β-hairpin peptides consisting of two series of alternating valine and lysine amino acids connected by a $V^{D}PPT$ tetrapeptide working as a β-turn [6667]. These peptides have a random coil structure which can spontaneously form a β-hairpin structure when the temperature is raised. These peptides interact with each other through hydrogen bonding and van der Waals forces and self-assemble laterally. Also, due to hydrophobic interactions between their hydrophobic faces, they form bilayers as shown in Fig. 2.5. Although neither of these peptides showed an immune response *in vitro* [68], MAX1 was not able to encapsulate C3H10t1/2 mesenchymal cells due to slow gelation, whereas MAX8 was able to homogeneously encapsulate the cells [69]. A very interesting characteristic of these peptides is that they undergo shear-thinning. Thus, their viscosity decreases and they begin to flow when subject to a shear stress, but can revert to their previous rigid structure when the stress is removed. This capability enables them to be injected via syringes. Experiments have shown that cells delivered using this method are able to maintain their viability during shear thinning [6970]. This class of peptides has been further developed to be responsive to light or change in pH and ionic strength [20].

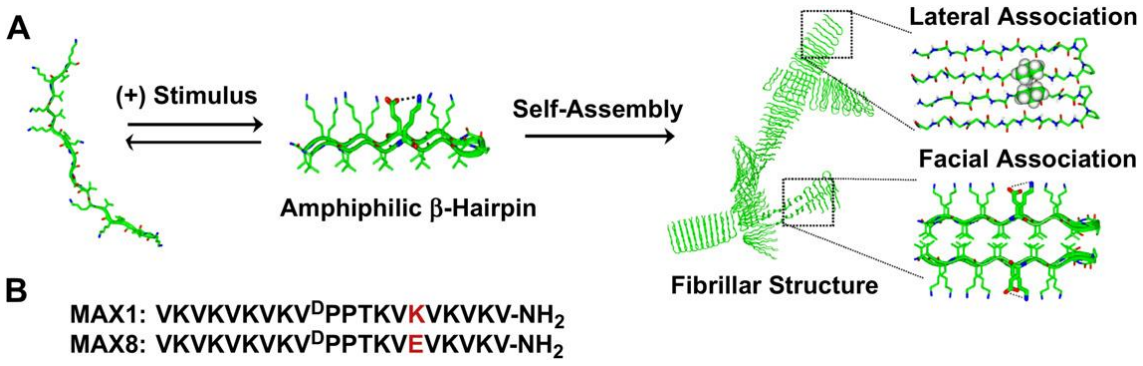

Figure 2.5 (A) Folding of peptides to form β-hairpin structure and self-assembly of β-hairpins through lateral (hydrogen bonding and van der Waals interaction) and facial (hydrophobic interaction) association. (B) Amino acid sequences of MAX1 and MAX8 β-hairpin peptides. "Reprinted from [68], Copyright (2015), with permission from Elsevier".

2.2.3 α-helical peptides

α-helical coiled-coil peptides developed by Woolfson et al. are another class of peptides forming self-assembling fibers (SAFs) [71–75]. SAFs consist of two 28-amino acid sequences containing repeats of a coiled-coil heptad sequence $(g_P a_H b_P c_P d_H e_P f_P)_n$, in which *H* stands for a hydrophobic amino acid and *P* for a polar amino acid (Fig. 2.6A). In this heptad sequence, hydrophobic amino acids isoleucine and leucine in the *a* and *d* positions, respectively, introduce an inter-helical hydrophobic interaction that facilitates dimerization. The insertion of asparagine residues (which preferentially interact with each other) at some specific *a* positions stabilizes the dimerization. Opposite charges at the *e* and *g* positions help the two coiled-coil peptides to twist and form parallel fibrils. *b*, *c* and *f* sites can be occupied by polar residues that facilitate electrostatic fibril aggregations and enable fibers to form (Fig. 2.6B) or by residues with hydrophobic or hydrogen-bond interactions that yield thinner fibers with more flexibility. Experiments have shown that the hydrogel can support growth and differentiation of PC12 cells for sustained periods in cultures [74]. However, large-scale production of long peptides for various applications remains a challenge [23].

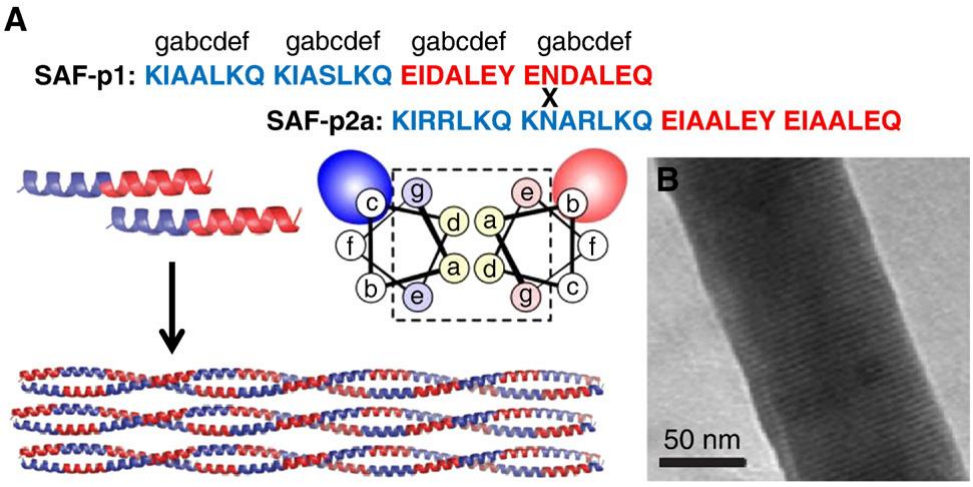

Figure 2.6 (A) Coiled-coil α-helical peptides with a 28-amino acid sequence composed of four repeats of a heptad. Rational substitution of each site in the heptad will result in a staggered two complementary α-helical fibril. (B) A thick fiber formed by aggregation of several fibrils due to placement of polar residues at *b*, *c* and *f* sites. "Reprinted from [20], Copyright (2015), with permission from Elsevier".

2.2.4 Ultrashort peptides

It has been shown that short peptides can also self-assemble into β-sheets as well. Fmoc-diphenylalanine (Fmoc-FF) and Fmoc-RGD can form nanofibers due to π-π interactions and also form hydrogels [76]. The mixing of these peptides promotes cell attachment to the hydrogel and has been successfully used to encapsulate dermal fibroblasts.

A new class of ultrashort peptides developed recently by Hauser et. al. consists of linear aliphatic amino acids with decreasing hydrophobicity moving from left to right in the sequence connected to a hydrophilic head such as Ac-LIVAGD (Fig. 2.7A) [77]. These peptides self-assemble into helical fibrils and then into fibers due to aggregation and ultimately can form hydrogels that entrap up to 99.9% water and resemble ECM collagen fibers (Fig 2.7B-D). The hydrogels made of these ultrashort peptides are very stiff and thermally stable. They have also been used successfully to culture some mammalian primary cells [78].

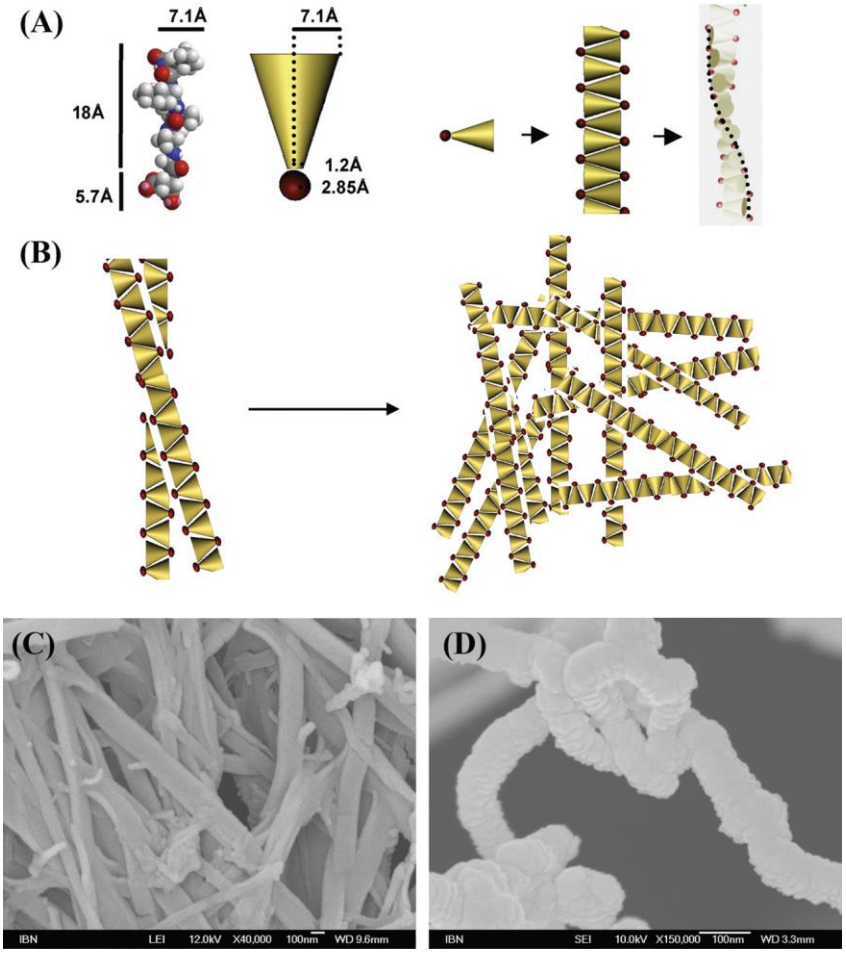

Figure 2.7 (A) Schematic showing self-assembly of ultrashort peptide Ac-LIVAGD (Ac-LD_6) to form a single α-helical fiber. (B) Schematic showing aggregation of single fibers into 3D scaffolds. Condensed fibers of the Ac-LD_6 (L) at concentrations of (C)15 mg/ml and (D) 20 mg/ml. "Reprinted from [23], Copyright (2015), with permission from John Wiley and Sons"

2.2.5 Hybrid peptide amphiphiles with hydrophobic alkyl chains

Peptide amphiphiles (PA) developed by Stupp and co-workers involve self-assembling peptides connected to a hydrophobic long alkyl group [79]. These peptides form nanofibers consisting of cylindrical micelles in water in which the alkyl tails are oriented toward each other at the centre and the amino acid residues are oriented toward the water (Fig. 2.8a). These peptides have been used for bone tissue engineering and have shown to enhance attachment, proliferation and further differentiation of mesenchymal stem cells (MSC) to osteoblasts [80]. Recently, a new peptide of

this type consisting of the hydrophilic peptide VVVAAAEEE(COOH) linked to a C_{16} alkyl tail at the N-terminus was shown to self-assemble as nanofibers by injection in saline media [81]. Heating solutions of these nanofibers before gelation led to their alignment. This approach was used to orient MSCs in a 3D environment by mixing the cells while the peptide solution was first heated and then cooled before transferring it to a saline media using a pipette (Fig. 2.8b-d).

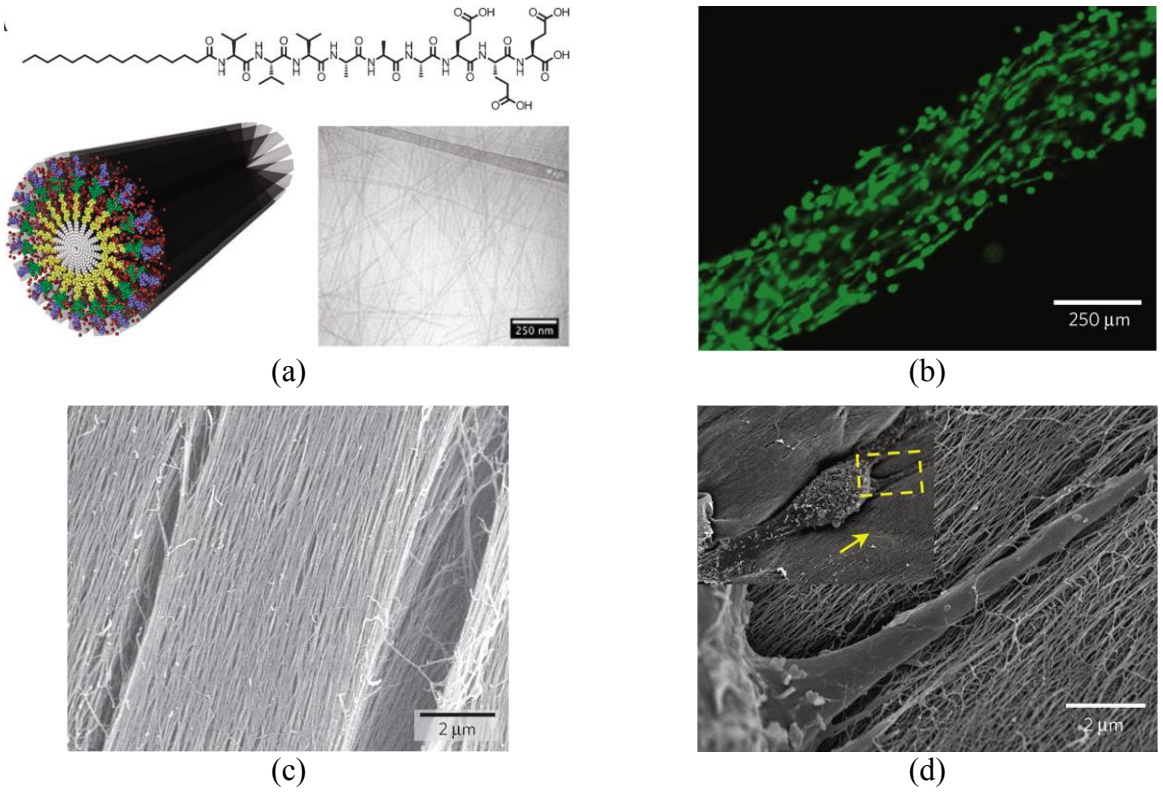

Figure 2.8 (a) Self-assembly of peptide amphiphiles to cylindrical nanofibers and cryo-TEM image of self-assembled aggregates [82]. (b) Directed MSCs cultured and calcein-stained in aligned PA hydrogels. (c) SEM image of aligned PA fibers. (d) SEM image of a cell on aligned structure (inset: zoom-out image; arrow indicates alignment direction). "Reprinted by permission from Macmillan Publishers Ltd: [Nature Materials] ([81]), copyright (2015)".

2.3 Hydrogels for biomedical applications

Hydrogels are commonly used biomaterials for tissue engineering and 3D cell cultures due to their high biocompatibility and the similarity of their physical and mechanical properties to that of living tissue [83–87]. These similarities provide a compatible environment for cells and promote

behavior to be similar to that observed *in vivo*. Hydrogels can also be modified chemically to mimic living tissues that makes them more biocompatible and perform better in the body [83–85,88].

2.3.1 Hydrogel scaffolds for tissue engineering

Different types of materials have been used to date to make hydrogel scaffolds for different types of tissues. These include synthetic materials such as polylactic acid (PLA) [8990], polyethylene oxide (PEO) [91], polyglycolic acid (PGA) [92], polyvinyl alcohol (PVA) [9394], polyethylene glycol (PEG) [95], as well as polysaccharide hydrogels consisting of hyaluronic acid (HA) [96], chitosan [97], agarose [98] and alginate [99]. Production of these synthetic polymers is reproducible which makes them attractive for researchers. However, hydrogels formed this way have major drawbacks such as large fiber/pore sizes, the use of toxic reagents for gel formation, low degradation under physiological conditions, improper charge density, low nutrient diffusion rate and the formation of acidic products due to degradation [100]. On the other hand, protein-based hydrogels using collagen [101], gelatin [102], fibrin [103], elastin [104], silk fibroin [105] and Matrigel™ are more biocompatible and biodegradable and provide a better platform for cell attachment and growth. However, they suffer from batch-to-batch variations and unwanted contaminants such as growth factors, proteins and viruses which can interfere with cell function [83,100].

2.3.1.1 Self-assembling peptide hydrogels

Based on the above-mentioned considerations, the best option would be to use a natural synthetic material. Self-assembling peptides are very promising from this point of view. Although they are formed from amino acids, can be found throughout the body ubiquitously, they can also be synthesized with precise control of its chemical composition. This should minimize the effects of contaminants and enable the effects of different cues on cell behavior in the prepared scaffold to be clearly distinguished. Their biodegradation products are natural amino acids that are used in the body and can be functionalized with different bioactive motifs for different cells and tissues. Also, nano-sized fibers and pores of hydrogels formed from these peptides resemble the structure of living tissues in the body. This provides an environment that closely mimics *in-vivo* cell-cell and cell-scaffold interactions. In addition, fiber crosslinking by which hydrogels form from these peptides does not require any chemical additives, UV irradiation or heat treatment which can lead

to lower biocompatibility, unlike the situation with other biopolymer-based hydrogels. Finally, these peptide hydrogels can be formed by injection which enables them to encapsulate cells for 3D cultures.

To date, different types of self-assembling peptide hydrogels have been used for tissue engineering applications. RADA16-I hydrogels with the commercial name of PuraMatrix™ have been used for different types of cells including osteoblasts, neurons and keratinocytes [23 100] (Fig.2.9A). The advantage of this peptide compared with other self-assembling peptides such as EFK8 is its similar sequence to RGD tripeptide found in fibronectin which mediates cell attachment. It has been shown to be effective as a 3D cell culture platform for anti-cancer drug screening. Cells in 3D cultures show higher drug resistance compared to those in 2D cultures [21]. Furthermore, the sequence of this peptide has been modified to extend its functionality and range of cells that can be seeded [106] (Fig. 2.9B). Interestingly, the introduction of cell-interactive motifs to the RADA16-I sequence has not been found to impede its self-assembly while enhancing the cell behavior [57–60]. The presence of matrix metalloproteinase cleavage sites has also been observed to speed up hydrogel biodegradation without interrupting RADA16-I self-assembly [61–63]. However, its mechanical strength drops after neutralization to physiological pH values and can be disrupted when subsequently subjected to stress [107] .

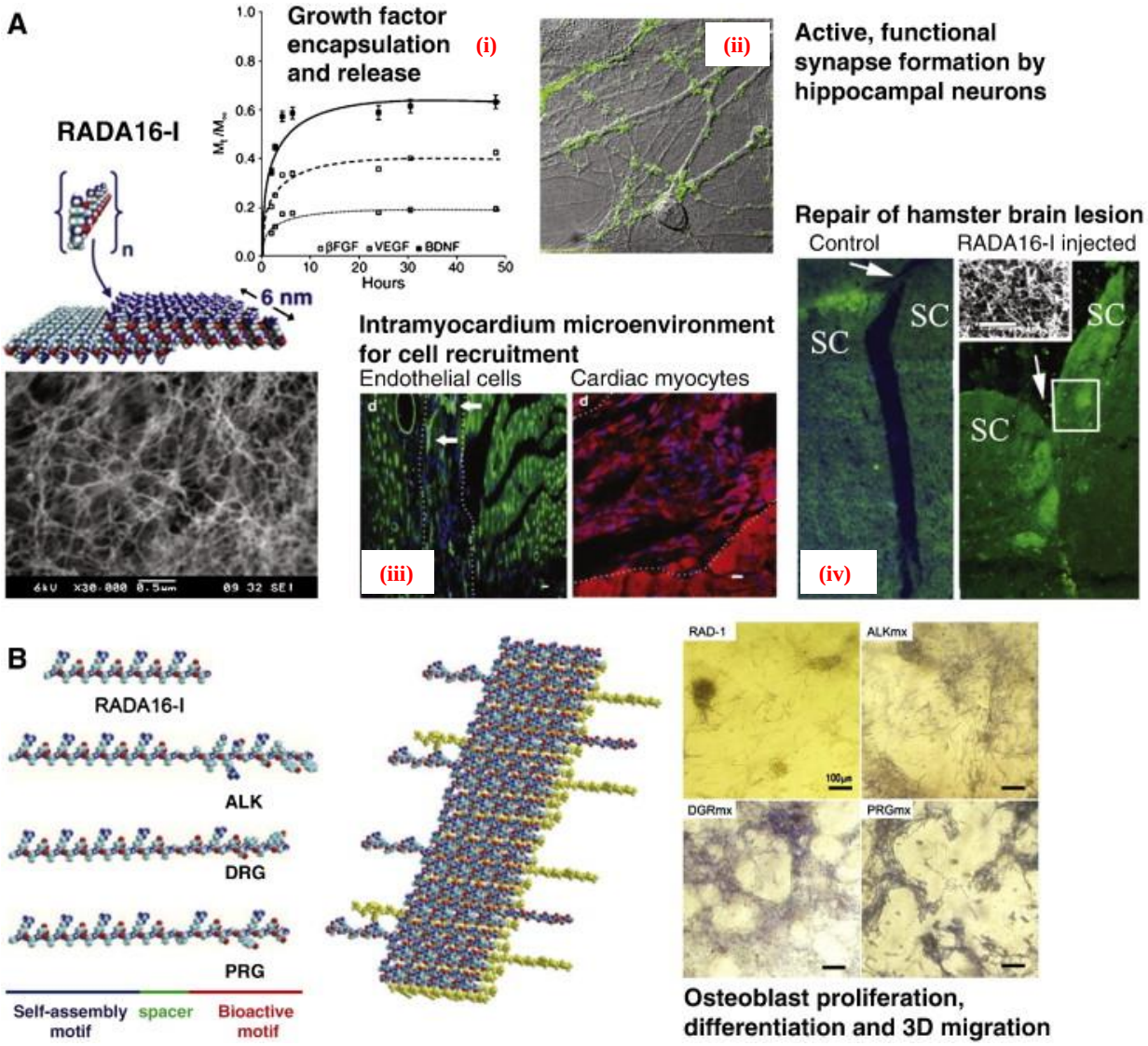

Figure 2.9 (A) Self-assembly of RADA16-I peptide to β-sheet nanofibers which can form hydrogel with following applications: (i) controlled release of different growth factors, (ii) cell culture substrate for primary rat hippocampal neurons forming active and functional synapses it, (iii) scaffolds for endothelial cell migration into mice myocardium (shown by arrows), (iv) scaffolds for neuron migration and repairing hamster brain lesions. (B) Modification of RADA16-I sequence with different bioactive motifs and self-assembly to β-sheet nanofibers as well as modification of sequence with ALK as scaffolds for osteoblast proliferation, differentiation and 3D migration. "Reprinted from [20], Copyright (2015), with permission from Elsevier".

2.3.2 Hydrogels for 3D cell culture and tumor studies

3D cell cultures are other important applications of hydrogels. Hydrogels have been used as 3D scaffolds for drug discovery and cancer tumor studies *in vitro* [86,87,108]. Drug screening and tumor modelling studies show that a 3D environment for cancer cells in such applications is necessary. It has been widely shown in different reports that tumor cells in a 3D scaffold show different behavior from that in a 2D environment in terms of growth rate, morphology and drug resistance [86,109–112]. The extracellular matrix (ECM) and the physical conditions in the microenvironment have significant effects on the behavior and gene expression of cancer cells *in vivo*. In contradiction to the classical theory of cancer that considers accumulated gene mutations as the main origin of cancer, tissue organization field theory (TOFT) considers the cell-microenvironment interaction as the starting point for cancer [113114]. It has been reported that the placement of malignant tumor cells in a normal microenvironment can stop tumor progression and revert the cancer cells to a normal phenotype [115,116]. These results not only show the potential of the tumor microenvironment as a target for cancer therapy [117] but also demonstrate the use of bio-mimetic 3D scaffolds as models of healthy ECM to treat the tumors *in vivo* and avoid metastasis [108,113118]. For these reasons, attention has turned to the tumor microenvironment as an important controlling factor for cancer in recent years.

2.3.2.1 Effect of tumor microenvironment stiffness

Although considerable progress has been made in the treatment of tumors through surgery, chemotherapy and radiation, prediction of the likelihood that metastasis will occur is still lacking [119]. It has been well documented that tuning the scaffold stiffness can affect the growth and differentiation of cells [120–125]. The stiffness of the microenvironment has been shown to greatly affect tumor formation, progression and metastasis [126127,128]. This occurs through regulation of cell proliferation and differentiation by which the cells become dysfunctional [119,129–131]. Fig. 2.10 shows the effect of matrix stiffening on the growth and morphology of mammary epithelial cells. An increase in matrix stiffness leads to a more stretched morphology and disruption of cell-cell adherent junctions as indicated by β-catenin weakening. Thus, synthetic scaffolds with tunable mechanical properties can serve as useful artificial 3D microenvironments to study cancer cells, spheroids and tumors [132–136].

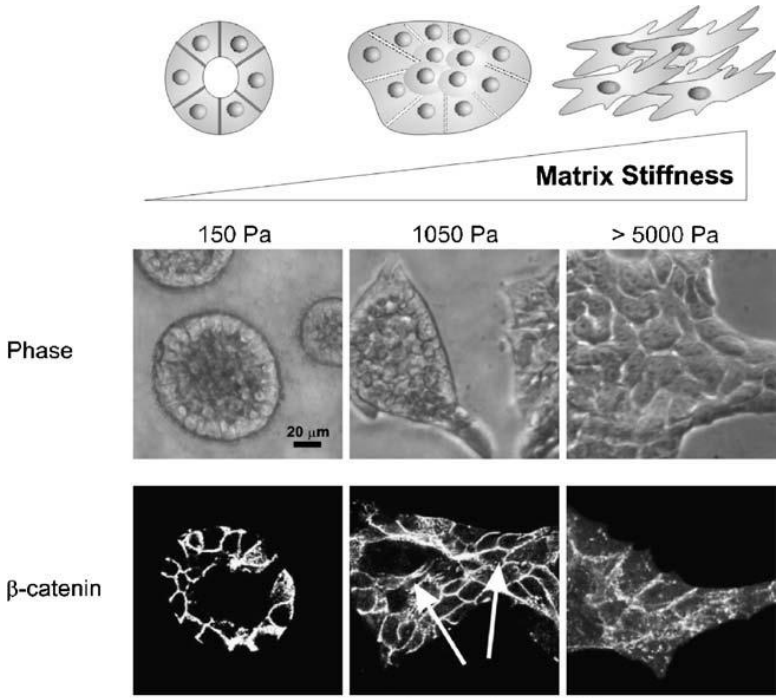

Figure 2.10 Effect of matrix stiffness on mammary epithelial cell (MEC) growth and morphogenesis. Phase-contrast and confocal images of immunostained 3D MEC colonies after 20 days showing progressively disrupted colony morphology as matrix stiffness increases (top). Disruption of cell–cell adherence junctions and luminal clearance with even a modest increase in matrix elastic modulus (E = 1050 Pa central panel; β-catenin). "Reprinted from [127]., Copyright (2015), with permission from Springer".

2.3.3 Hybrid hydrogels with CNTs

Due to their remarkable electronic and mechanical properties, carbon nanotubes have been incorporated into hydrogels to modify their physical and mechanical properties for a variety of tissue applications [137–144]. In the past few years, the incorporation of CNTs in collagen hydrogels has been shown to increase the electrical conductivity of the hydrogels and to enable better control of their mechanical properties [145–152]. Conductive hydrogels are useful for mimicking and regenerating tissues in which electrical signals are propagated such as in cardiac muscles and neural tissue [139,141–143,148,149,151–153]. At the same time, it has been shown that the mechanical properties of the scaffold play a major role in the behavior and fate of cells, particularly stem

cells [120,122,125,154]. This opens up the possibility of using soft hydrogels for a wider range of tissues by using CNT-based scaffolds to improve their mechanical properties.

2.4 Electrochemical biosensors

2.4.1 Mediatorless biosensors

Since the 1970s, direct electron transfer between redox proteins and electrode surfaces and its application for mediatorless electrochemical biosensors have been extensively studied. The most efficient method to make a redox protein-based electrochemical biosensor is to establish direct electron transfer between the protein and electrode. The use of a mediator facilitates not only the electron transfer between the electrode and enzyme but also various interfering reactions. Mediatorless biosensors can offer better selectivity since they are able to operate in a potential range closer to the redox potential of the protein itself and thus make interfering reactions less likely to occur [155156]. In addition, most *in-vivo* devices are mediatorless to avoid any possible leaching of the mediator and consequential toxic effects. Mediated systems also tend to be less stable during extended continuous operation [157]. Normally direct adsorption of proteins on the electrode surface leads to their denaturation and loss of their catalytic and electrochemical activity [158]. Thus, an important first step in designing a mediatorless biosensor is to immobilize the protein without denaturation.

2.4.2 Hydrogen peroxide biosensors based on hemoglobin

Hemoglobin (Hb) is an important protein in red blood cells as a reversible oxygen carrier in the body through its four polypeptide chains which contain electroactive heme groups. It has been reported that Hb also can catalyze the reduction of hydrogen peroxide [159]. The ability to rapidly and accurately determine hydrogen peroxide concentration is very important since it is the product of many enzymatic reactions and is also commonly found in food, clinical, pharmaceutical, industrial and environmental systems [159–161156]. A number of techniques such as HPLC [161], titrimetry [162], spectrometry [163], chemiluminescence [164] and electrochemical methods [165] are currently available for hydrogen peroxide determination.

Electrochemical methods for hydrogen peroxide analysis have attracted extensive interest because they are fast, less prone to interferences and relatively inexpensive [161]. Basically, two types of amperometric enzyme-based H_2O_2 probes can be used − mediated biosensors and mediatorless biosensors. Although the mediated H_2O_2 biosensors can detect very low concentrations by use of electron transfer mediators such as ferrocene derivatives [166], hexacyanoferrates [167], tetrathiafulvalene [168] or phenazine methosulphate [169], the danger exists that mediator molecules can contaminate the sample or electrode system or can diffuse from the enzyme layer [170]. Mediatorless biosensors which operate through the direct electron transfer between redox proteins and electrode have gained increasing attention because they do not suffer from this leakage problem and have potentially simpler design without the need for a chemical mediator.

2.4.3 Direct electron transfer from Hb

In addition to its ability to electrocatalyze H_2O_2 reduction, Hb is an ideal model protein for the study of the direct electron transfer of heme molecules due to its commercial availability, reasonable cost and well-known structure. However, the direct electrochemical reaction of Hb on an electrode is very difficult for a number of reasons. Since the heme group resides inside the Hb structure and is surrounded by the protein polypeptide chains, the electrons being transferred must travel a large distance to the electrode surface and a mediator is often required to help transport them. Once adsorbed, Hb on the surface frequently denatures and loses its electrochemical activity and bioactivity. Hb becomes a barrier to electron transfer on the electrode surface once it becomes denatured [171]. Finally, Hb located at the electrode surface may not have a favorable orientation for electron transfer. To date, different methods and nanomaterials including Au, Pt and CdTe nanoparticles as well as graphene (Fig. 2.11), CNTs and TiO_2 nanorods have been employed to overcome the above obstacles and facilitate direct electron transfer from Hb to the electrode [159,161,172–183]. These methods mainly operate by providing a strong electronically conducting environment for Hb molecules on the surface. Although promising results have been observed using these nanomaterials, the biosensor efficiency of Hb –based H_2O_2 biosensors is still lower than other ones using different types of heme proteins such as HRP and CAT [156].

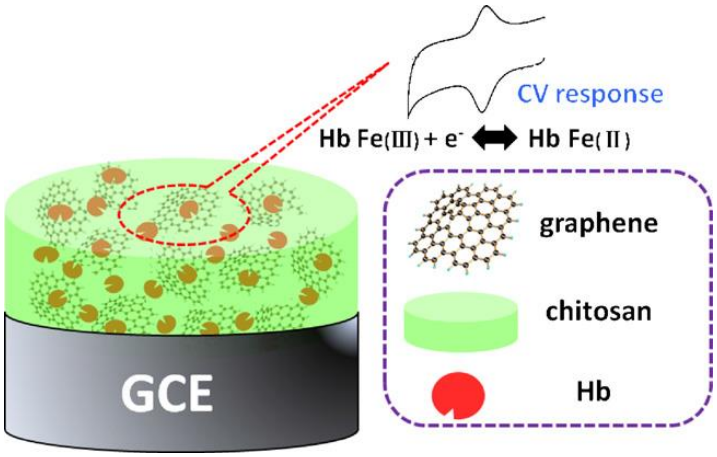

Figure 2.11 Schematic construction of Hb-graphene-chitosan/GCE. "Reprinted from [181], Copyright (2015), with permission from Elsevier".

2.4.4 CNTs for electrochemical biosensors

To date, CNT-based electrodes have been widely used as electrochemical sensors and have shown many advantages. First, the CNT-modified electrodes can catalyze redox reactions of analytes. It has been reported that the oxidation of analytes such as dopamine, H_2O_2 and NADH are catalyzed at surfaces of various types of CNT-modified electrodes [11]. Second, biomacromolecules such as enzymes and DNA can be immobilized on the CNT-modified electrodes and maintain their biological activity. Third, CNTs are good materials for fabrication of the electrodes since they are small and form linear structures that are strong and very stable chemically. These characteristics are advantageous for modifying electrode surfaces. Fourth, CNTs can be functionalized mostly through the carboxyl groups on their ends where enzymes, etc. can be immobilized for the development of various types of sensors. The fifth advantage of CNTs is their good electronic conductivity. It has been suggested that the improvement in the rate of electron transfer is due to the curvature of the tubes that has a beneficial effect on the energy bands close to the Fermi level [30]. The CNT conductivity is also affected by changes in their structure such as twisting and bending which may be utilized for sensing purposes. The combination of these advantages with others such as their porous nature also give them good wettability for a number of solvents, a better electrode-electrolyte interface and large surface

area. The central hollow cores and outside walls are effective at adsorbing and storing gases such as oxygen, hydrogen and nitrogen oxide [25].

As mentioned previously, the active sites in redox proteins and enzymes are typically buried within a hydrophobic polypeptide chain and the redox centers of proteins or enzymes are electrically insulated and inaccessible to the electrode surface. This makes it difficult to carry out direct electrochemistry of proteins and enzyme on conventional electrodes such as gold, platinum and glassy carbon. However, CNTs can serve as molecular wires that connect the electrode surface to the active site of enzymes. Consequently, the direct or enhanced electrochemistry of several proteins and enzymes without the need of mediators has been achieved. A number of enzyme-based electrochemical biosensors using CNT-modified electrodes based on this approach have been reported [184185175].

2.4.5 Self-assembling peptides for electrochemical biosensors

Recently, the potential of using ionic-complementary peptides in biocompatible electrodes to immobilize glucose oxidase covalently and fabricate glucose biosensors was demonstrated [4849]. These peptides can self-assemble on surfaces in the form of β-sheet layers that have considerable biological and physiological stability [5450] and good *in vitro* and *in vivo* biocompatibility [55186].

Chapter 3[1]

Dispersion of multi-walled carbon nanotubes in water using ionic-complementary peptides

Abstract

We demonstrate the non-covalent modification of multi-walled carbon nanotubes (MWNTs) immersed in aqueous solution using the ionic-complementary peptide EFK16-II. This modification which presumably arises through the interaction between the hydrophobic side of the EFK16-II and MWNT sidewalls and orients hydrophilic functional groups toward the solution phase and enables them to form highly stable dispersions in water. This stability can be attributed to the electrostatic repulsion between self-assembled peptides on the MWNTs. This repulsion as determined by zeta potential measurements increases as the pH diverges from the isoelectric point of ~ 6.7 for EFK16-II. This trend is confirmed by dynamic light scattering (DLS) measurements of the suspensions showing a decrease in their particle size as the zeta potential increases. These EFK16-II-MWNT suspensions have been used to modify mica surfaces. Atomic force microscopy (AFM) and scanning electron microscopy (SEM) images show that this leads to a uniform distribution of individual modified MWNTs on the mica surfaces. Transmission electron microscopy (TEM) reveals images of well dispersed fibres with dimensions similar to that of individual MWNTs. Tissue culture plates previously contacted with EFK16-II-modified MWNTs have been shown to have enough biocompatibility for growth and attachment of cells. The biocompatibility and enhanced electrical conductivity that should result from the modification with these EFK16-II-MWNT suspensions opens up their use in a number of potential biomedical applications such as the design of bio-electrode interfaces and fabrication of biosensors with high sensitivity.

[1] This chapter is adapted from a paper "Sheikholeslam, M.; Pritzker, M.; Chen, P. Dispersion of multi-walled carbon nanotubes in water using ionic-complementary peptides. *Langmuir,* 2012, 28, 12550–12556".

3.1 Introduction

Since the discovery of carbon nanotubes (CNTs) in 1991[4], considerable interest has been shown in incorporating them in chemical and biochemical sensors and nano-scale electronic devices and utilizing them for tissue engineering applications due to their remarkable electronic and mechanical properties. CNT-modified electrodes have better conductivity than graphite-based ones and have been shown to exhibit superior performance than those based on single metals such as Au, Pt and other carbon-based nanomaterials such as C60 and C70 [25–29]. Their electronic properties give CNT electrodes the ability to mediate electron transfer reactions with electroactive species in solution. To date, CNT-based electrodes have been widely used in electrochemical sensing. Furthermore, they are capable of providing suitable interfaces for the signal transfer and neurite outgrowth of neurons as well as supporting the attachment and growth of osteoblast, fibroblast and cardiac cells [28].

One of the main methods to prepare a CNT-modified electrode is to coat its surface with a CNT-containing suspension. However, the first obstacle for electrode modification is that the strong van der Waals forces between carbon nanotubes leads to their aggregation and poor dispersion in water and other solvents, which severely limits their usefulness. Although CNT dispersions can be stabilized in organic solutions such as DMF, ethanol and acetone and then used to modify electrodes to enhance their electrochemical response, these organic solvents typically denature biomolecules and so limit their application as biosensors [11]. Thus, the ability to form stable CNT-containing suspensions in aqueous solutions has attracted considerable attention. Although covalent stabilization of CNTs (using a method such as acid treatment) can successfully produce such suspensions, this approach has its problems since it tends to diminish the excellent optical and electronic character of CNTs and impede their inherent conductivity. Consequently, the formation of suspensions by non-covalent stabilization of CNTs may be a more promising method. For this purpose, the modification of CNTs by polymers and surfactants has been studied [44]. When polymers or non-ionic surfactants are used, a CNT suspension can be successfully dispersed through steric stabilization by an adsorbed surfactant or polymer layer. The hydrophobic part of the surfactant makes contact with the CNTs, while its hydrophilic part is oriented toward the solution. When ionic surfactants adsorb onto CNTs, electrostatic repulsion

between their similarly charged ends is the dominant factor, impeding nanotube aggregation and stabilizing the suspensions [44].

The use of peptide-based molecules has been explored as an option for dispersion of CNTs. The association of CNTs with peptides is expected to be useful in biosensor and tissue engineering applications and in the development of new bioactive nanomaterials. The biological potential of carbon nanotubes in immunology was investigated by Pantarotto *et al.* [12] who demonstrated enhanced *in vivo* antibody response from covalently linked nanotube-peptide conjugates. Toward this end, peptide sequences with specific affinities for carbon nanotubes using phage display have been identified [1314]. These peptides contain sequences rich in histidine and tryptophan at specific locations. Also, nanotubes have been successfully dispersed in aqueous solutions by pre-treating with amphiphilic peptide sequences which contain phenylalanine at specific locations and can fold into α-helixes on nanotube sidewalls [1516]. The main interaction responsible for suspending carbon nanotubes in water is reported to be π-π stacking between the aromatic rings in the amino acids and the nanotubes. Arnold *et al*. [17] investigated an approach utilizing peptide amphiphile (PA) molecules whereby amino acid sequences are covalently coupled to a hydrophobic alkyl tail. Since the surface of carbon nanotubes is non-polar and hydrophobic, peptide amphiphiles in an aqueous solution are expected to self-assemble on this surface and thereby minimize the interfacial energy of the nanotube-water interface through hydrophobic interaction between the tail and the carbon nanotubes and as a result exposing the hydrophilic sequence to the water.

Recently, the potential of using ionic-complementary peptides in biocompatible electrodes to immobilize glucose oxidase and fabricate glucose biosensors was shown [4849]. These peptides can self-assemble on surfaces in the form of β-sheet layers that have considerable biological and physiological stability [5450] and good *in vitro* and *in vivo* biocompatibility [55186].

Herein we report a non-covalent method of dispersing MWNTs in aqueous solutions using a simple self-assembling ionic-complementary peptide EFK16-II that has both a hydrophilic side (containing lysine and glutamic acid residues) and a hydrophobic side (containing phenylalanine). The self-assembly of this type of peptide on both hydrophilic (mica) and

hydrophobic (HOPG) surfaces has been previously shown [48187]. The hydrophobic side of the peptide is oriented toward HOPG while the hydrophilic side faces toward the solution. Thus, one would expect EFK16-II to assemble on the sidewalls of MWNTs through a similar mechanism when they are sonicated together in an aqueous solution. One of the advantages of this approach over previously reported ones for CNT modification is that these peptides can self-assemble in the form of thin β-sheet layers, which are about one nanometer thick and hence should not present a hindrance to CNT conductivity which is important in biosensor and bio-electrode fabrication. In this way, the orientation of the hydrophilic side of the peptides toward the solution would enable the MWNTs to be dispersed in an aqueous environment. Furthermore, the hydrophilic side of the peptide contains eight carboxyl and amino groups, which have been shown to be capable of immobilizing the GOx enzyme in a glucose biosensor without denaturation of the enzyme [48]. Consequently, this approach has the potential to improve the biocompatibility of MWNTs and immobilize a variety of proteins such as enzymes and antibodies on their sidewalls. Another potentially important benefit of modification of CNTs with these types of peptides is the enhancement of electrical conductivity suitable for bio-electrode interfaces. Toward this end, the use of self-assembling peptides to disperse CNTs may be effective.

3.2 Materials and Methods

3.2.1 Materials

Three peptides were used in this study: i) crude peptide EFK16-II with a sequence of FEFEFKFKFEFEFKFK, ii) EAK16-II with the same sequence except all Fs were replaced with As and iii) EK8 with a sequence of EKEKEKEK, where F corresponds to phenylalanine, A to alanine, E to glutamic acid and K to lysine. All peptides were purchased from CanPeptide Inc. (Québec, Canada) and used without any further purification. At neutral pH, F and A are neutral hydrophobic residues, while E and K are negatively and positively charged, respectively. The N terminus and C-terminus of the peptides were protected by acetyl and amino groups, respectively, to minimize end-to-end electrostatic interaction between peptides. The peptide stock solutions were prepared in pure water (18.2 MΩ; Millipore Milli-Q system) at a

concentration of 0.5mg/ml and stored at 4°C before use. The MWNTs (more than 85% purity) were purchased from NANOHUB Co., Ltd (Seoul, South Korea). Grade V-4 muscovite mica ($KAl_2(AlSi_3)O_{10}(OH)_2$) obtained from SPI Supplies (West Chester, PA, USA) was the substrate used for the atomic force microscopy (AFM) experiments. Mica was not used as the substrate to obtain the scanning electron microscopy (SEM) images since it is a poor conductor and gold-coating could hide some of the smaller MWNTs. Instead, much more highly conducting highly ordered pyrolytic graphite (HOPG) purchased from SPI Supplies (West Chester, PA, USA) was used as the substrate for these experiments.

3.2.2 Methods

3.2.2.1 Mica modification with EFK16-II-modified MWNTs

The stock suspensions used to modify mica were prepared by combining together EFK16-II and MWNT in pure water (18.2 MΩ; Millipore Milli-Q system) and sonicating the mixture for 10 min using a Qsonica XL-2000 probe sonicator at a power of 5W. The concentrations of both peptide and MWNT were 0.5mg/ml unless otherwise stated. The suspension was centrifuged at a speed corresponding to 6000 × g for 2h to settle and remove the MWNT aggregates from the suspension and leave behind individual suspended MWNTs in the supernatant. Once the supernatant was decanted, it was analyzed by a variety of techniques such as dynamic light scattering (DLS), zeta potential measurement and AFM and also used for cell culture experiments. Then mica was modified with the prepared suspension by contacting it with 100 μL of the supernatant for 20 min unless otherwise stated. After modification, the mica sample was rinsed with pure water three times.

3.2.2.2 Atomic force microscopy

Surfaces of mica modified with EFK16-II alone and EFK16-II-modified MWNT were investigated using a PicoScan™ AFM (Molecular Imaging, Phoenix, AZ) in air. To prepare the AFM samples, 100μl of a 0.5 mg/ml EFK16-II solution or EFK16-II-modified MWNT stock suspension was injected onto a freshly cleaved mica surface and incubated for 20min. It was then washed 3 times with Milli-Q water and left to dry for 1-2 h. Silicon crystal tips (type NCL,

Nanosensors^{TM}) with a radius of 10nm were used for AFM imaging using the tapping mode. The AFM tip resonance frequency used for imaging was between 160 and 180 kHz.

3.2.2.3 Dynamic light scattering (DLS)

Dynamic light scattering experiments were performed on the EFK16-II-modified MWNT assemblies using a Nano ZS Zetasizer (Malvern Instruments, Worcestershire, UK) with the appropriate viscosity and refractive index settings and the temperature maintained at 25°C during the measurements. A disposable capillary cell was used. The scattered light intensities of freshly prepared samples were collected at an angle of 173°. Three measurements were made for each sample. From these intensity data, the size distribution of the peptide assemblies in solution was obtained using the multimodal algorithm CONTIN provided in the software package Dispersion Technology Software 5.1 (Malvern Instruments, Worcestershire, UK).

3.2.2.4 Zeta potential

The surface charge of EFK16-II-modified MWNT assemblies in freshly prepared solutions at 25°C was determined from zeta potential measurements also obtained using the Nano ZS Zetasizer (Malvern Instruments, Worcestershire, UK) in disposable capillary cells. The pH of the peptide solution was adjusted to the desired value using small amounts of 2 M NaOH or 2 M HCl. Since the change in peptide concentration (<1%) due to the addition of NaOH or HCl was negligible, no correction of the peptide and MWNT concentrations for the volume change was made for this measurement. Three zeta potential measurements were obtained for each sample.

3.2.2.5 Scanning and transmission electron microscopy (SEM & TEM)

SEM images of the samples were obtained using a LEO 1560 Field Emission SEM. Samples were prepared following a similar procedure used for AFM analysis except that HOPG served as the substrate, as mentioned previously. Transmission electron microscopy (TEM) was performed with a Philips CM20 electron microscope at an accelerating voltage of 200 kV. The samples were prepared by contacting 10 μl of fresh EFK16-II-modified MWNT solution on a 400-mesh holey carbon grid for 10 min. Then any remaining solution was drawn off the edge of the grid with tissue paper and the sample was air-dried for 20 min before introduction into the TEM unit.

3.2.2.6 Cell culture

Human M4A4 GFP cells were cultured in 24-well tissue culture plates in the presence of Dulbecco's Modified Eagle's medium with 10% fetal bovine serum (pH 7.4) and then transferred to an incubator with 5% CO_2 environment at 37.0°C. Also Chinese Hamster Ovary (CHO-K1) cells were cultured using the same procedure in F-12K medium with 10% fetal bovine serum (pH 7.4) and incubated with the same conditions. Optical images were taken using an EVOS fl digital inverted microscope after 5 days of incubation.

3.3 Results and Discussion

3.3.1 Dispersion of MWNTs using EFK16-II peptide

The carbon nanotubes have been dispersed in water-based suspensions having a MWNT:EFK16-II weight ratio of 1:1. The concentration of EFK16-II is set to 0.5 mg/ml to ensure assembly of the peptide on the MWNT sidewalls. Figures 3.1a–c show dispersions of MWNTs after sonication (without centrifugation). Figures 3.1d–g present images of the supernatants obtained after centrifugation of suspensions prepared under different conditions. As shown in Figure 3.1a, when unmodified MWNTs are immersed in water after sonication, they immediately agglomerate and settle to the bottom of the vial indicating that the suspension in water is unstable and MWNTs cannot be dispersed. Not surprisingly, the supernatant obtained after centrifugation is entirely clear and contains no solids (Figure 3.1d). When unmodified MWNTs are immersed in ethanol, they immediately appear to become dispersed (Figure 3.1c). However, further examination reveals that the suspension so formed is not stable. Although not shown here, aggregates begin to form if the suspension is allowed to stand for 24 hours. Centrifugation causes most of the solids to settle out, leaving only a very small amount in the supernatant (Figure 3.1f). Furthermore, the solids remaining in the supernatant eventually agglomerate if allowed to stand longer (Figure 3.1g). The most stable suspensions are obtained when the MWNTs are modified with EFK16-II. As shown in Figure 3.1b, a uniformly dispersed suspension in water immediately forms. The suspension shows no evidence of any agglomeration when allowed to stand for long periods of time. When the suspension is centrifuged, a very large amount of finely dispersed MWNTs still remains in the supernatant. Little or none of these nanotubes in the supernatant

settle out even after standing for 6 months (Figure 3.1e). These observations indicate that EFK16-II is a very effective dispersant for these MWNTs. This success appears to bear out the proposal put forth in the Introduction section that EFK16-II should be able to assemble on the MWNTs with its hydrophobic side oriented toward the sidewalls and its hydrophilic side facing toward the solution, resulting in non-covalent functionalization of the MWNTs and effectively rendering them hydrophilic. The same mechanism has been reported previously for different types of peptides. [1517] An advantage of the approach presented here is that a pre-existing amino acid sequence was used rather than one that had been specifically designed to interact with the carbon nanotubes, as in the approach reported by Wang *et al.* and Su *et al.* [1314] In addition, the presence of phenylalanine residues on the hydrophobic side of the EFK16-II which is in contact with the MWNTs should make the affinity for each other stronger through π-π interactions.

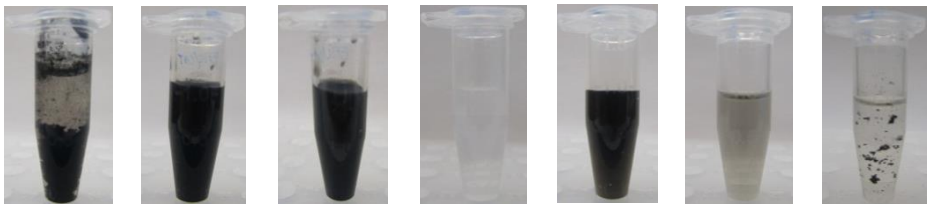

(a) (b) (c) (d) (e) (f) (g)

Figure 3.1 MWNT probe-sonicated suspensions (a) in water, (b) modified with EFK16-II in water, (c) in ethanol. Supernatant after centrifugation of MWNT suspensions (d) unmodified in water immediately after centrifugation, (e) modified with EFK16-II in water; 6 months after centrifugation, (f) unmodified in ethanol immediately after centrifugation, (g) unmodified in ethanol 4 days after centrifugation.

3.3.2 Importance of EFK16-II sequence in dispersing MWNTs

To further investigate the effects of hydrophobic and π-π interactions on the stability of these MWNT suspensions, we repeated the dispersion experiments but replaced EFK16-II with two related peptides EAK16-II and EK8. When suspensions of these peptides and MWNTs form in water, they exhibit similar pH (3.5-4.2) and zeta potential (~55 mV) since their charged residues are the same. The main differences in these peptides are their abilities to participate in π-π interactions and their degree of hydrophobicity, which decreases in the following order: EFK16-

II > EAK16-II > EK8. Phenylalanine can form π-π interactions, unlike alanine. EK8 is less hydrophobic than the others since it does not contain any hydrophobic amino acids in its sequence. Consequently, any hydrophobic interaction will occur between its peptide backbone and MWNTs. Figure 3.2 shows the suspensions obtained after centrifugation at 6k × g for 2 hours. As is evident, EK8 is least effective at dispersing MWNTs; most of the MWNTs settled out after centrifugation due to weak peptide-MWNT interactions. On the other hand, relatively little MWNT settles out when either EFK16-II or EAK16-II is present, showing that both of these peptides are good dispersants for MWNTs. Although not clearly distinguishable in the images, somewhat more MWNTs are found to settle out when EAK16-II is used, indicating that EFK16-II is the slightly stronger dispersant of the two. These trends suggest that hydrophobic interactions play a stronger role in determining the stability of these MWNT suspensions than do π-π interactions. The hydrophilic side of these peptides contains residues with carboxyl and amino groups that become charged in water. Thus, electrostatic repulsion between these charged hydrophilic peptide residues that are oriented outward into the solution prevent the agglomeration of the MWNTs.

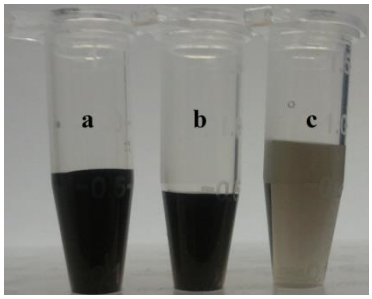

Figure 3.2 Different peptide-MWNT suspensions after centrifugation at 6k × g; (a) EFK16-II, (b) EAK16-II and (c) EK8.

3.3.3 Effect of pH on zeta potentials and size of the MWNTs suspensions

Due to the presence of these carboxyl and amino groups, the stability of MWNT suspensions in water should be affected by the pH. Experiments were therefore carried out to investigate the effect of pH on their zeta potentials and the stability of their suspensions. As shown in Figure

3.3a, the zeta potential of the particles is very positive under acidic conditions and decreases in magnitude as the pH is raised toward 6.0 before changing sign and increasing in magnitude with further increase in pH. This trend is understandable given that the isoelectric point (pI) of EFK16-II is known to be pH ~ 6.7 [188]. The peptide would be expected to exhibit a net positive charge at pH below the pI of EFK16-II and a net negative charge at higher pH. This behavior also explains the strong stability of the EFK16-II-modified MWNT suspensions shown in Figure 3.1 when one considers that the pH of these suspensions formed in deionized water is measured to be 3.9. As shown in Figure 3.3a, the zeta potential of EFK16-II-modified MWNT particles is very positive at this pH, indicating that the electrostatic repulsion between the particles should be large and the resulting suspension very stable under these conditions.

The extent of repulsion between the particles and the stability of their suspensions should also be reflected in their degree of aggregation. Figure 3.3b shows the average size of the EFK16-II-modified MWNTs in suspension at different pHs. These results show clearly that as the charge of the particles rises, the smaller is their size. This is confirmed in the photographic images of the suspensions obtained at pH 2.2, 6.5 and 11.2 that are presented in Figure 3.4. The dispersions of modified MWNT formed in water are homogeneous at acidic and alkaline pHs where the peptide chains in the modified MWNTs are highly charged (Figures 3.4a and c), whereas the suspensions become unstable when the pH is adjusted close to the pI of EFK16-II (Figure 3.4b). As expected, the agglomeration of modified MWNTs is strongly influenced by the electrostatic interaction between EFK16-II peptides. As the repulsion between the peptide chains increases, so does the dispersibility of the MWNTs. Reduction of the repulsion between the peptide chains in the modified MWNTs leads to their aggregation.

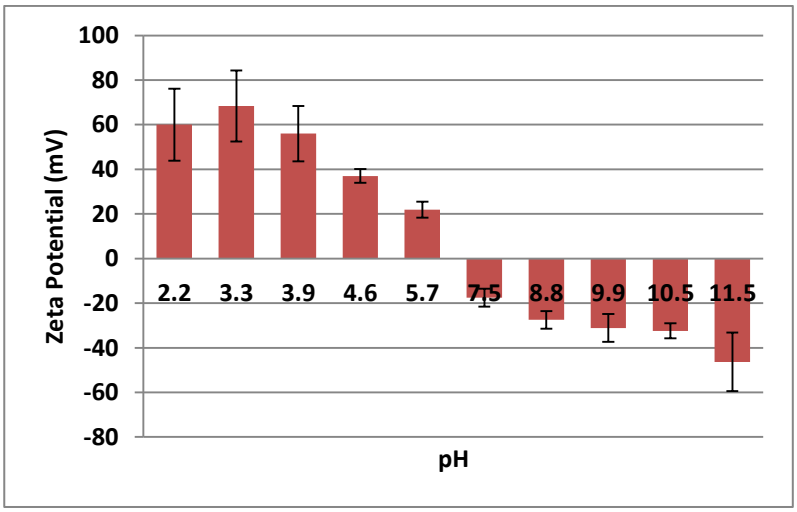

(a)

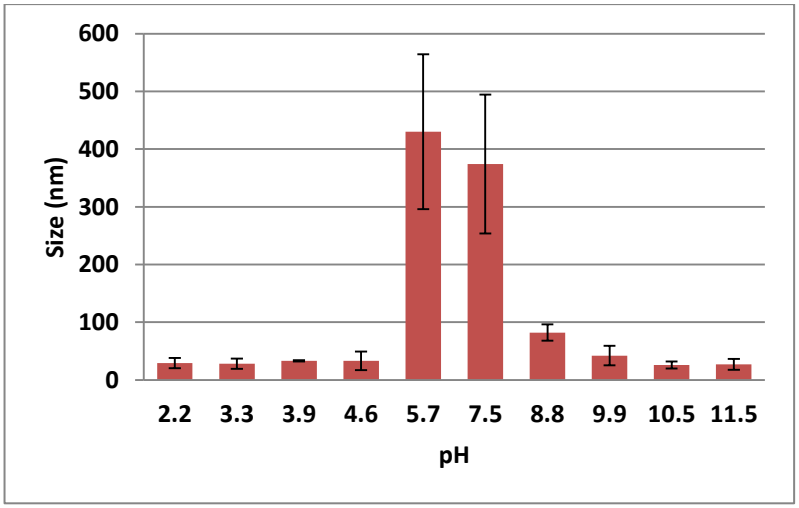

(b)

Figure 3.3 (a) Zeta potential and (b) size of EFK16-II-modified MWNTs as a function of pH

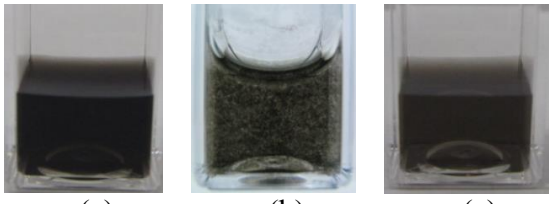

(a) (b) (c)

Figure 3.4 Photographs of EFK16-II-modified MWNT dispersions at different pHs: (a) 2.2, (b) 6.5 and (c) 11.2. All solutions were centrifuged (at 6k×g for 2h) to separate isolated and dispersed MWNTs from the aggregates before pH adjustment.

3.3.4 Assessing individual dispersion of MWNTs by AFM, SEM and TEM

Atomic Force Microscopy images show that individual EFK16-II-modified MWNTs are uniformly distributed over a mica surface (Figure 3.5a). These images have been analyzed using a procedure for tip deconvolution explained elsewhere [53] to estimate the diameters of the MWNTs. The height profile along the green line shown in Figure 3.5a has been obtained to gain an estimate of the dimensions of a MWNT lying on the surface. As shown below the AFM image, this analysis reveals that the MWNT has a diameter between 5 to 15 nm as it lies along the surface which agrees with the information concerning the dimensions of the nanotubes provided by the vendor. This confirms that the nanotubes remain in a non-aggregated state when modified with EFK16-II. For the purposes of comparison, Figure 3.5b shows an image of a mica surface that had been modified by a sonicated solution containing EFK16-II but no MWNTs. In this solution, many more self-assembled peptides (an example of one such assembly is indicated by the arrow) appear on the surface of mica than that shown in Figure 3.5a when MWNTs are present. Although EFK16-II often forms fibrils on the surface [48], it appears that the different conditions of our experiments, such as the use of probe sonication to dissolve the peptide in water, favors the formation of globular assemblies rather than fibrils. Similar behavior has been reported for the peptide EAK16-IV at a different pH [189]. The difference in the number of peptide assemblies that appear depending on whether or not MWNTs are present (Figures 3.5a and b) can likely be attributed to the uptake of EFK16-II by the MWNTs which should leave many fewer free peptide molecules available to self-assemble on the surface.

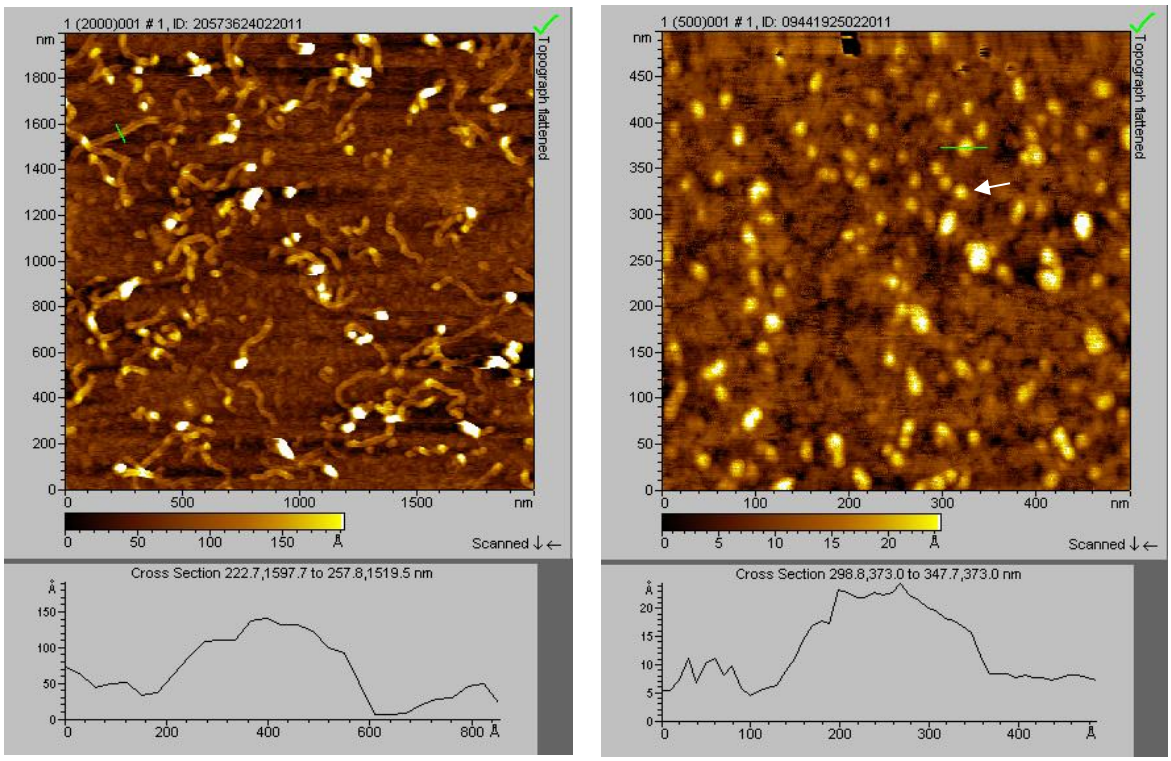

(a) (b)

Figure 3.5 AFM images of (a) mica surface modified with EFK16-II-modified MWNTs and (b) mica surface modified with probe-sonicated EFK16-II as a control sample in the absence of MWNTs. Also shown are the height profiles (indicated by green lines) across an MWNT in (a) and an EFK16-II assembly in (b) indicated by an arrow.

Figure 3.6 shows SEM and TEM images of MWNTs after modification with EFK16-II. As mentioned in section 3.2.2.5, a procedure similar to that used for AFM analysis was followed to prepare samples for SEM imaging except that HOPG served as the substrate. It is clear from these images that most of the MWNTs are present as individual fibers. This provides further evidence of the effect of peptide in overcoming the hydrophobic forces between these nanotubes and dispersing them in water. The amount of MWNT fibers that lie on the surface can be increased by prolonging the modification time and repeating the modification process. Examination of the TEM images shows that the MWNTs have diameters in the range of 5-20 nm which again agrees with the information provided by the vendor.

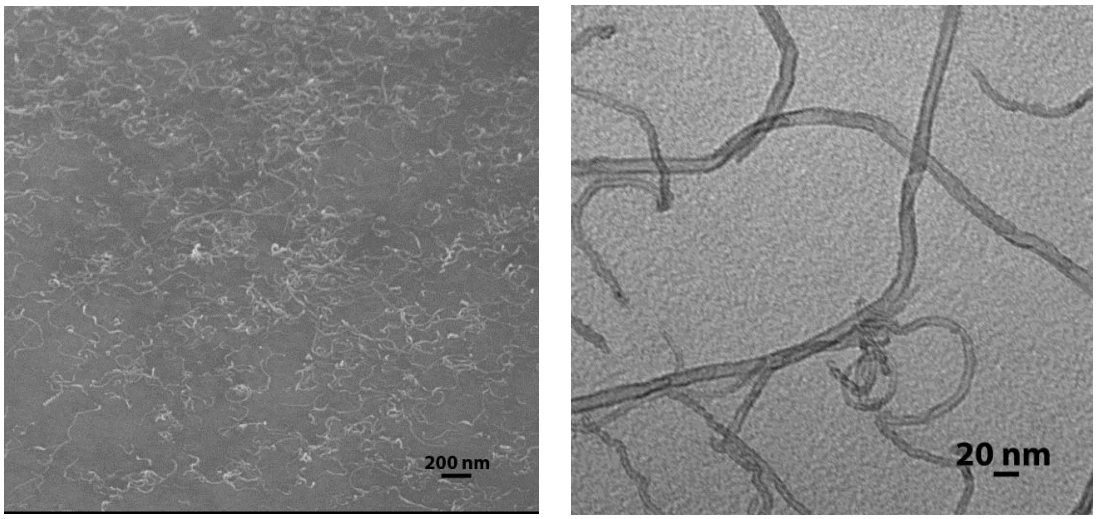

(a) (b)

Figure 3.6 (a) SEM image of the surface of HOPG modified with EFK16-II-modified MWNTs and (b) TEM image of EFK16-II-modified MWNTs on holey carbon grid.

3.3.5 Cell attachment and growth on the peptide and peptide-MWNT-modified surfaces

To demonstrate the potential of the modified surfaces for biomedical applications, we conducted cell attachment and proliferation experiments in 24-well tissue culture plates modified with the EFK16-II-modified MWNT. It should be noted that these tissue culture plates were surface-treated using corona discharge by the manufacturer, which has the effect of adding oxygen-containing chemical groups and/or opening the benzene ring. This makes the surface more hydrophilic and causes the plates to acquire a negative charge required for cell attachment and growth when immersed in the culture medium. Thus, the plates should be in a similar state as the mica used previously in this study and so one would expect the self-assembly of EFK16-II to proceed similarly on the plates. Figure 3.7 shows the optical images of the human M4A4 GFP and Chinese hamster ovary (CHO-K1) cells. These cells are good choices for assessing the biocompatibility of the plates since they exhibit a distinctive morphology if they can attach and grow on the surface and so can be easily distinguished from the situation where they cannot attach and grow and so die. Figure 3.7 shows optical images of (a) M4A4 GFP and (d) CHO-K1 cells 5 days after seeding on the culture plates modified with EFK16-II-modified MWNTs and images of (b) M4A4 GFP and (e) CHO-K1 cells 5 days after seeding on EFK16-II modified

plates in the absence of MWNTs. Also, images of the same cells on bare unmodified plates are shown in Figure 3.7c and f. Although more cells appear to grow on the unmodified plates, cells are still able to readily attach, spread and proliferate on the plates treated with the EFK16-II-modified MWNTs, indicating that this modified surface is sufficiently biocompatible for cell attachment and proliferation. A comparison of Figures 3.7a and b reveals a higher population and more homogeneous distribution of cells on plates treated with the EFK16-II-modified MWNTs than those modified with EFK16-II. This suggests that the presence of MWNTs appears to provide better conditions for attachment and growth of M4A4 GFP cells on this surface. Another contributing factor could be the higher surface roughness in the presence of MWNTs which can facilitate cell anchorage and attachment to the surface and yield a more even distribution of cells over the surface.

Contact angle measurements conducted on the plate surfaces show that they decrease from about 52° to about 14° and 12° upon modification of the bare plate with EFK16-II-modified MWNT and with EFK16-II alone, respectively (Figure 3.8). Thus, the decrease in the cell population after surface modification occurs simultaneously with an increase in hydrophilicity of the plates. Nevertheless, the decrease in cell population resulting from the treatment of the plates with EFK16-II-modified MWNTs is not too large and is likely outweighed by the positive effects conferred by the presence of MWNTs on the plate surface.

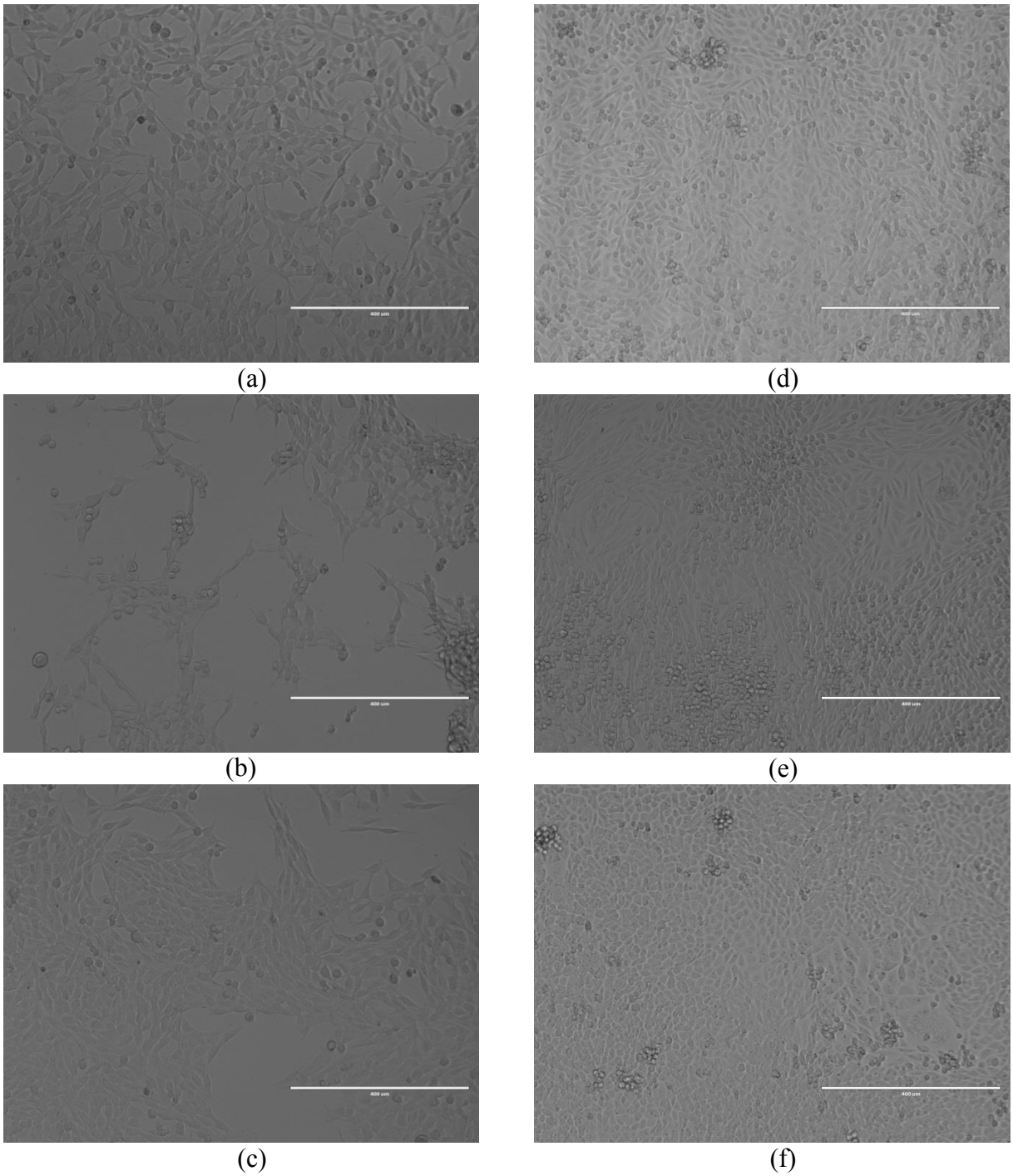

Figure 3.7 Optical microscopic images of (a) M4A4 GFP and (d) CHO-K1 cells that have attached and grown for 5 days after seeding in a 24-well tissue culture plate modified with EFK16-II-modified MWNT; optical images of (b) M4A4 GFP and (e) CHO-K1 cells 5 days after seeding in culture plates modified with EFK16-II; optical images of (c) M4A4 GFP and (f) CHO-K1 cells 5 days after seeding in unmodified wells.

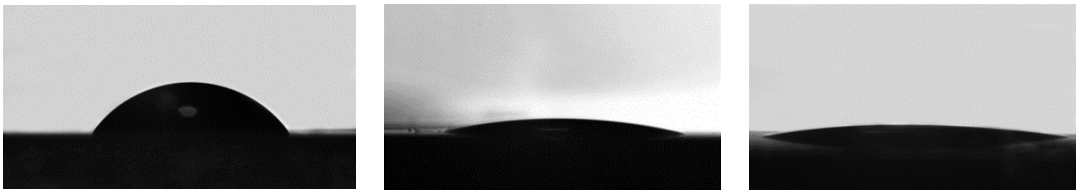

(a) (b) (c)

Figure 3.8 Photographs of a water droplet on different surfaces: (a) bare plate (contact angle ~ 52°), (b) plate modified with EFK16-II-modified MWNT (contact angle ~ 14°) and (c) plate modified with EFK16-II (contact angle ~ 12°).

3.4 Conclusions

From this study on the combined use of the ionic-complementary peptide EFK16-II and MWNTs, EFK16-II appears to self-assemble on the sidewalls of MWNTs and disperse them in water through a non-covalent functionalizing mechanism based on hydrophobic and π-π interactions. The stability of suspensions containing EFK16-II-modified MWNTs in water depends very strongly on pH. They remain stable for long periods of time at pH below about 5 and above about 8 where the modified particles are highly charged. On the other hand, at pHs close to the isoelectric point of EFK16-II (pH ~6.7), MWNTs agglomerate and their suspensions become unstable. Furthermore, experiments using tissue culture plates modified with EFK16-II-modified MWNTs show that they provide a biocompatible surface for attachment and growth of different kinds of cells.

Chapter 4[2]
Hybrid Peptide-Carbon Nanotube Dispersions and Hydrogels

Abstract

Scanning probe microscopy (SPM) techniques based on nano-mechanical measurements (topography, adhesion, modulus) and electric force microscopy (EFM) have been used to examine mica surfaces modified with the ionic-complementary peptide EFK8 alone and with EFK8–single-walled carbon nanotube (SWNT) dispersions in water in order to gain a deeper understanding of the interaction between nanotubes and ionic-complementary peptides. Through the use of these techniques, it has been shown for the first time that peptide fibers can be distinguished from SWNTs and peptide-wrapped SWNTs. SPM images reveal features consistent with two types of helical structures: EFK8 fibers wrapped around each other during self-assembly and EFK8 fibers wrapped around SWNTs. In this second structure, EFK8 chains should be oriented with their hydrophobic sides oriented toward the SWNTs and their hydrophilic sides toward the water, thereby enabling the dispersion of the nanotubes in aqueous media. We have also demonstrated the formation of hybrid EFK8-SWNT hydrogels that have potentially superior physical and mechanical properties over those of other hydrogels and opens up new applications for this type of material. To the best of our knowledge, this is the first work reporting the formation of a composite hydrogel made of an ionic-complementary peptide and carbon nanotubes.

[2] This chapter is adapted from a paper "Sheikholeslam, M.; Pritzker, M.; Chen, P. Hybrid peptide–carbon nanotube dispersions and hydrogels. *Carbon,* 2014, 71, 284–293".

4.1 Introduction

In the past two decades, ionic-complementary peptides have been used for a wide range of applications ranging from anti-cancer drug delivery to biocompatible hydrogels as scaffolds for 3D cell cultures and tissue engineering [22,47–52]. Before the introduction of these peptides, 3D cell cultures required the use of either synthetic scaffolds (such as PLLA and PGA biopolymers, calcium phosphate mesh and PEG gels) that unfortunately did not have the same fiber and pore size and chemical features of the natural extracellular matrix (ECM) or animal-derived materials (including bovine collagen and gelatin, fibronectin and Matrigel). The inclusion of these materials could contaminate the cell culture with undefined material and cause problems related to cell signaling, protein content and reproducibility [190]. It has been shown that the use of ionic-complementary peptides can provide a better scaffold for cells alleviating the above mentioned problems [190].

Since their discovery in 1991 [4], carbon nanotubes (CNTs) have attracted the attention of many researchers in different fields of engineering and science and emerged as one of the leading multifunctional materials in the field of nano-engineering. They have shown great promise for applications in biomedical engineering by enhancing the properties of biomaterials such as composite materials for tissue engineering [27,28,31–35] and in the fabrication of biomedical devices such as biosensors [25,26].

Hydrogels are interesting materials for use in tissue engineering due to their structural similarity with actual tissues in the body and their biocompatibility. Consequently, they are being used as scaffolds to fabricate new tissues. Due to their remarkable electronic and mechanical properties carbon nanotubes (CNTs) have been incorporated into hydrogels to modify their physical and mechanical properties for a variety of tissue applications [137–144]. In the past few years, the incorporation of CNTs in collagen hydrogels has been shown to increase the electrical conductivity of the hydrogels and to enable better control of their mechanical properties [145–152]. Conductive hydrogels are useful for mimicking and regenerating tissues in which electrical signals are propagated such as in cardiac muscles and neural tissue [139,141–143,148,149,151–153]. At the same time, it has been shown that the mechanical properties of the scaffold play a major role in the behavior and fate of cells, particularly stem cells [120,122,125,154]. This opens up the possibility of

using soft hydrogels for a wider range of tissues by using CNT-based scaffolds to improve their mechanical properties.

The first problem in using CNTs in biomedical applications is to overcome the van der Waals forces between CNT fibers so that they can be dispersed particularly in aqueous media and/or chemically functionalized. We have previously demonstrated this can be achieved through the addition of the ionic-complementary peptide EFK16-II that non-covalently stabilizes multi-walled carbon nanotubes (MWNTs) in aqueous solution via hydrophobic and π-stacking interactions [191]. In the current chapter, we report on the dispersion of single-walled carbon nanotubes (SWNTs) in aqueous media with another ionic-complementary peptide EFK8 (FEFEFKFK) containing the same amino acids but with half the number of residues in an EFK16-II sequence. Being an ionic complementary peptide with the same amino acid groups, EFK8 should interact with carbon nanotubes as EFK16-II does through hydrophobic bonding and π-stacking.

Although our previous study showed evidence of a strong interaction between EFK16-II and the MWNTs, it did not yield information concerning the particular structure formed by the peptide and nanotube in aqueous solutions. In the current study, we turn our attention to the interaction between EFK8 and SWNTs and use several high-resolution surface probe microscopy (SPM) techniques to reveal some details of the structure they form. Finally, we investigate a potential application of this EFK8-SWNT interaction by demonstrating whether it is possible to form a hybrid hydrogel involving the peptide and nanotube in aqueous media. To the best of our knowledge, the formation of a composite hydrogel made of an ionic-complementary peptide and carbon nanotubes has not been previously reported.

4.2 Materials and Methods

4.2.1 Materials

The ionic complementary peptide EFK8 with a sequence of FEFEFKFK where F corresponds to phenylalanine, E to glutamic acid and K to lysine was used in this study. This peptide was synthesized in our laboratory using an Aapptec Apex 396 peptide synthesizer. At neutral pH, F is a neutral hydrophobic residue, while E and K are negatively and positively charged, respectively.

The peptide was protected by acetyl and amino groups at the N terminus and C-terminus, respectively, to prevent end-to-end electrostatic interactions between peptides. EFK8 was dissolved in pure water (18.2 MΩ; Millipore Milli-Q system) at a concentration of 0.5mg/ml to prepare the peptide stock solution and then stored at 4°C before use. The metallic SWNTs (carbon > 90%, carbon as SWNT > 77%) were purchased from Sigma-Aldrich Co (catalog# 727777, lot# MKBH7136V). The substrate used for atomic force microscopy (AFM) was Grade V-4 muscovite mica purchased from SPI Supplies (West Chester, PA, USA).

4.2.2 Methods

4.2.2.1 Peptide synthesis

All amino acids (Fmoc protected), activator 2-(6-chloro-1H-benzotriazole-1-yl)-1,1,3,3-tetramethylaminium hexafluorophosphate (HCTU) and Rink Amide-AM resin were obtained from Aapptec LLC (USA). All other solutions were purchased from Acros Organics (USA). The EFK8 peptide with a molecular weight of 1162.60 g/mol was synthesized in our laboratory using the solid-phase peptide synthesis (SPPS) method using an Aapptec Apex 396 peptide synthesizer (Aapptec LLC, USA) before being purified by repeated precipitation in cold ether. Then it was freeze-dried and the final powder stored in a refrigerator. Matrix-assisted laser desorption ionization time of flight mass spectroscopy (Q-TOF Ultima Global, Waters, Milford, MA, USA) was used to measure the molar mass of the synthesized peptide.

4.2.2.2 SWNT dispersion preparation

The stock suspensions were prepared by combining EFK8 and as-received SWNT (carbon > 90%, carbon as SWNT > 77%) together at a 1:1 mass ratio in pure water (18.2 MΩ; Millipore Milli-Q system) to yield concentrations of 0.5mg/ml for both the peptide and SWNTs. The concentration of 0.5mg/ml for the SWNTs is based on the mass of as-received material and so may include components that are not actual SWNT. The suspensions were then mixed for 1 hour using a Qsonica XL-2000 probe sonicator at a power of 1W and centrifuged at a speed of 30,000 × g for 30 min to produce a supernatant that was decanted for later use in AFM experiments and hydrogel formation. The centrifugation speed falls in the recommended range by the SWNT supplier (Sigma-Aldrich) to remove impurities and produce good dispersions for AFM imaging.

4.2.2.3 Atomic and electric force microscopy

A Dimension Icon® AFM (Bruker Nano Surfaces, Santa Barbara, CA) was used in air to conduct examination of mica surfaces modified with EFK8 and EFK8-SWNTs. The samples investigated by AFM were prepared by incubating 50µl of 0.5 mg/ml EFK8-modified SWNT stock suspensions on a freshly cleaved mica surface for 30 sec. The surface was then washed 3 times with Milli-Q water and left to dry for 1-2 h. Silicon nitride tips (type SCANASYST-AIR, Bruker) with a radius of 2 nm were used for AFM imaging in the PeakForce® QNM mode. In this mode, a force-distance measurement is conducted at every single point of the image and nano-mechanical properties are extracted from the collected data. The user selects the maximum interaction between the probe and surface during a scan termed the peak force set-point. As the tip moves from point to point along a scan, it is automatically moved to a distance from the surface corresponding to the peak force set-point. The probe is then retracted from the surface and the interaction force continually monitored. This force decreases as the tip-sample distance increases, passing through a point where it becomes zero (due to a balance between repulsive and attractive forces between the tip and the sample) and then to a point where it becomes a minimum. At this point, the tip detaches from the sample. This minimum force gives a measure of the adhesion of the tip to the sample. The sample modulus which is a measure of sample stiffness can also be determined by fitting the Derjaguin-Muller-Toporov model to the force-distance relationship that is measured during the retraction of the tip [192]. The fitting and parameter estimation are carried out by software for every force-distance curve.

Electric force microscopy (EFM) using the Icon AFM was conducted in air on samples prepared on mica surfaces. This technique enables electric properties on a sample surface to be mapped by measuring the electrostatic force between the surface and a biased oscillating AFM cantilever. The EFM signal is generated from the shift in the phase lag between the drive signal and cantilever response resulting from the effect of the electrical field on the resonant frequency of the oscillating cantilever above the surface. The Icon AFM unit employed in this study was operated using the LiftMode™ in which the tip scanned every line twice; the first scan measured the topography using the tapping mode, while the second one detected the electric field at a designated height above the surface. The second scan was conducted with the tip held at a lift

height of 25 nm and a bias voltage of 2 V relative to the sample. The tips used in this technique consisted of silicon coated with platinum-iridium (type SCM-PIT, Bruker) and had a radius of 20 nm and resonance frequency close to 75 kHz.

4.2.2.4 Transmission and scanning electron microscopy

Transmission electron microscopy (TEM) was performed with a Philips CM20 electron microscope at an accelerating voltage of 100 kV. The samples were prepared by contacting 10 μl of fresh EFK8-modified MWNT solution on a 400-mesh holey carbon grid for 2 min. Then any remaining solution was drawn off the edge of the grid with tissue paper and the sample was air-dried for 20 min before introduction into the TEM unit. Hydrogel samples required special preparation so that they could be examined by SEM. The first step involved dehydration in stages by successive immersion in 30%, 50%, 70%, 90% and 100% ethanol solutions over 2 days. Once dehydrated, the hydrogels were dried using the critical point method employing supercritical CO_2. Once dried, the scaffolds were sputtered with gold for 100 sec prior to imaging with SEM. The SEM images of all samples were obtained using a Zeiss Ultra Plus SEM.

4.2.2.5 Hydrogel formation

EFK8 and EFK8-SWNT solutions were added to inserts with membranes at their bottoms suspended in a 24-well cell culture plate (BD Biosciences, San Jose, CA). Hydrogel formation was promoted by the monovalent salts present in the cell culture medium (F-12K with 10% fetal bovine serum) injected into the space between each insert and well wall so that they could reach the well bottom. The salt then diffused from the media across the membrane into the peptide or peptide-CNT dispersion to trigger hydrogel formation. The solutions were left for 2 hour at room temperature to ensure hydrogel formation was complete.

4.3 Results and Discussion

4.3.1 EFK8-SWNT hybrid dispersion and their interaction

A SWNT:EFK8 weight ratio of 1:1 was used to disperse the SWNTs in water. To ensure self-assembly of EFK8, a peptide concentration of 0.5mg/ml was chosen. Figure 4.1a shows the prepared dispersion after 30 min centrifugation at the speed of 30000 × g. These results clearly

indicate that the SWNTs have been dispersed through the addition of the peptide, confirming that they have been rendered hydrophilic through their interaction with the EFK8, similar to that observed previously when EFK16 was used [191]. Being an ionic-complementary peptide, EFK8 has both a hydrophilic (including E and K) and a hydrophobic side (including F). Presumably, the peptide has oriented itself with its hydrophobic side pointing toward the SWNT and its hydrophilic side toward the external solution. A TEM image of a portion of the dispersion that has been dried (Figure 4.1b) shows evidence of a number of SWNTs that are individually dispersed as a result of the interaction with EFK8 although the peptide is too small to be visible.

To examine the interaction at higher resolution, we also obtained AFM images of the EFK8-SWNT sample. A representative example is presented in Figure 4.1c. The highlighted region shows evidence consistent with one strand wrapping around another fiber to form a structure consistent with a helical pattern along its length. This can be seen more clearly in the image of the highlighted region in Figure 4.1c shown at higher magnification (Figure 4.1d) and in the 3-D image of the highlighted region in Figure 4.1d shown at still higher magnification. In addition, many small fibers that are distributed over the surface appear to be unassociated with other fibers. Presumably, these are self-assembled EFK8 fibers. The presence of these EFK8 fibers on the surface shows that not all of the peptides interact with the SWNTs and are consumed to disperse them. Instead, a significant portion self-assembles to form EFK8-only fibers independently of the presence of the nanotubes. This is an important observation since these free peptides would still be available to participate in other processes under the appropriate conditions. One example is hydrogel formation if higher concentrations of the peptide are added. The inset in the bottom left corner of Figure 4.1c shows an AFM topography image of a sample obtained in the presence of EFK8-only with no SWNT present. A structure consistent with the helical pattern appearing in the EFK8-SWNT images is evident along many of the fibers in this inset, suggesting that EFK8 is capable of forming helices during self-assembly. This is also consistent with a previously reported study showing that a similar peptide KFE8 forms helices during self-assembly in the absence of carbon nanotubes [193], which is discussed in more detail later in this chapter.

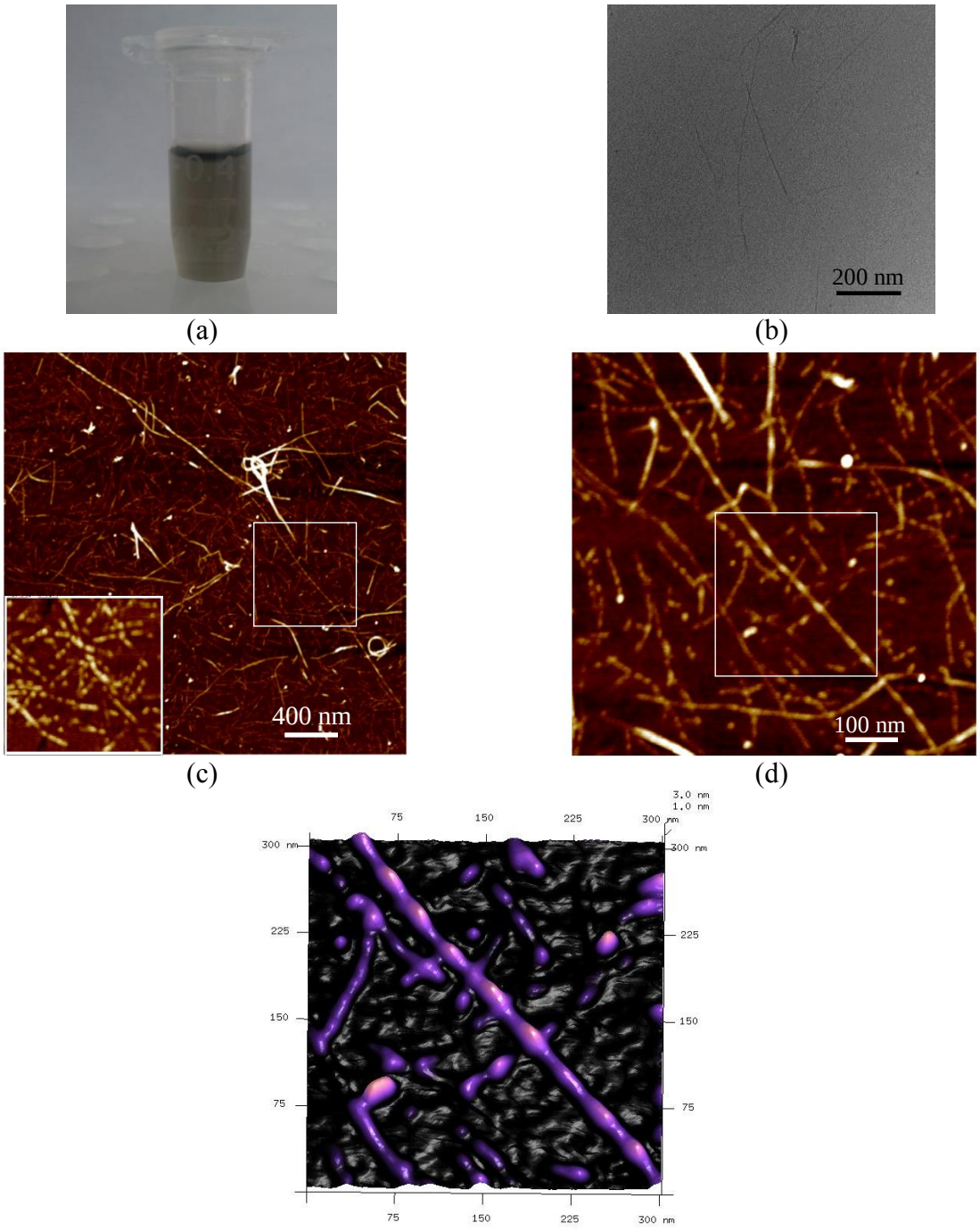

Figure 4.1 EFK8-SWNT dispersion in water: (a) optical image of dispersion in an Eppendorf vial, (b) TEM image of dried dispersion, (c) AFM image of dried dispersion, (d) high magnification image of the region shown in (c) and (e) 3-D image of the highlighted region in (d). Inset in bottom left corner of (c) is a 350 nm^2 AFM image of self-assembled EFK8 fibers.

4.3.2 Nano-mechanical study of EFK8-SWNT hybrid dispersion

However, the main difficulty in interpreting the topography image shown in Figure 4.1c is that it is not possible to unambiguously conclude that the long wrapped fiber is in fact an EFK8-wrapped SWNT. Another possible interpretation is that a couple (or more) peptide have bundled together and formed this long fiber, as has been previously reported by Marini et al. [193]. To examine this question further, we obtained AFM images of the EFK8-SWNT samples in the PF-QNM mode and analyzed the data collected from the topography, adhesion and modulus channels. This new technique has been recently used to map the mechanical properties of some polymers and proteins [194–198]. However, to the best of our knowledge, this is the first time that it has been applied to investigate the interaction between peptides and CNTs. Our main intention here is to use this technique to identify and distinguish between the various fibers rather than to determine their properties *per se*. This can open up a powerful new tool to characterize hybrid nanostructures. In the PF-QNM mode, the AFM conducts a force-distance measurement at every single pixel of the image. Different types of data such as topography, adhesion, modulus, dissipation, etc. are then quantitatively extracted from these measured force-distance curves. In the current analysis, we have combined topography, adhesion and modulus data to better distinguish between peptide-wrapped SWNTs and peptide bundle fibers.

To make sure that enough long peptide fibers and EFK8-wrapped SWNTs exist and a better comparison of their adhesion and modulus measurements can be made, we incubated both peptide and peptide-SWNT dispersions for five days. Figures 4.2a-c show the images of a sample containing EFK8 only. The same portion of the sample is viewed in these images, but processed using the topography (Figure 4.2a), adhesion (Figure 4.2b) and modulus (Figure 4.2c) data collected during the same scan using the PF-QNM mode. Due to the large incubation time, peptide fibers have bundled together and grown thicker and longer. The adhesion and modulus channels both show a homogeneous distribution of fiber adhesion and modulus over the surface (Figures 4.2b and c). The topography, adhesion and modulus images of a sample obtained when EFK8 and SWNT are combined together are presented in Figures 4.2d, e and f, respectively. The topography image (Figure 4.2d) appears to be similar to that obtained in the EFK8-only sample with many fibers entangled together and largely indistinguishable from each other. However,

some fibers in the adhesion image appear brighter than others (Figure 4.2e). In such an image, the brighter an object appears, the greater is its adhesion to the AFM probe. Based on the nature of the peptides and carbon nanotubes, we would expect a softer object such as EFK8 to exhibit stronger adhesion than a harder one such as SWNT. Consequently, darker fibers (shown by dotted blue arrow) in the adhesion image may correspond to SWNTs and lighter ones (red arrow) to the peptide. In a modulus image, fibers that appear bright have higher modulus than darker ones. The image shown in Figure 4.2f obtained using this channel confirms the conclusion reached based on the topography and adhesion data. The same fibers indicated by the dotted blue arrows have both lower adhesion (Figure 4.2e) and higher modulus (Figure 4.2f) which is consistent with that expected if they consist of SWNTs. Thus, by combining information gathered from these three data channels, peptide fibers and SWNTs can be distinguished from each other.

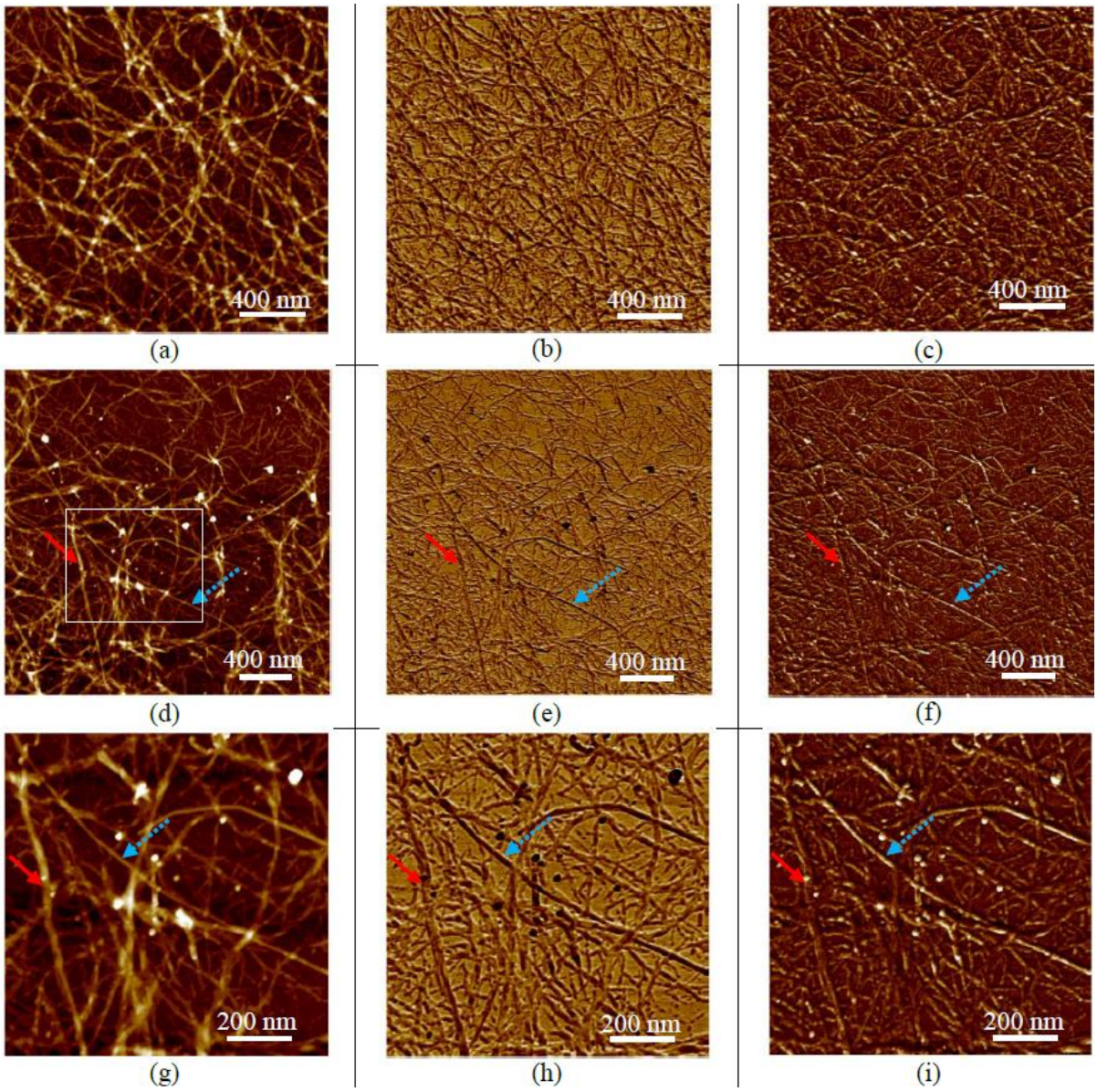

Figure 4.2 AFM images of EFK8 peptide fibers: (a) topography, (b) adhesion and (c) modulus maps. AFM images of EFK8-SWNT fibers: (d) topography, (e) adhesion and (f) modulus maps. Blue dotted arrow shows a SWNT, while the red arrow shows an EFK8 fiber. Region highlighted in (d) is shown at higher magnification using (g) topography, (h) adhesion and (i) modulus data

4.3.3 EFM study of EFK8-SWNT hybrid dispersion

The EFM technique has also been used to further distinguish between the SWNT and peptide fibers and confirm the conclusions reached using AFM. This technique employs a conductive tip to detect electric field variations over a sample surface. It has been previously employed to examine peptide nanotubes [199,200] and compare SWNT and DNA conductances [201], but no study on its use to distinguish CNTs from peptide nanofibers and investigate their interaction has been reported.

Figure 4.3a shows an EFM topography image of EFK8-SWNT on mica. This image is shown at higher resolution in Figure 4.3c. Both small and long fibers appear in these images. On the basis of the topography images, it is straightforward to identify the small fibers as being peptide due to their size and self-assembly, but the situation is less certain for the longer ones since they could be either bundles of peptide fibers or peptide-wrapped SWNTs from their appearance. For example, consider the two fibers indicated by the blue dotted arrows in the topography and phase images in Figure 4.3. One fiber which is straight and oriented in a north-south direction can be very clearly seen, while the second one which is somewhat curved and is oriented primarily in an east-west direction is much fainter. This difference suggests that the fiber oriented in the north-south direction lies at a greater height and/or is much thicker than the one lying in the east-west direction. In the high magnification topography image (Figure 4.3c), a sequence of alternating brighter and duller segments is evident along the length of the fiber in the north-south direction, consistent with the expected pattern if an outer wrapping is wound around the fiber. On the other hand, such a pattern is not visible along the fiber oriented in the east-west direction. Based on the species present, the outer wrapping surrounding the fiber in the north-south direction can only be the EFK8 peptide. However, it is not clear whether the EFK8 peptide is wrapped around an SWNT or if the entire structure is a bundle of peptide fibers wound around each other.

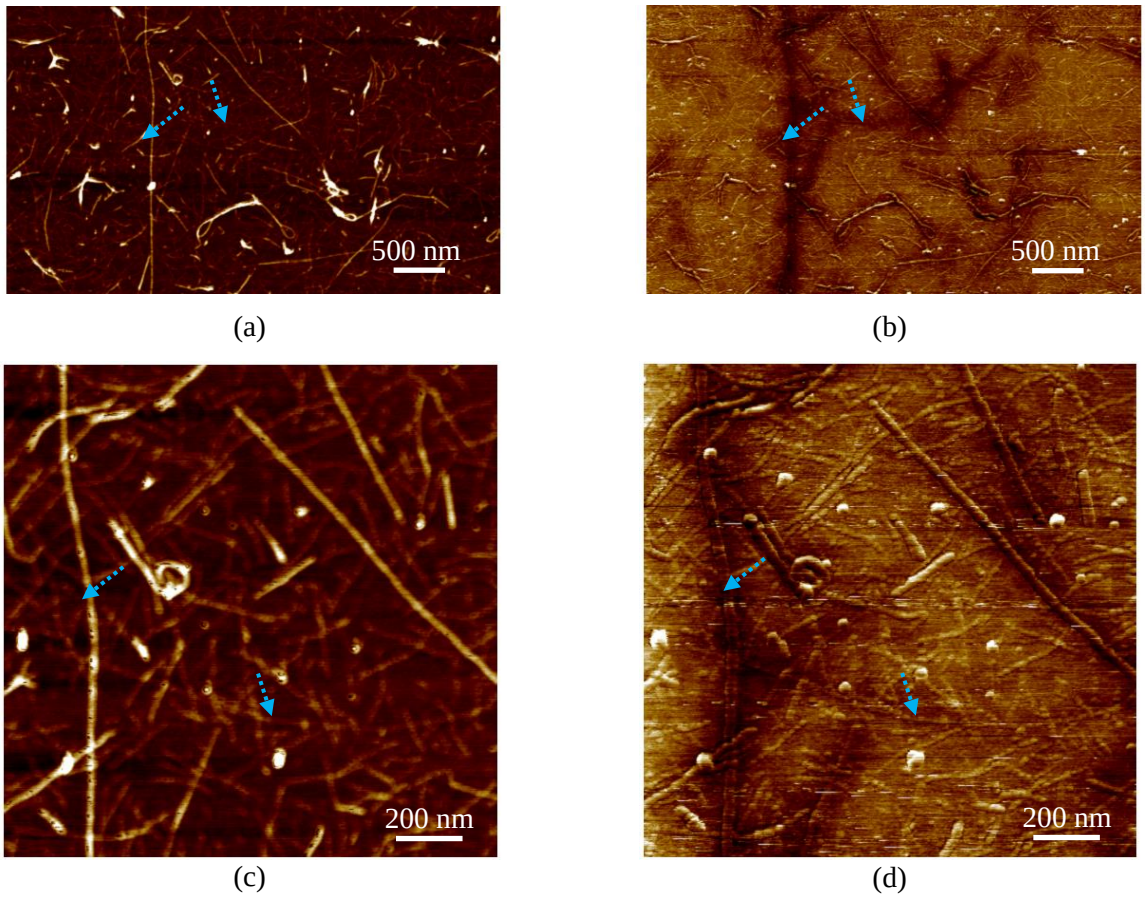

Figure 4.3 EFM images of the EFK8-SWNT dispersion: (a) topography and (b) phase maps showing the large effect of SWNTs on the phase shift. Higher resolution images of (a) and (b) are shown in (c) and (d), respectively.

However, through use of the EFM technique, a distinction between these two alternatives can be made. During EFM measurements, the tip interacts more strongly with the electronically conductive SWNTs than with EFK8 that contains charged amino acids glutamic acid (E) and lysine (K). As a result, the tip experiences a larger change in its resonance frequency measured as a greater phase shift when it interacts with the SWNTs than with EFK8. This difference makes the SWNT fibers appear darker brown in color than do the EFK8 fibers. When the EFM phase image of the SWNT-EFK8 sample is obtained, brown haloes appear around both fibers oriented in the north-south and east-west directions (Figures 4.3b and d). These are telltale signs of the phase shift associated with SWNTs. Taken together, Figures 4.3c and d provide evidence that the

fiber oriented in the north-south direction consists of EFK8 peptides wrapped around an SWNT. Although such a structure has not been reported to the best of our knowledge, peptides have been previously shown to be able to form helical structures. Marini et al [193] presented clear evidence that the peptide KFE8 can form left-handed double helical fibers made up two anti-parallel β-sheets at the beginning of its self-assembly in the absence of CNTs. These helices were measured to have 19.1±1.2 nm pitch and 7.1±1.1 nm thickness. Based on the proposed mechanism for KFE8, the sheet forming the inner helix has its hydrophobic side oriented toward the hydrophobic side of the sheet forming the outer helix. These sheets wrap together so that the hydrophilic sides of the sheets are always exposed to the solution.

Since the peptide EFK8 considered in the current study contains the same amino acid groups and has a very similar sequence as KFE8 (FKFEFKFE), the same forces as above should operate when it comes into contact with a hydrophobic substance such as carbon nanotubes in an aqueous solution. Thus, if SWNTs are present in a solution containing EFK8, they can serve a similar role as the inner helix in the self-assembly of KFE8 and fit inside the outer helix formed by the peptide. The peptide should wrap around hydrophobic SWNT with its hydrophobic side oriented inward toward the SWNT and its hydrophilic side pointing toward the external solution.

When immersed and sonicated in aqueous solutions containing an ionic-complementary peptide such as EFK8, hydrophobic SWNTs will have strong affinity for other SWNTs and the hydrophobic side of the peptide. At the same time, surface effects will drive both the SWNTs and the hydrophobic side of the peptide to minimize their contact with the solution. These competing influences can be accommodated by a mechanism in which EFK8 peptides self-assemble, similar to that proposed by Marini et al. [193] for KFE8. However, they can also be accommodated by the peptide fibers winding themselves around the SWNTs with their hydrophobic side in continual contact with the nanotubes and their hydrophilic side oriented outward toward the solution. The larger the portion of SWNT surface that is covered, the more hydrophilic the entire structure is rendered. Such a configuration explains how the addition of ionic-complementary peptides such as EFK8 enables the dispersion of SWNTs in aqueous solutions to take place.

One of the main obstacles in using SWNTs for a variety of applications has been the difficulty in obtaining nanotubes with a narrow size distribution. This is a significant limitation since SWNT diameter strongly influences a number of its properties (from semiconducting to conducting) and its ultimate performance in different applications. Thus, it would be very desirable to develop a separation technique that can produce nanotubes with a narrow size distribution. One possible approach for developing such a method would be to take advantage of the observation that EFK8 can wrap around nanotubes and render them hydrophilic [202–204]. If this peptide has a preference to form helices with a certain pitch, it may have a greater tendency to wrap around SWNTs with a particular diameter than others. In this way, it can be employed to selectively separate SWNTs with a certain diameter from a mixture of nanotubes having a range of sizes. Obviously, many other peptides in addition to EFK8 can be used to carry out this separation. Although DNA molecules have been previously considered for this purpose and studies conducted to assess their effectiveness [202–204], the observation in the current study that peptides can also wrap around SWNTs opens up the possibility that they can be used to separate SWNTs. Moreover, peptides may be a better choice than DNA since they can be custom-designed with different amino acid groups and sequence lengths and thereby tailored to separate SWNTs with a desired diameter. Given the importance of controlling SWNT size, further research on this topic is warranted.

It is also important to note that the two fibers indicated by arrows in Figure 4.3 exhibit strong phase shifts in the EFM phase image although their heights appear to be very different. At the same time, peptide fibers on the surface that appear to have the same height of each of these two SWNTs do not exhibit strong phase signals. These observations confirm that the effects of topography to interfere with and confound phase images, which can be a limiting factor in the use of the EFM technique, are not significant in this case.

Beyond experimental work, a number of computational studies based primarily on molecular dynamics methods have been conducted to gain a better understanding of the nature of the interaction between different biopolymers such as DNA with CNTs and their resulting structures [205–208]. Most have found that π-stacking and hydrophobic interactions are the main attractive forces between CNTs and these biopolymers, which is consistent with the effects observed in our

current study. However, no computational study concerned specifically with the interaction between EFK8 and SWNTs has been reported, but would be a valuable topic for future research. Such an analysis would complement the current study and help in the design of peptide sequences that can provide better and diameter-specific SWNT dispersions in aqueous media.

4.3.4 EFK8-SWNT hybrid hydrogel

To this point, we have used different AFM techniques to characterize EFK8-SWNT interactions and dispersions. However, from a practical point of view, the dispersion of CNTs in water using ionic-complementary peptides opens up the potential for a new class of hybrid materials ideal for many of the same applications as these functional peptides, but with more flexibility and enhanced mechanical and electrical properties. Among the most promising of these hybrid materials are hydrogels that have many potential applications, particularly for tissue engineering. Being an ionic-complementary peptide, EFK8 can form hydrogels in solution upon addition of a small amount (millimolar) of monovalent salt contained in cell culture media or another solution [190]. The role of the salt is to screen the electrostatic interaction between charged amino acids in the peptide sequence which is the main factor preventing the aggregation of peptide fibers and dispersion of CNTs as well.

Using the procedure described in section 4.2.2.5, we first formed a hydrogel by contacting F12-K cell culture medium with a solution containing EFK8, but no SWNTs (Figure 4.4a-left). From our understanding of the mechanism for hydrogel formation based on EFK8 alone, it should also be possible to form a hybrid hydrogel from an EFK8-SWNT dispersion by adding medium. Our AFM images of EFK8-SWNT dispersions reveal the existence of unattached free peptides in addition to those bound to SWNTs (Figures 4.2 and 4.3).

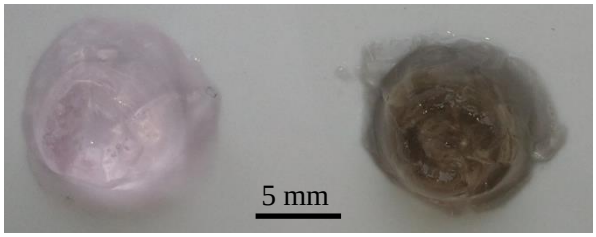

(a)

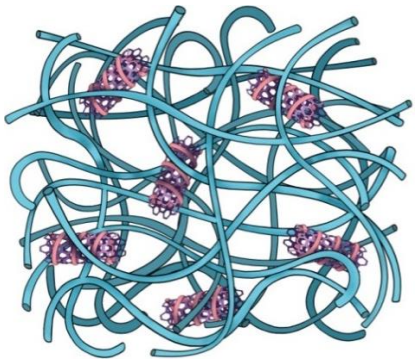

(b)

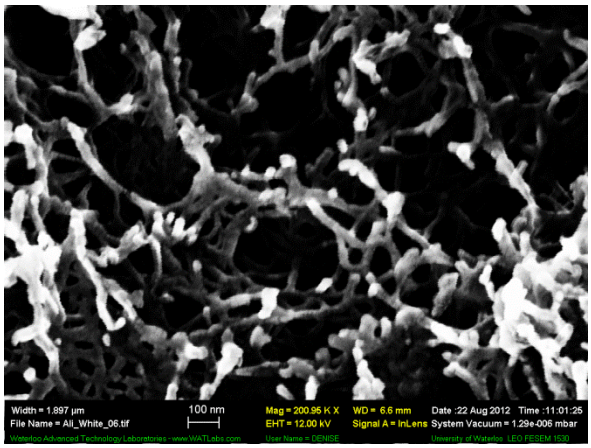

(c)

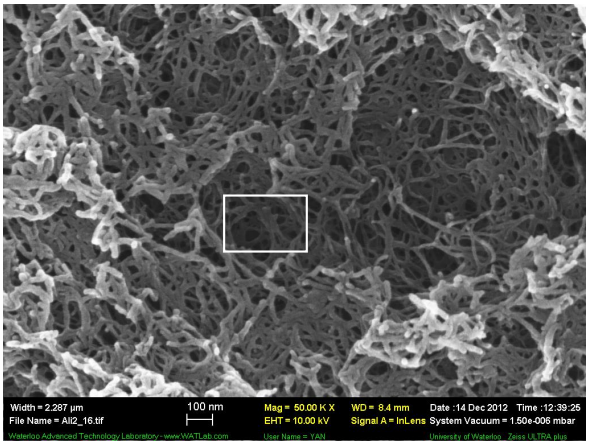

(d)

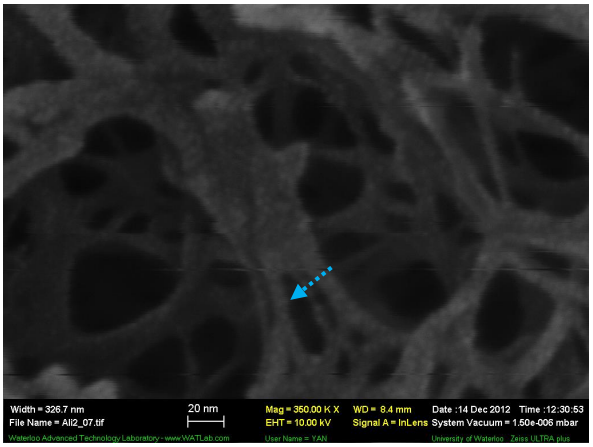

(e)

Figure 4.4 (a): EFK8 (left) and EFK8-SWNT hybrid (right) hydrogels. (b) Conceptual diagram of hybrid hydrogel structure made up of a scaffold (in blue) of peptide fibers containing EFK8-wrapped-SWNTs. SEM images of (c) EFK8 hydrogel, (d) EFK8-SWNT hydrogels. Highlighted region in (d) is shown at higher magnification in (e).

Both forms of the peptide contain charged amino acid groups that are exposed to the solution and available to form bonds with charged groups in other peptide fibers and so should contribute to hydrogel formation. The free peptides should operate exactly as they do in peptide-only solutions, while the peptides wrapped around SWNTs are oriented with their hydrophilic sides (containing charged amino acids) exposed to the solution. These ideas have been borne out by the fact that we were able to form hydrogels following the procedure described in section 4.2.2.5 (Figure 4.4a-right). Figure 4.4b shows a schematic view of the hybrid hydrogel consisting of peptide fibers forming the main scaffold (in blue) surrounding EFK8-wrapped-SWNTs. These hydrogels are homogeneous and differ in appearance from those produced from EFK8 alone primarily due to their gray color that arises from the entanglement of SWNTs in the peptide scaffold. SEM images of the EFK8 and EFK8-SWNT hybrid hydrogels dried using the critical point technique are shown in Figures 4.4c and d, respectively. The EFK8 hydrogel structure consists of a network of peptide fibers entangled with each other similar to the structure observed in real tissues of the body [190]. As shown in Figure 4.4c, the structure of the hybrid hydrogel appears quite similar to the EFK8 hydrogel. Due to the fact that the SWNT and peptide fibers have similar thicknesses and that the fibers become thicker when SWNTs are wrapped by the peptide or hydrogels form, it is very difficult to distinguish between EFK8 fibers and SWNTs in the SEM images. Figure 4.4e shows a magnified view of the highlighted region in Figure 4.4c. It should be noted that some fibers (e.g., the one indicated by the blue dotted arrow) in this image have much smaller diameters than others and may be SWNTs entangled in the peptide scaffold.

4.4 Conclusions

Scanning probe microscopy (SPM) examination of mica surfaces modified with EFK8 peptide alone and with EFK8 and SWNTs together provides new evidence that this peptide can wrap around the nanotubes, thereby rendering them hydrophilic and enabling their dispersion in aqueous media. For the first time, nano-mechanical measurements during atomic force microscopy (AFM) examination of the peptide-SWNT samples have been successfully used to distinguish peptide fibers from SWNTs. The electric force microscopy (EFM) technique was also successfully applied to identify SWNTs and distinguish them from self-assembled EFK8 peptide fibers, something which was not possible using regular AFM imaging. Finally, by adding salt to

EFK8-SWNT dispersions, we showed that hybrid EFK8-SWNT hydrogels can be formed. Work is currently underway to investigate the possibility of tuning their mechanical and electrical properties such as stiffness and conductivity by appropriate adjustment of the experimental conditions (e.g., peptide and SWNT concentration) during hydrogel formation. If successful, this should have a large impact on a wide variety of applications, particularly tissue engineering.

Chapter 5
Peptide and Peptide-Carbon Nanotube Hydrogels as Scaffolds for Tissue & 3D Tumor Engineering

Abstract

EFK8 peptide hydrogels and EFK8-SWNT hybrid hydrogels have been prepared and used to culture NIH-3T3 fibroblast and A549 cancer cells. In the first part of the study, the effect of the presence of SWNTs in the hydrogels on NIH-3T3 cell behavior cultured on hydrogels is investigated. Inverted light and confocal microscopy images reveal that when the hydrogels contain EFK8 only, the cells grow with spherical morphology and form isolated colonies. In the presence of SWNT, cell behavior and growth change significantly to a stretched morphology and spread individually and homogeneously over the surface. In addition, evidence shows that cells tend to migrate into the hybrid hydrogels. Furthermore, cells exhibit a faster proliferation rate when seeded on the hybrid hydrogel. An increase in the EFK8 solution concentration also leads to an increase in the hydrogel compressive modulus whereas the addition of SWNTs does not appear to have any effect on this property. Thus, the beneficial effect of SWNTs on the cell behavior does not appear to be caused by modification of the compressive modulus and is probably due to SWNTs serving as locations for cell anchorage that facilitate cell attachment, spreading and migration. Cells encapsulated in both types of hydrogels show the same behavior as in 2D cultures by forming colonies on EFK8 and spreading individually on the hybrid hydrogel. In the second part of the study, the potential of EFK8 hydrogels to promote the formation of spheroidal cancer cells is evaluated. The cells form spheroids when cultured on EFK8 hydrogels prepared at a peptide concentration of 1.25 mg ml^{-1}, but show a more stretched morphology and migratory phenotype when seeded on the stiffer hydrogel formed from 5 mg ml^{-1} EFK8. On the other hand, cells adopt a stretched morphology with high mobility when seeded on a hybrid EFK8-SWNT hydrogel formed from 1.25 mg ml^{-1} EFK8. Again, this behavior can be attributed to the facilitating effect of SWNTs on cell adhesion and migration.

5.1 Introduction

Hydrogels are commonly used biomaterials for tissue engineering and 3D cell cultures due to their high biocompatibility and the similarity of their physical and mechanical properties to that of living tissue [83–87]. These similarities provide a compatible environment for cells and enable their behavior to be similar to that observed *in vivo*. Hydrogels can also be modified chemically to mimic living tissues so that they become more biocompatible and perform better in the body [83–85,88].

Different types of materials have been used so far to make hydrogel scaffolds. Synthetic materials such as poly (lactic acid) (PLA) [8990], poly (ethylene oxide) (PEO) [91], poly (glycolic acid) (PGA) [92], poly (vinyl alcohol) (PVA) [9394], poly (ethylene glycol) (PEG) [95], as well as polysaccharide hydrogels including hyaluronic acid (HA) [96], chitosan [97], agarose [98] and alginate [99] have been investigated for use with different types of tissues. Production of these synthetic polymers is reproducible which makes them attractive for researchers. However, hydrogels formed this way have major drawbacks such as large fiber/pore sizes, the use of toxic reagents for gel formation, low degradation under physiological conditions, improper charge density, low nutrient diffusion rate and acidic products due to degradation [100]. On the other hand, protein-based hydrogels using collagen [101], gelatin [102], fibrin [103], elastin [104], silk fibroin [105] and Matrigel^{TM} are more biocompatible and biodegradable and provide a better platform for cell attachment and growth. However, they suffer from batch-to-batch variations and unwanted contaminants such as growth factors, proteins and viruses which can interfere with cell function [83,100]. On the whole, the best option would be to use a natural synthetic material. Self-assembling peptides are very promising from this point of view. They are formed from amino acids and found ubiquitously in the body; at the same time, they can be synthesized with precise control of its chemical composition. This should minimize the effects of contaminants and enable the distinction between the effects of different cues on cell behavior in the prepared scaffold. Their biodegradation products are natural amino acids that are used in the body and can be functionalized with different bioactive motifs for different cells and tissues. Also nano-sized fibers and pores of these hydrogels mimic the structure of living tissues in the body. This provides an environment that closely mimics in-vivo cell-cell and cell-scaffold interactions. In

addition, fiber crosslinking by which hydrogels form from these peptides does not require any chemical additives, UV irradiation or heat treatment which can lead to lower biocompatibility, unlike the situation with other biopolymer-based hydrogels. Finally, these peptide hydrogels can be formed by injection which enables them to encapsulate cells for 3D cultures.

To date, different types of self-assembling peptide hydrogels have been used for tissue engineering applications. RADA16-I hydrogels with the commercial name of PuraMatrix™ have been used for different types of cells [100]. The advantage of this peptide compared with other self-assembling peptides such as EFK8 is its similarity to the RGD tripeptide, a sequence within fibronectin that mediates cell attachment. Furthermore, the sequence of this peptide has been modified to extend its functionality and range of cells that can be seeded [106]. However, its mechanical strength drops after neutralization to the physiological pH which leads to its disruption when subjected to stress [107]. EFK8 is another type of self-assembling peptide with better mechanical strength due to stronger hydrophobic interactions participating in self-assembly process conferred by the presence of phenylalanine. We have previously shown that EFK16-II and EFK8 peptides can disperse SWNTs and be combined to form hybrid peptide-CNT hydrogels upon adding a small amount of salt [191,209].

Another important application of hydrogels is for 3D cell cultures. Hydrogels have been used as 3D scaffolds for drug discovery and 3D cancer tumor studies in vitro [86,87,108]. A 3D environment for cancer cells for these applications appears to be necessary based on the results of drug screening and tumor modelling. Reports show that the growth rate, morphology and drug resistance of tumor cells in a 3D scaffold are different from that in a 2D environment [86,109–112]. When cells are in vivo, both the extracellular matrix (ECM) and the physical properties of the microenvironment contribute significantly to the behavior and gene expression of cancer cells. In contrast with the classical theory of cancer which posits accumulated gene mutations to be the main cause of cancer, tissue organization field theory (TOFT) introduces the cell-microenvironment interaction as the starting point for cancer [113114]. It has even been reported that the placement of malignant tumor cells in a normal microenvironment can revert the cancer cells to a normal phenotype [115,116]. With this approach, not only the tumor microenvironment can be a target for cancer therapy [117] but also bio-mimetic 3D scaffolds can serve as useful models of

healthy ECM to treat the tumors in vivo and avoid the local formation of new tumors [108,113118]. For these reasons, attention in recent years has been increasingly focused on the tumor microenvironment as an important controlling factor for cancer.

Although treatment of tumors through surgery, chemotherapy and radiation has progressed tremendously, the ability to accurately predict the metastatic potential of a tumor is still missing [119]. It has been well documented that tuning the scaffold stiffness can affect the growth and differentiation of different types of cells [120–125]. Stiffness has been shown to be an important characteristic of the microenvironment that affects tumor formation, progression and metastasis [127,128]. Microenvironment stiffness affects these stages by regulating cell proliferation and differentiation so that the cells become dysfunctional [119,129–131]. Thus, synthetic scaffolds with tunable compressive modulus can serve as useful artificial 3D microenvironments to study cancer cells, spheroids and tumors [132–136].

In the current work, we have investigated the effect of the presence of SWNTs in EFK8 hydrogels on the NIH-3T3 fibroblast cell adherence, proliferation, migration and spreading as well as the hydrogel compressive modulus. Also, the potential of EFK8 as a 3D scaffold with tunable compressive modulus to study A549 cancer cell spheroid formation has been examined. Finally, the effect of SWNT on the metastatic behavior of the cancer cells is investigated.

5.2 Materials and Methods

5.2.1 Materials

The ionic complementary peptide EFK8 with a sequence of FEFEFKFK where F corresponds to phenylalanine, E to glutamic acid and K to lysine was used in this study. This peptide was synthesized in our laboratory using an Aapptec Apex 396 peptide synthesizer. At neutral pH, F is a neutral hydrophobic residue, while E and K are negatively and positively charged, respectively. The peptide was protected by acetyl and amino groups at the N terminus and C-terminus, respectively, to prevent end-to-end electrostatic interactions between peptides. EFK8 was dissolved in pure water (18.2 MΩ; Millipore Milli-Q system) at a concentration of 0.5mg ml^{-1} to prepare the peptide stock solution and then stored at 4°C before use. The metallic SWNTs (carbon > 90%, carbon as SWNT > 77%) were purchased from Sigma-Aldrich Co (catalog#

727777, lot# MKBH7136V). NIH-3T3 and A549 cells were purchased from ATCC. DMEM (high glucose) and F12-K medium solutions as well as fetal bovine serum (FBS) were obtained from HyClone™. Penicillin/streptomycin mixtures containing 10000 units penicillin and 10 mg streptomycin, Fluoroshield™ with DAPI and anti-β-catenin antibody produced from rabbits (C2206) were acquired from Sigma-Aldrich. Actin Green™ 488 ReadyProbes® reagent, Calcein AM (C3099) and Ethidium Homodimer-1 (EthD-1) (E1169) were purchased from Life technologies. AffiniPure Donkey anti-Rabbit IgG (Jackson Immunoresearch laboratories Inc) was used as the secondary antibody.

5.2.2 Methods

5.2.2.1 Peptide synthesis

All amino acids (Fmoc protected), activator 2-(6-chloro-1H-benzotriazole-1-yl)-1,1,3,3-tetramethylaminium hexafluorophosphate (HCTU) and Rink Amide-AM resin were obtained from Aapptec LLC (USA). All other solutions were purchased from Acros Organics (USA). The EFK8 peptide with a molecular weight of 1162.60 g mol^{-1} was synthesized in our laboratory using the solid-phase peptide synthesis (SPPS) method using an Aapptec Apex 396 peptide synthesizer (Aapptec LLC, USA) and then purified by repeated precipitation in cold ether. The resulting peptide was then freeze-dried to yield a powder that was stored in a refrigerator. Matrix-assisted laser desorption ionization time-of-flight mass spectroscopy (Q-TOF Ultima Global, Waters, Milford, MA, USA) was used to measure the molar mass of the synthesized peptide.

5.2.2.2 SWNT dispersion preparation

The stock suspensions were prepared by combining EFK8 and as-received SWNT (carbon > 90%, carbon as SWNT > 77%) together at a 1:1 mass ratio in pure water (18.2 MΩ; Millipore Milli-Q system) to yield concentrations of 0.5 mg ml^{-1} of both the peptide and SWNTs. The concentration of 0.5 mg ml^{-1} SWNT is based on the mass of as-received material and so may include components that are not actual SWNT. The suspensions were then mixed for 1 hour using a Qsonica XL-2000 probe sonicator at a power of 1W and centrifuged at a speed of 30,000 × g for 30 min to produce a supernatant that was decanted for hydrogel formation. The

centrifugation speed falls in the recommended range by the SWNT supplier (Sigma-Aldrich) to remove impurities.

5.2.2.3 Hydrogel formation

Transparent PET membrane inserts with 1.0 μm pore size (BD Biosciences, San Jose, CA) were placed in 24-well cell culture plates. Then EFK8 and EFK8-SWNT solutions were added to the inserts. Hydrogel formation was promoted by the monovalent salts present in the cell culture medium injected into the space between each insert and well wall so that they could reach the well bottom. The salt then diffused from the media across the membrane into the peptide or peptide-CNT dispersion to trigger hydrogel formation. The solutions were left for 30 min exposed to UV light inside the biosafety hood at room temperature to ensure hydrogel formation was complete. Then 400 μl cell culture medium was layered on top of the hydrogel and the plate was transferred to a 37.0°C incubator. After an hour, approximately two-thirds of the medium was gently removed and replaced with 400 μl of fresh medium before being placed in the 37.0°C incubator for another 1h. Finally, the medium on top was replaced as before and the medium in the well below the insert was replaced with 800 μl fresh medium and the plate was left in the incubator overnight.

5.2.2.4 Cell culture

Mouse NIH-3T3 fibroblast cells (12000 cells/well) were cultured on hydrogels formed in the 24-well inserts in the presence of Dulbecco's Modified Eagle's medium (DMEM, high glucose) with 10% fetal bovine serum and 1% penicillin/streptomycin (pH 7.4) and then transferred to an incubator (5% CO_2) at 37.0°C. Medium on top of the hydrogel and inside the wells were changed every 2-3 days. Human A549 lung cancer cells cultured in F12-K medium containing 10% FBS and 1% penicillin/streptomycin (pH 7.4) and maintained as described above.

5.2.2.5 Morphological and immunostaining

A LIVE/DEAD® reagent was used for morphological staining by adding calcein AM (8μM) and EthD-1 (18μM) to the live cells, leaving for 30 min. To carry out staining, the medium was gently removed from the inserts and the cells were fixed in 4% paraformaldehyde for 20 minutes

at room temperature, washed 3 times with PBS and the cells were permeabilized with 0.5% Triton X-100 for 10 min. Then the hydrogels were washed three times with PBS. Following this step for morphological staining of the cells, one droplet of Actin Green^{TM} probe was added to the hydrogel and left for 30 min followed by washing 3 times with PBS. Finally, Fluoroshield^{TM} with DAPI was added and left for 1 hour followed by 3 sequential washes with PBS. Immunostaining involved the same fixation and permeabilization steps as above followed by incubating the hydrogels in a PBS solution containing 10% fetal bovine serum for 12-16 hours to block non-specific binding sites. Then the primary antibody (rabbit anti-β-catenin) was added to this blocking solution at the ratio of 1:500 and the contents were incubated at 4°C overnight. After washing the hydrogels with blocking solution 4 times (2 hours per wash), the secondary antibody was added to the blocking solution at a ratio of 1:250 and contents incubated for another 4 hours. After 3 washes with PBS, the hydrogels were incubated in Fluoroshield^{TM} with DAPI for 1h and washed 3 final times with PBS.

5.2.2.6 3D cell encapsulation

The first step in the procedure was to dilute the 5 mg ml^{-1} EFK8 stock solution to 2.5 mg ml^{-1} by mixing with a sterile 20% sucrose solution. After trypsinizing and spinning down the cells, the medium was removed and cell pellet was re-suspended in a sterile 10% sucrose solution to make sure no medium remained. Then the cells were again collected by centrifugation and re-suspended in the 10% sterile sucrose solution so that their concentration was 8×10^5 cell/ insert which is twice the desired level. Then the cell suspension was quickly mixed with an equal amount of the EFK8 (2.5 mg ml^{-1})/sucrose (10%) solution to generate a final cell suspension (4×10^5 cell/ insert) in EFK8 (1.25 mg ml^{-1}) and 10% sucrose. From this suspension, a 100 µl aliquot was pipetted to each insert previously placed in the 24-well plate containing 250 µl medium in each well. After 5 min, 400 µl medium was gently layered onto the hydrogels. Then the plates were placed in the 37.0°C incubator and the medium was changed following the same procedure used to form the hydrogels (section 5.2.2.3).

5.2.2.7 Optical, confocal and scanning electron microscopy

Optical images were taken using an EVOS fl digital inverted microscope after 1, 3 and 5 days of incubation. For confocal imaging, the hydrogels were removed from the inserts and placed in chambered coverglass facing down. A droplet of PBS was added to prevent hydrogels from drying during imaging. Confocal images were taken using a Zeiss LSM 510 Meta Confocal Microscope. The hydrogel samples were dried prior to SEM imaging by first dehydrating in stages by successive immersions in 30%, 50%, 70%, 90% and 100% ethanol solutions over a 2 day period. Once dehydrated, the hydrogels were dried using a custom-made critical point drier (CPD) employing supercritical CO_2. Then the scaffolds were fixed on aluminum stubs using carbon paste and gold sputtered for 100 sec prior to imaging with SEM using an FE-SEM (LEO 1530) unit.

5.2.2.8 Micro-indentation

The compressive moduli of the hydrogels were measured using a micro-indenter equipped with a 0-25 g load cell (GSO-25, Transducer Techniques) and a hemispherical (D: 6mm) PDMS probe at a maximum load of 1g and speed of 5μ/s. The compressive modulus was measured at 2 or 3 locations of each hydrogel sample. For each of the two types of hydrogel studied, replicate measurements were conducted on three different samples formed on different days. The data presented here represent the averages over all these measurements. The compressive modulus was calculated from the slope of the resulting stress-strain curve over the linear portion from 0 to 5% strain.

5.3 Results and Discussion

5.3.1 Effect of SWNT on cell attachment, morphology, spreading and proliferation

NIH-3T3 cells seeded on top of the EFK8 and hybrid EFK8-SWNT hydrogels and incubated for 1, 3 and 5 days are shown in Fig. 5.1. The images show that the cells grow on EFK8 hydrogel with time and move toward each other on the surface to form colonies (Fig. 5.1a-c). Then the colonies become more populated and the areas between them become almost free of cells. Also most of the cells show a rounded morphology rather than the stretched one expected of this type

of cell. This suggests that the cells do not adhere very well to EFK8 hydrogels and thus need to form colonies. By forming colonies, they use other cell bodies and the ECM to attach, survive and grow rather than the hydrogel.

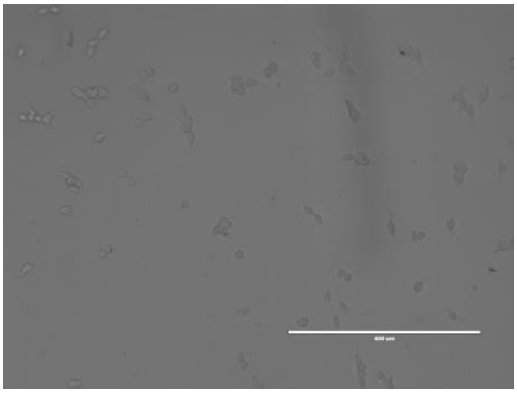

(a)

(e)

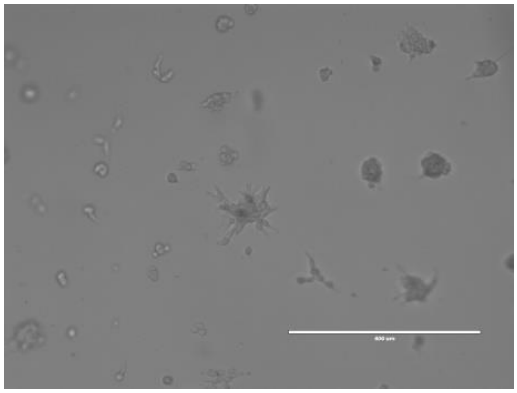

(b)

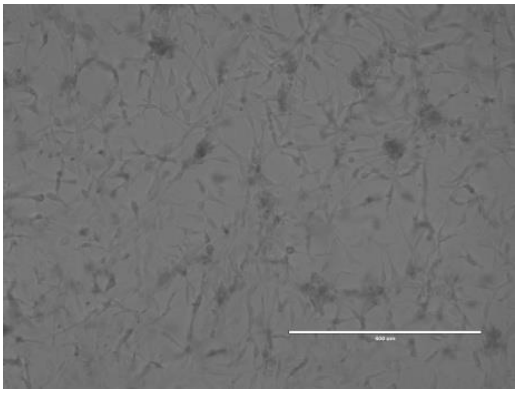

(f)

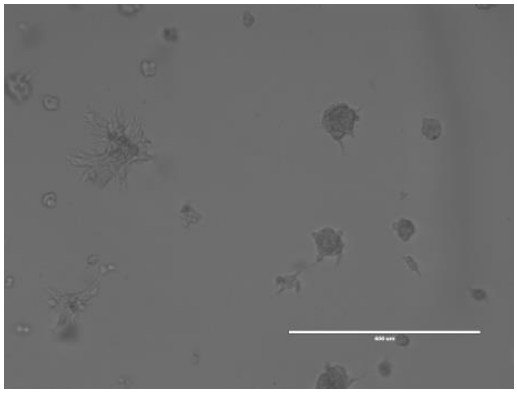

(c)

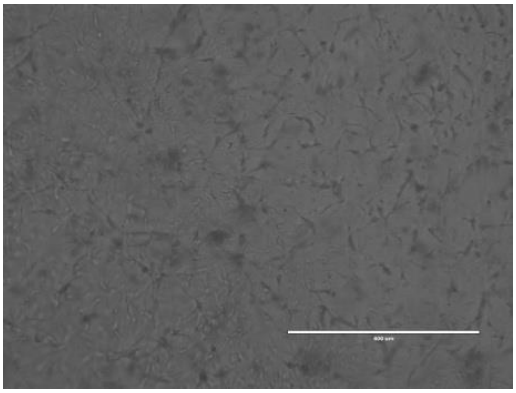

(g)

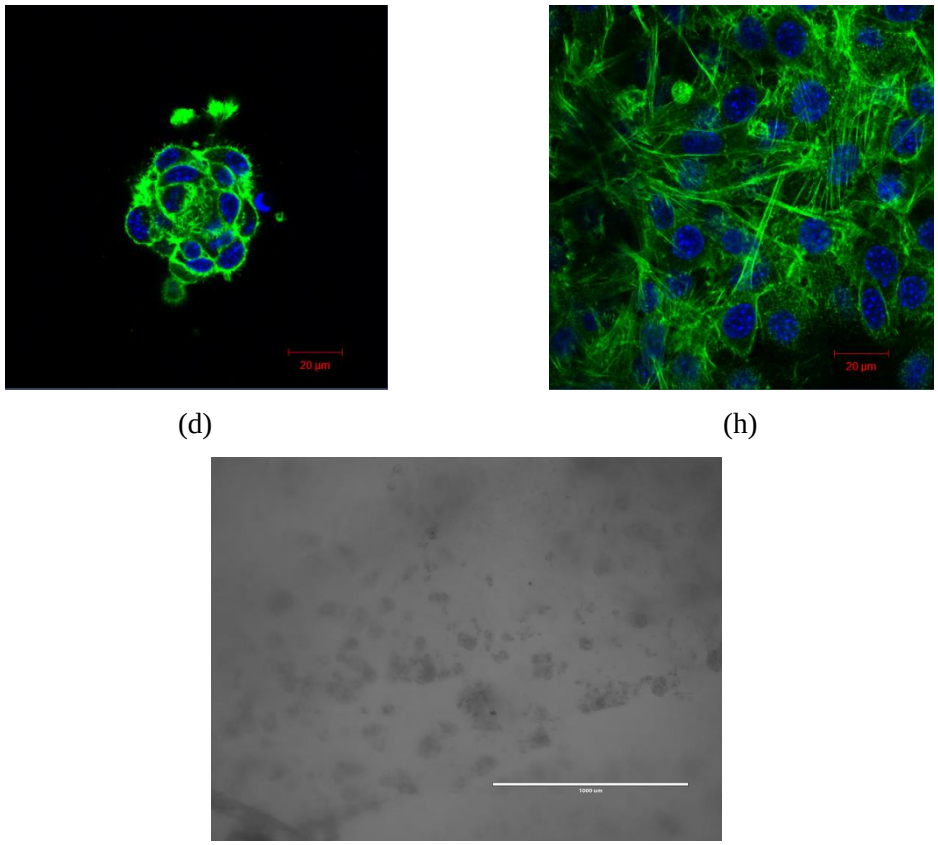

(d) (h)

(i)

Figure 5.1 NIH-3T3 cells seeded and cultured on EFK8 hydrogel after (a) 1, (b) 3 and (c) 5 days of seeding and on EFK8-SWNT hybrid hydrogels after (e) 1, (f) 3 and (g) 5 days of seeding (scale bar: 400 μm length). Confocal microscopy images of (d) EFK8 and (h) EFK8-SWNT at higher magnification (scale bar: 20 μm length). Cells were stained for f-actin using Actin Green™ (green) and for nuclei with DAPI (blue)). (i) RADA16-I hydrogel disrupted 1 day after seeding the cells (scale bar: 1000 μm length).

On the other hand, cells seeded on EFK8-SWNT hydrogels grow and spread more homogeneously on the surface over time (Figs. 5.1e-g). Most of the cells have spindle-like morphology, signifying healthy cells. This shows that the hybrid hydrogel provides a suitable scaffold for the cells to attach, grow and migrate over the surface and fill the available space homogeneously. It is likely that the SWNTs in the EFK8 scaffold provide sites for cells to anchor via focal adhesion and mediate cell attachment. Focal adhesion occurs at sites that mediate cell attachment and is responsible for cell membrane contraction and expansion during cell migration

and spreading. This is in agreement with the previous reports on the effect of carbon-based nanomaterials such as CNTs and graphene on the cell behavior due to their strong affinity with the cells and specially as a result of their aromatic structure which can increase the local concentration of ECM proteins such as collagen, laminin and fibronectin. [210211]. Although these materials have been found to enhance cell attachment, proliferation and differentiation, the mechanism by which they interact with cells has not been studied. The confocal microscopy images in Figs. 5.1d and h show cells on EFK8 and EFK8-SWNT hydrogel, respectively, after 3 days incubation. In these higher magnification images, the difference in the cells in these two environments is more obvious. It is also apparent that the cells have larger nuclei in addition to stretched cytoskeletons when they are contacted with the hybrid hydrogel.

Also included are cells seeded on RADA16-I hydrogel as a control sample (Fig. 5.1i). The resulting image shows that although the cells can attach and proliferate very well with a spindle-like morphology on the RADA16-I hydrogel (due to similarity of the peptide sequence to RGD) the hydrogel is disrupted after one day and cannot maintain its initial shape which can hinder its application for transplanting *in-vivo*.

Fig 5.2 shows the SEM images of fixed cells in the hydrogels after dehydrating and drying the hydrogels using CPD. Colonies with mostly rounded shape cells are apparent in the dried EFK8 hydrogel (Fig. 5.2a). A higher magnification of one of the cell colonies is shown in Fig. 5.2b. Fig 5.2c depicts the morphology of individual cells spread over the hybrid EFK8-SWNT hydrogel. The differences evident in Fig. 5.2 depending on the type of hydrogel are consistent with that shown in Fig. 5.1. Higher magnification images of an individual cell on the hybrid hydrogel are shown in Figs. 5.2c-f. Many protrusions at the cell edges are apparent at higher magnification, demonstrating the role of SWNTs in improving cell attachment to the EFK8 scaffold.

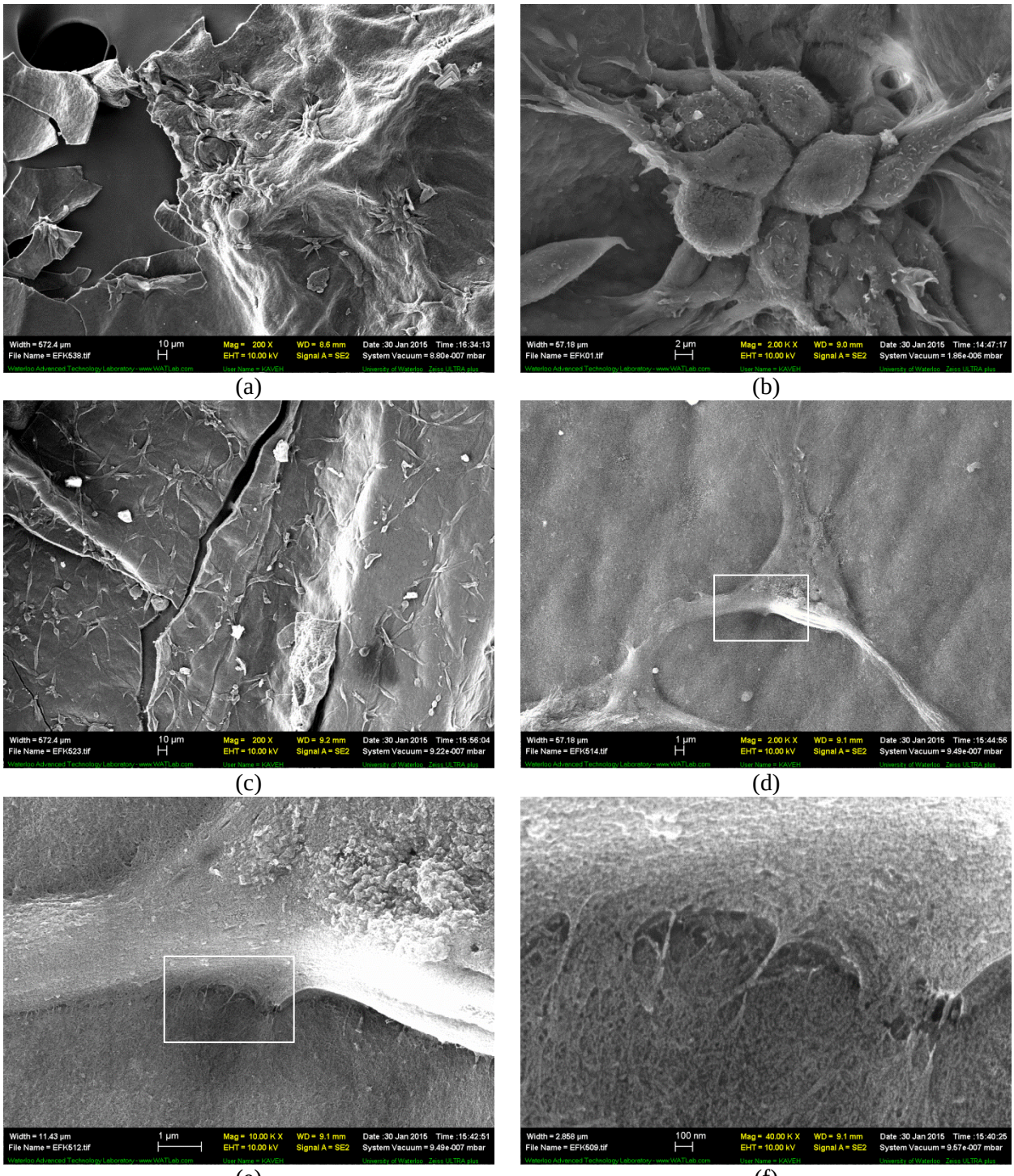

Figure 5.2 (a-b) NIH-3T3 cell colonies on EFK8 hydrogel at different magnifications. (c-f) Individually spread cells on the hybrid EFK8-SWNT hydrogel at different magnifications. Cell protrusions responsible for cell attachment to the scaffold are apparent in (f).

Comparison of the images in Fig. 5.1 suggests that cells grow faster on the EFK8-SWNT hydrogel and more cells are living in this scaffold after 5 days. To compare the proliferation rate on the two hydrogels, the gels were disrupted and the cells collected and counted using a hemocytometer after 1, 3 and 5 days of culture (Figure 5.3). This analysis shows that the number of cells is almost the same on both hydrogels 1 day after seeding. However, over the period from day 1 to day 3 after seeding, cells grow and proliferate faster on the hybrid hydrogel, again showing the effect of SWNTs on the proliferation of the cells. The difference in the number of cells continues to grow over the period from day 3 to day 5. Based on the corresponding optical images, the hybrid hydrogel is completely covered with cells by day 5 while considerable free space is available on the EFK8 hydrogel after the same incubation time.

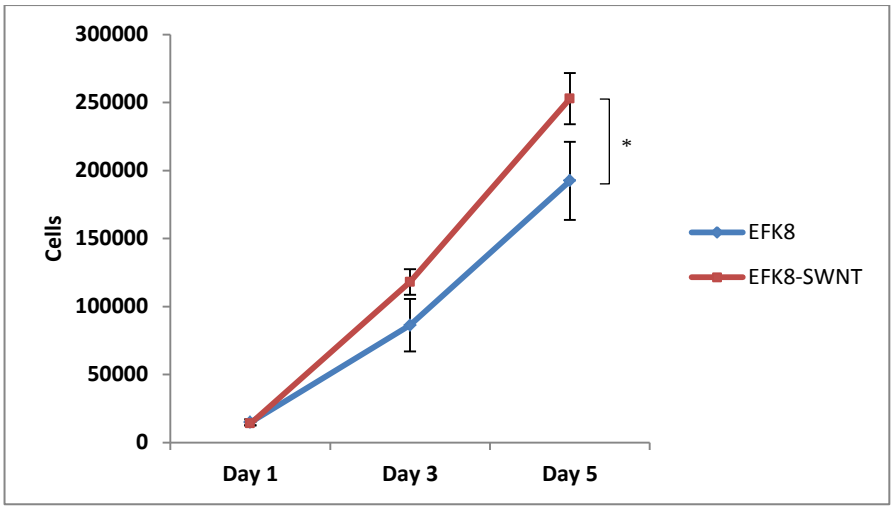

Figure 5.3 NIH-3T3 cell proliferation on the EFK8 and EFK8-SWNT hydrogels incubated for 1, 3 and 5 days after seeding. All data represent mean ± s.d. *$P < 0.05$.

Thus, based on these microscopy images and cell counting data, the presence of SWNTs in the EFK8 hydrogel appears to significantly improve cell behavior in terms of attachment, morphology, spreading and proliferation rate.

5.3.2 Effect of SWNT on cell migration

To better investigate cell migration in the two types of hydrogels, a small droplet of EFK8-SWNT dispersion was placed on the EFK8 solution and then gelation was triggered in both types of the hydrogels in the same sample. In this way, isolated hybrid EFK8-SWNT hydrogels were distributed over the surface of the EFK8 hydrogel. Then the sample was examined using light and confocal microscopy. Fig. 5.4a is an optical image showing stretched cells populating an EFK8-SWNT hydrogel that appears as the dark central region and is surrounded by cell colonies that form in the EFK8 hydrogel after 3 days of seeding cells. This clearly shows the contrast between the stretched morphology that cells can assume on the hybrid hydrogel and the rounded shapes in the colonies that form when the hydrogel consists of EFK8 alone. A confocal image of the same region is presented in Fig. 5.4b to better highlight the cell population on the hybrid hydrogel. Images at different focal planes in the vertical z-direction were obtained and combined to yield 3-dimensional images of the cells within the hydrogel. Figs. 5.4c and d show reconstructed 3-dimensional images of these cells at two different angles. Although cells were originally seeded only on the very top of the hydrogel, cells appear to have migrated downward into the hydrogel over time presumably due to the presence of SWNT in the hybrid hydrogel. Furthermore, the cells near the bottom of the hybrid hydrogel also appear to be stretching in the vertical direction, suggesting that this is the direction of their proliferation and growth. This effect further depicts the role of CNT in the scaffold in improving cell-scaffold interactions and enhancing cell growth and migration.

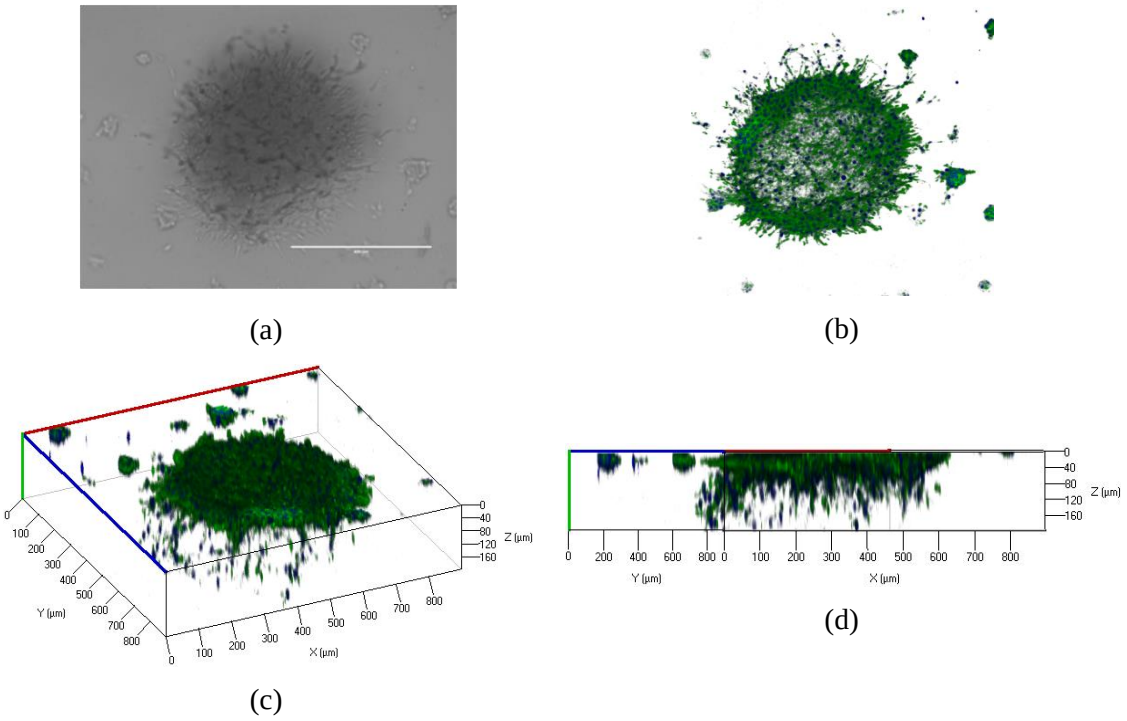

Figure 5.4 Optical (a) and confocal (b) microscopy images of an EFK8-SWNT hydrogel embedded in an EFK8 hydrogel. Z-stack images (c,d) obtained at different angles show the 3-dimensional structure of the cells within the hybrid hydrogel.

Comparison of optical images taken on days 1 and 3 after initial seeding (Fig. 5.5a, b) shows that although cells are distributed evenly over the EFK8 hydrogel at day 1, they have clustered into distinct colonies in the EFK8 background by day 3 as the distance between cells has grown. This trend is consistent with the proposal that EFK8 alone does not support cell attachment very well. At the same time, examination of a series of optical images over time suggests that cells in the EFK8 background area, especially those that are close to the EFK8-SWNT drop, are migrating individually or in colonies toward the CNT-containing drop. This tends to leave behind a region closest to the EFK8-SWNT drop that is largely free of cells and colonies. Figures 5.5c-q show a sequence of optical images of the same region taken at 1-hour intervals. An example of cells and colonies observed to migrate to the CNT-containing region over a period of time are indicated by arrows (Fig. 5.5c-q). This process might be possible through the transmission of

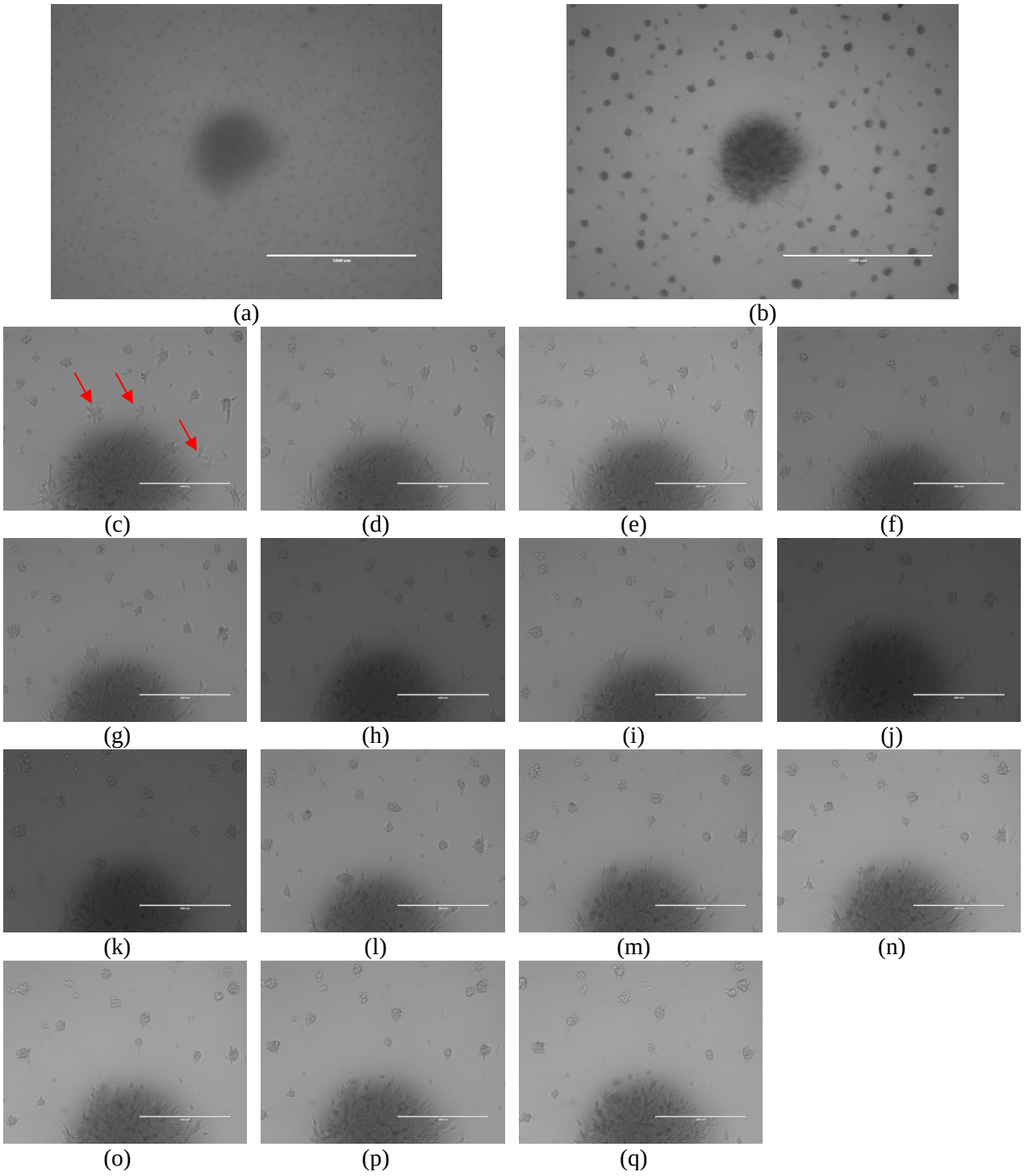

Figure 5.5 Optical images of EFK8 hydrogel modified with an EFK8-SWNT drop at the center taken on (a) day 1 and (b) day 3 after seeding. Higher magnification images (c-q) of the SWNT-containing region taken at 1-hour intervals. The arrows indicate cells or colonies that may be migrating toward the EFK-SWNT region.

some chemical or electrical signal from cells in the EFK8-SWNT region that this is a more favorable area for growth to those in the surrounding EFK8 region.

5.3.3 Cell patterning using EFK8-SWNT hybrid hydrogel

The large contrast in cell behavior on the two types of hydrogels (Fig. 5.4) indicates that cells can be easily patterned on EFK8 gels by pipetting an EFK8-SWNT hydrogel precursor onto its surface. Fig. 5.6a shows an EFK8 hydrogel surface patterned with four hybrid hydrogels. After 5 days, the SWNT-containing regions are filled with stretched cells in contrast with the background EFK8 hydrogel which contains primarily cell colonies. Most of the patterning methods are either complicated or require expensive UV irradiation. However, this method of pipetting a hydrogel surface with another type of hydrogel precursor is extremely simple. The size of the second hydrogel that forms the pattern can be controlled by the amount of precursor contained within the pipette and the pipette tip diameter. Once deposited, it gels at the same time as the background hydrogel. A 3-dimensional pattern eventually forms as the cells migrate not only along the surface but also vertically into the underlying gel. This technique is also very suitable for cell printing in which cells can be incorporated into the second hydrogel precursor at a desired concentration homogeneously distributed in the patterns.

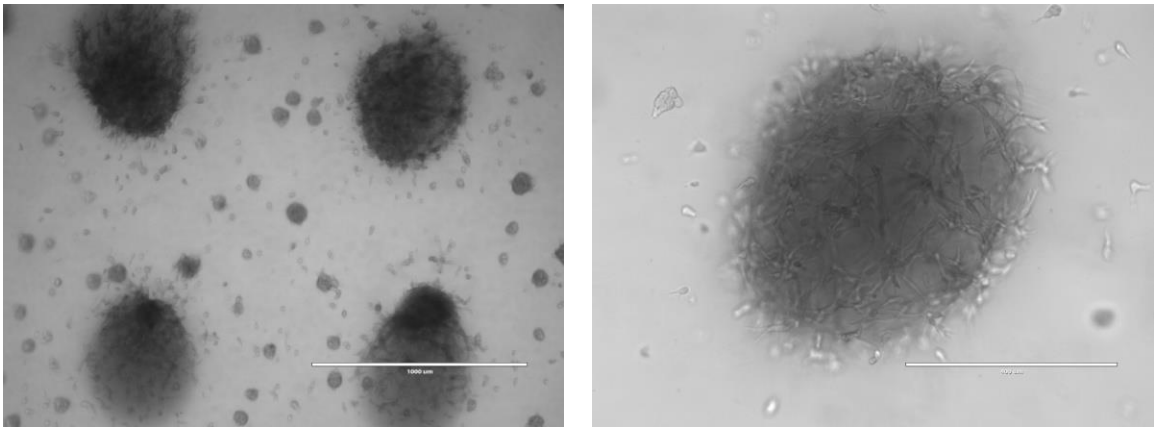

(a) (b)

Figure 5.6 (a) EFK8 hydrogel patterned with EFK8-SWNT hydrogels observed at (a) lower and (b) higher magnifications.

5.3.4 3D encapsulation of cells inside hydrogels

One of the major applications of hydrogels in tissue engineering is to encapsulate and deliver cells to a desired target *in-vivo*. Typically, the hydrogel is transplanted into the injured area after surgery to gain access. However, an advantage of injectable hydrogels is the minimal wound produced during transplantation. To do so, cells should be already encapsulated in the hydrogel precursor dispersion prior to injection. To test this idea, cells were dispersed in EFK8 and EFK8-SWNT dispersions and hydrogels formed. Fig. 5.7 presents optical images of cells in EFK8 and EFK8-SWNT hydrogels after 1, 3 and 5 days of encapsulation. As can be seen, cells show the similar behavior to that observed previously when they were seeded on top of a pre-existing EFK8 hydrogel and pre-existing hybrid hydrogel (Fig. 5.1). In the EFK8 hydrogel, cells stretch and migrate toward each other to form colonies over the period from day 1 to day 5 (Figs. 5.7a-c). Once again, this result indicates that cells cannot anchor and adhere very well to the scaffold in this hydrogel and shows the natural morphology of fibroblast cells. The images obtained on the hybrid hydrogel (Figs. 5.7d-f) show that no significant difference between cell morphologies is observed in the two types of hydrogels on day 1. However, the behavior changes thereafter as the cells exhibit stretched morphology and spread well inside the hybrid hydrogel by days 3 and 5, demonstrating good cell-to-scaffold attachment, growth and migration. These results also demonstrate that the EFK8-SWNT hydrogel is capable of encapsulating the cells without affecting the normal behavior of the cells, at least as far as observed in this study.

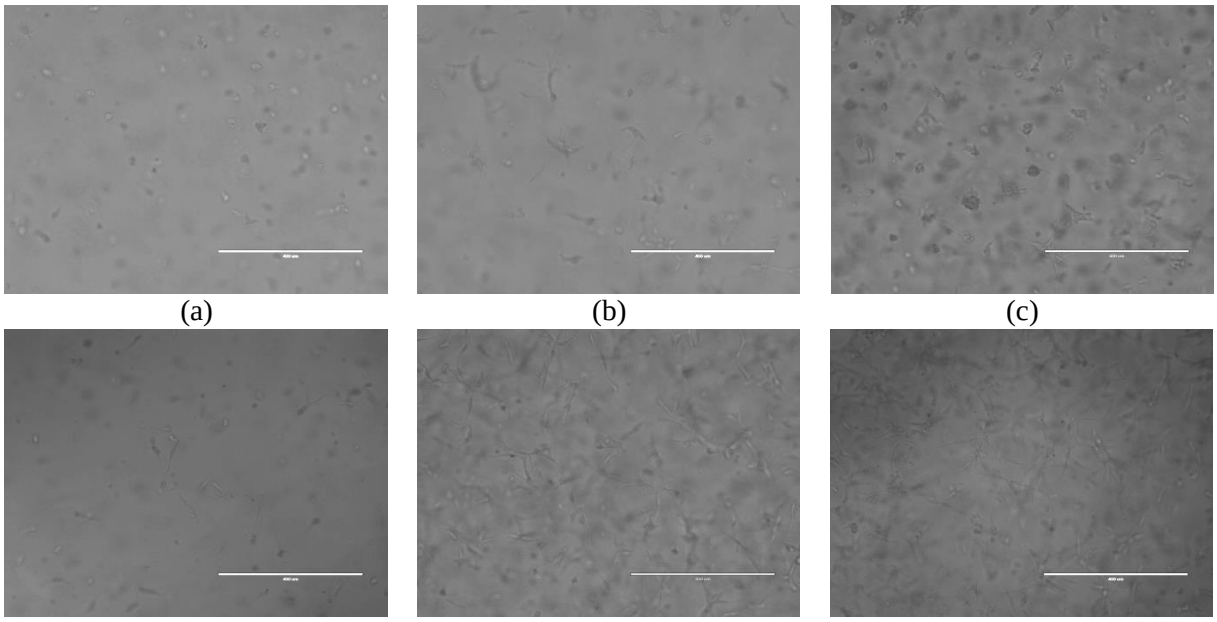

Figure 5.7 3D encapsulated cells 1, 3 and 5 days after encapsulation in EFK8 (a-c) and EFK8-SWNT (d-f) hydrogels, respectively.

5.3.5 Effect of SWNT on migration of 3D-encapsulated cells

Cell drops (that tend to appear as tori) were formed by pipetting a small amount of cell-EFK8 and cell-EFK8-SWNT dispersions in the medium and images collected over a 2-week period. Again no obvious difference between the hydrogels is apparent after day 1 (Figs. 5.8a and d). However, by day 5, most cells in the EFK8 hydrogel form large, concentrated colonies (Fig. 5.8b), while cells spread everywhere more uniformly with mostly stretched morphology in the EFK8-SWNT hydrogel (Fig. 5.8e). After 2 weeks, the SWNT hydrogel has turned black with very low transparency, presumably due to the proliferation of cells (Fig. 5.8f) However, over the same period, some transparency still exists in the EFK8 hydrogel (Fig. 5.8c).

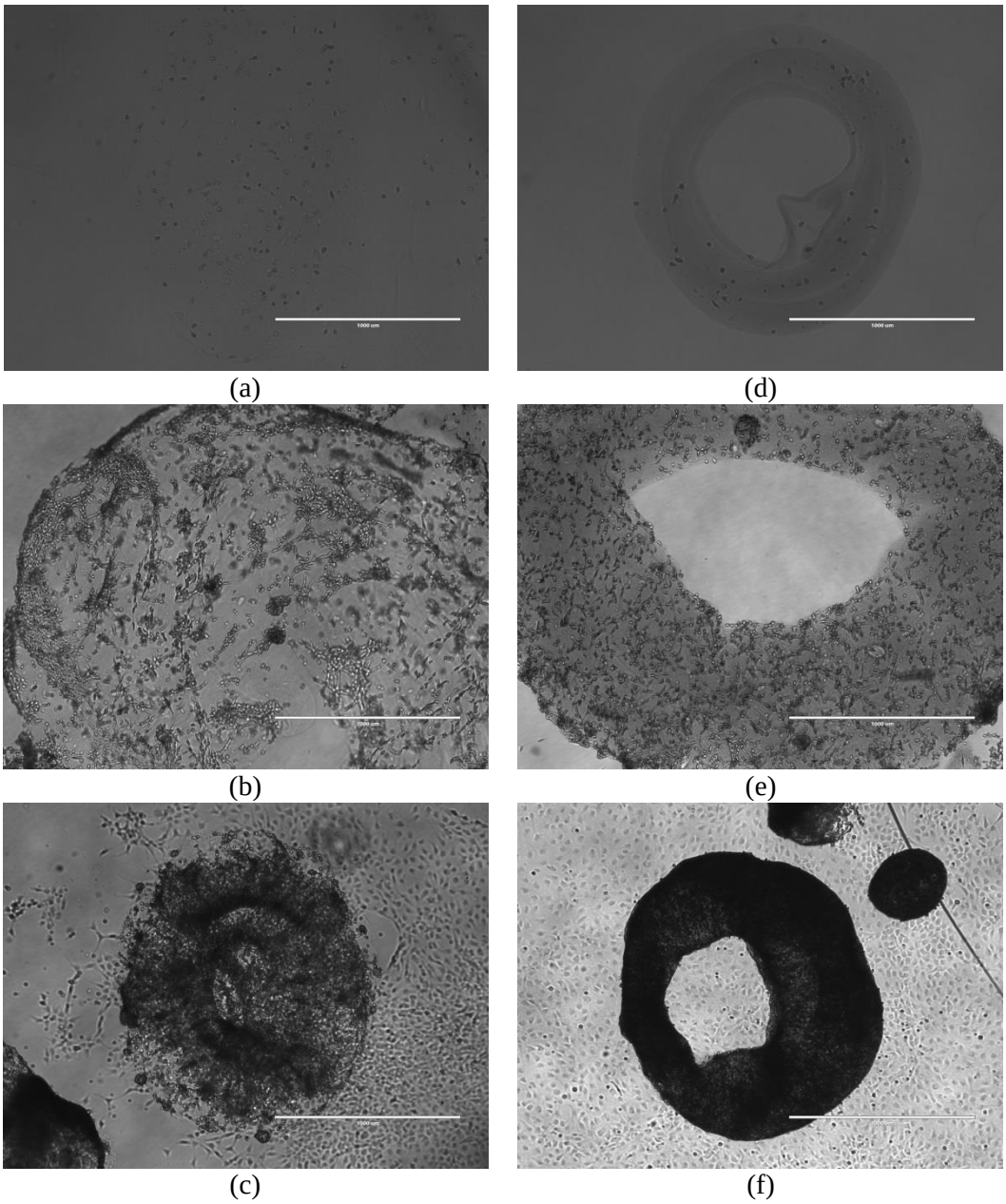

Figure 5.8 Optical images of cell drops formed in EFK8 (a: day 1, b: day 5 and c: 2 weeks) and EFK8-SWNT (d: day 1, e: day 5 and f: 2 weeks) hydrogels.

Also, some rod-shaped hydrogels containing a mixture of EFK8 and EFK8-SWNT dispersions were purposely formed to enable some comparisons regarding the ability of each hydrogel to promote and facilitate cell migration. The rod shown in Fig. 5.9a and b has an EFK8 hydrogel

head containing dispersed cells with the remainder being an EFK8-SWNT hydrogel containing no cells. A second rod (Fig. 5.9c, d) has an EFK8-SWNT hydrogel head with cells while the rest consists of EFK8 without cells. The EFK8-SWNT portions always appear darker than the EFK8 portions. For the case when cells were initially present only in the EFK8 head (Fig. 5.9a), a significant number of cells are observed in the EFK8-SWNT portions both close (Fig. 5.9b) and further away (Fig. 5.9c) from the head after 11 days. On the other hand, in the case where cells were initially present only in the EFK8-SWNT head (Fig. 5.9d), only a relatively low number of cells are found in the EFK8 portion close to the head (Fig. 5.9e) and virtually none are observed further away from the head (Fig. 5.9f) after 11 days. Taken together, these results suggest that cells appear to migrate a longer distance in regions containing SWNT, whereas they have more difficulty migrating to empty portions of the scaffold in the absence of the SWNT. Thus, this further shows the effect of SWNTs to facilitate 3D cell migration in the EFK8 hydrogel.

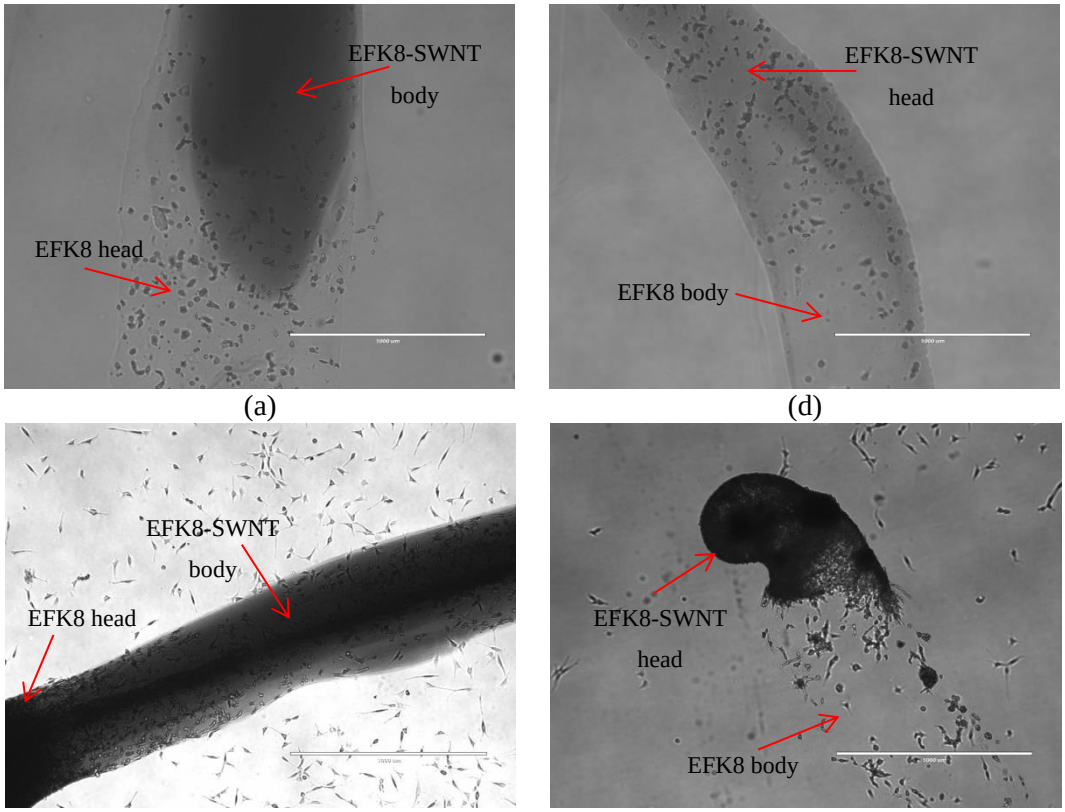

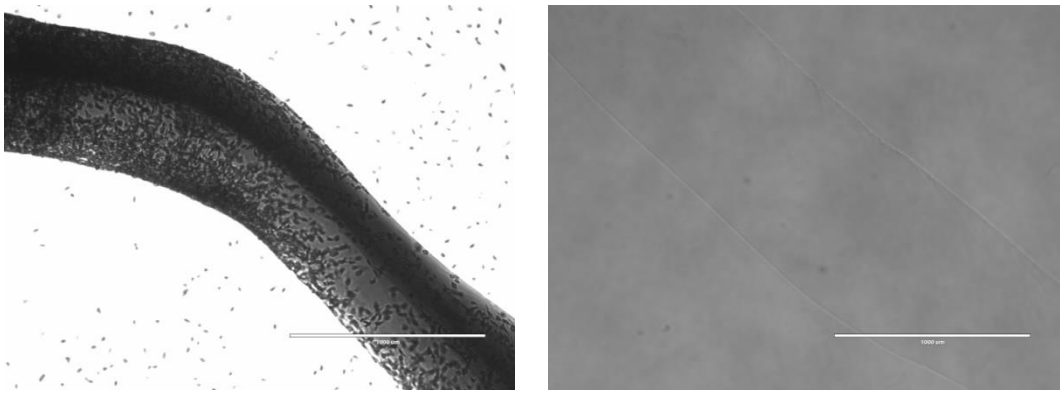

(c) (f)

Figure 5.9 3D cell migration in the mixed hydrogel rods. EFK8-SWNT hydrogel rod with a small cell-containing EFK8 hydrogel head after day (a) 1 and (b) 11, respectively. EFK8 hydrogel rod with a small cell-containing EFK8-SWNT hydrogel head after day (d) 1 and (e) 11, respectively. (c) EFK8-SWNT part of the rod at a larger distance from the head in (b). (f) EFK8 part of the rod at a larger distance from the head in (e).

5.3.6 Compressive modulus of hydrogels

The compressive moduli of EFK8 hydrogels formed at different peptide concentrations as well as the hybrid EFK8-SWNT hydrogel are presented in Fig. 5.10a. As can be seen, an increase in the peptide concentration raises the modulus of the EFK8 hydrogel. Also, a comparison of results obtained for the EFK8 and EFK8-SWNT hydrogels formed from the same peptide concentration of 1.25 mg ml^{-1} shows that the presence of SWNT in the EFK8 hydrogel does not significantly change its modulus. Thus, the previously noted difference in the cell behavior on these two hydrogels is not likely caused by a change in the stiffness, as has been reported in some previous studies [120–125]. This trend supports the conclusion that the difference is due to the ability of SWNT itself to provide appropriate sites for cell anchorage. This result is further confirmed by observing the behavior of NIH-3T3 cells cultured on a stiffer EFK8 hydrogel formed from a peptide concentration of 5 mg ml^{-1}. The image of these cells taken after 5 days and shown in Fig. 5.10b does not show any distinctive difference in the cell morphology on this hydrogel and the less stiff EFK8 hydrogel formed from 1.25 mg ml^{-1} previously presented in Fig. 5.1c. The cells form colonies even on this stiffer hydrogel, whereas the cell morphology is very different when cultured on the hybrid EFK8-SWNT hydrogel.

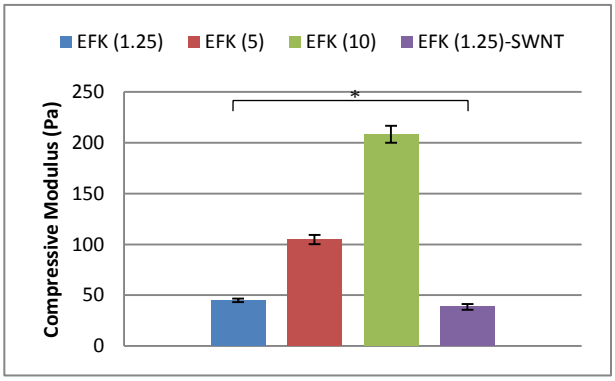

(a)

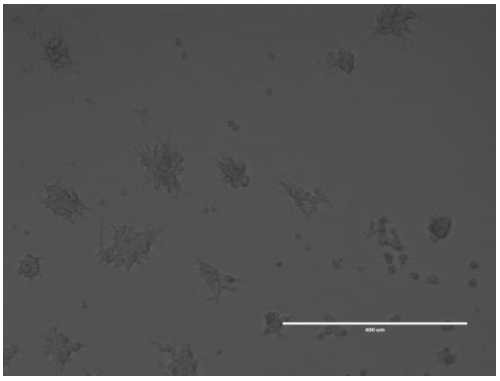

(b)

Figure 5.10 (a) Compressive modulus of various hydrogels. (b) Optical image of NIH-3T3 cells after 5 days of seeding on EFK8 hydrogel formed from peptide at concentration 5 mg ml^{-1}. All data represent mean ± s.d. $*P < 0.05$.

5.3.7 EFK8 and EFK8-SWNT hydrogels as scaffolds for engineering cancer cell spheroids

In the final stage of this study, due to the similarity of the stiffness of EFK8 hydrogels in this study to that of lung tissue [212], A549 lung cancer cells were chosen and seeded on the hydrogels to evaluate the suitability of EFK8 and EFK8-SWNT hydrogels as 3D cell culture platforms to study the formation of spheroidal cancer cells. As can be seen in Fig. 5.11 (top), cancer cells grow over time and form spheroidal colonies on an EFK8 hydrogel. Furthermore, these tumor-like spheroids grow over time on the hydrogel. This shows that an EFK8 hydrogel can be used as a 3D cell culture platform triggering cancer cells to form spheroids which is more similar to the morphology of real tumors than that obtained with 2D cell cultures.

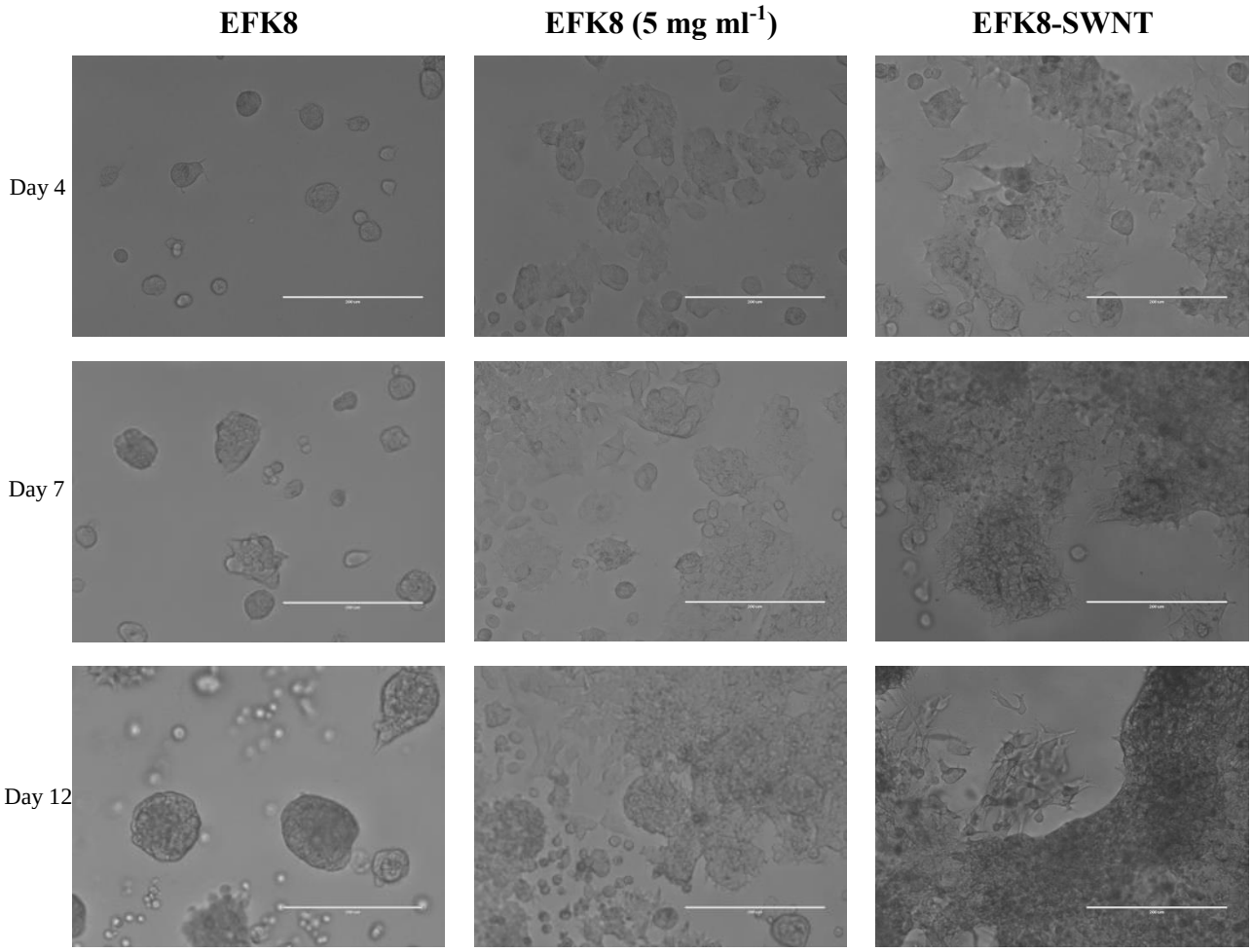

Figure 5.11 Optical images showing the evolution of A549 lung cancer cells seeded on different hydrogels. **Left column**: Formation of spheroidal colonies of cancer cells induced by seeding on an EFK8 hydrogel formed from 1.25 mg ml^{-1} peptide. **Middle column:** Evidence of cancer cell migration after seeding on EFK8 hydrogel formed from 5 mg ml^{-1} peptide. **Right column:** Evidence of cancer cell migration after seeding on EFK8-SWNT hybrid hydrogel formed from 1.25 mg ml^{-1} peptide. Scale bar is 200 μm.

To explore whether the compressive modulus of the hydrogel has any effect on the behavior of the cancer spheroids, A459 cells were seeded on a stiffer EFK8 hydrogel formed from 5 mg ml^{-1}. The optical images shown in Fig. 5.11 (middle row) indicate that seeding on a hydrogel with higher compressive modulus leads to stretched cells with a higher potential for spreading and migration than the cells in spheroids produced on EFK8. Faster spreading could cause tumor progression and metastasis. Interestingly, as shown in the bottom row of Fig. 5.11, the addition

of SWNTs to the EFK8 hydrogel formed from 1.25 mg ml^{-1} peptide leads to similar cell morphology (stretched cells with long protrusions) to that observed on EFK8 alone when formed from 5 mg ml^{-1} peptide. Earlier in this study, we showed that the presence of SWNTs in an EFK8 hydrogel improved normal cell attachment, spreading and migration. Thus, the behavior of A549 cells observed in Fig. 5.11 when seeded on EFK8-SWNT likely reflects the combined effects of the binding regions in the tumor microenvironment and the compressive modulus.

Fig. 5.12 a and b shows cells that have been stained using the Live/Dead® assay conducted on EFK8 hydrogels formed from both 1.25 and 5 mg ml^{-1} peptide. In these images, the difference in geometry of cell spheroids present on the hydrogel formed at 1.25 mg ml^{-1} peptide (Fig. 5.12a) to that of the stretched cells present on the hydrogel formed at the higher peptide concentration (Fig. 5.12 b) is obvious. Immunostaining of β-catenin normally concentrated at the cell-cell junctions using anti-β-catenin and of the cell nucleus using DAPI was also conducted. In the case of the EFK8 hydrogel formed from 5 mg ml^{-1} peptide (Fig. 5.12 d) and the EFK8-SWNT hydrogel (Fig. 5.12 e), some cells at the border of the tumors contain less concentrated green β-catenin on the edges and do not have sharp polygonal boundary that are characteristic of compact cells in colonies. This suggests that these cells are not strongly attached to their neighbor cells which should facilitate cell dissemination and metastasis. On the other hand, cells seeded on the EFK8 hydrogel formed from 1.25 mg ml^{-1} peptide form spheroids that pack together with sharp polygonal boundaries and have a more concentrated green β-catenin color on the edges (Fig. 5.12 c).

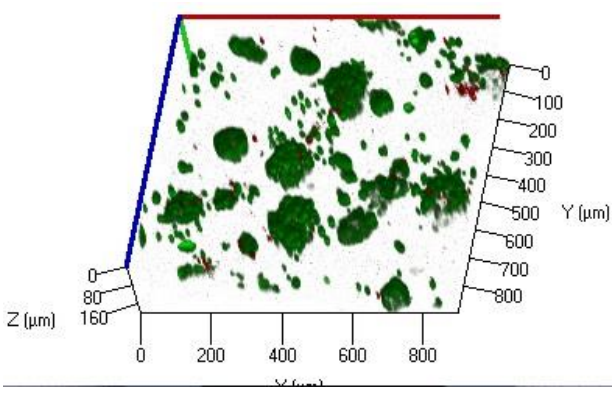

(a)

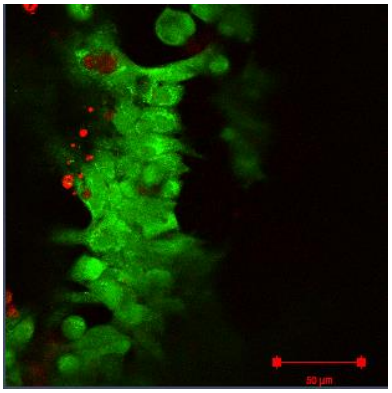

(b)

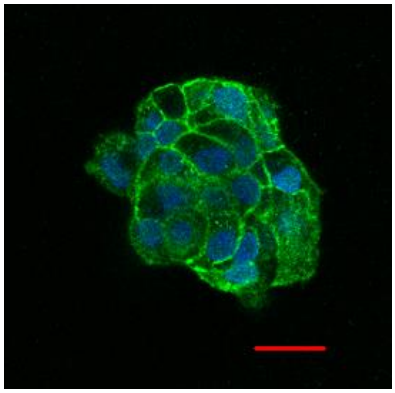

(c)

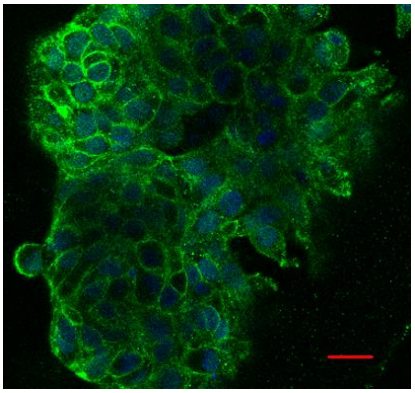

(d)

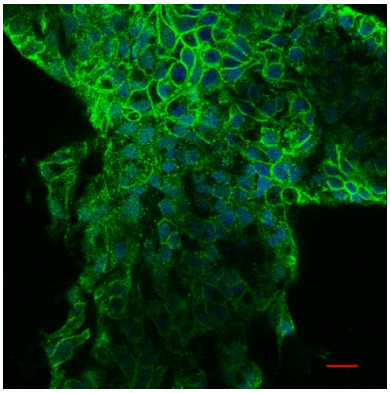

(e)

Figure 5.12 Morphological staining of A549 lung cancer cells using Live/Dead® assay reagent on (a) EFK8 hydrogel and (b) EFK8 (5 mg ml^{-1}) hydrogel (live cells are green and dead ones are red). A549 cells immunostained for β-catenin (green) and nucleus (blue). Immunostaining of the same cells on (c) EFK8, (d) EFK8 (5 mg ml^{-1}) and (e) EFK8-SWNT hydrogels. Scale bar corresponds to 20 µm length.

5.4 Conclusions

It was shown that the presence of SWNTs in the EFK8 hydrogel significantly increases NIH-3T3 cell attachment and leads to a spindle-like morphology, an indication of healthy cells. Also, cells grow faster on the SWNT-containing hydrogel. Also, it was observed that cells spread evenly and migrate more on the hybrid hydrogel rather than on an EFK8 hydrogel, both in 2D and 3D cultures. Furthermore, EFK8-SWNT is able to encapsulate the cells for use in delivery applications, while the presence of SWNTs in the hydrogel did not hinder the cell behavior observed in 2D cultures. Finally, EFK8-SWNT regions on the EFK8 hydrogel appear to attract cells from EFK8 areas.

An increase of the peptide concentration was found to raise the compressive modulus of the resulting hydrogels. However, the presence of the SWNT in the EFK8 hydrogel did not have an effect on its compressive modulus. Also, culturing the cells on a stiffer hydrogel made no significant difference to the apparent behavior of NIH-3T3 cells. Thus, we conclude that the improvement in the cell attachment, growth, spreading and migration on the hybrid hydrogel is not related to the change in modulus and instead is probably related to the enhanced cell-scaffold attachment. EFK8 hydrogels can also be used as 3D cell culture scaffolds for cancer cells. They were found to promote formation of A549 cancer cell spheroids which grow over time and so be useful for 3D drug screening. An increase in the compressive modulus of the hydrogel leads to cells which have a more stretched morphology and are able to migrate more easily over the surface. On the other hand, the addition of SWNTs to the EFK8 hydrogel (while keeping its modulus unchanged) results in cells with mobility similar to that observed on stiffer hydrogels, signifying the importance of cell-scaffold interactions to metastasis.

Chapter 6
Immobilization, Direct Electrochemistry and Electrocatalysis of Hemoglobin on Peptide-Carbon Nanotube-Modified

Abstract

The direct electrochemistry of hemoglobin (Hb) immobilized on a glassy carbon electrode (GCE) by mixing with a hybrid dispersion of EFK8 self-assembling peptide and single-walled carbon nanotubes (SWNTs) was investigated and shown to have effective properties as a biosensor for hydrogen peroxide (H_2O_2). Preliminary experiments involving cyclic voltammetry (CV) and electrochemical impedance spectroscopy (EIS) showed that the presence of SWNTs in the modifying peptide layer on GCE significantly enhanced the electrochemical response of the electrode for the ferricyanide/ferrocyanide redox couple. Also, when more layers of the peptide-SWNT dispersion were applied to the surface, the electrochemical response of the GCE was further increased. This behavior was then exploited to fabricate a biosensor for H_2O_2 by mixing hemoglobin with the hybrid peptide-SWNT dispersion and casting this mixture on a glassy carbon electrode. Subsequent CV and EIS analysis revealed successful immobilization of Hb on the electrode and the ability of the electrode to enable direct electron transfer from the Hb to the electrode surface. In particular, CVs obtained in 0.1M PBS (pH 7.0) showed that the immobilized Hb retained its bio-catalytic activity for Fe ions, indicating that it had not denatured and the hybrid layer remained biocompatible with Hb. Furthermore, this electrode was found to accurately measure the H_2O_2 concentration over the range from 20 to 9.6×10^2 μM in 0.1M PBS (pH 7.0) under mediatorless conditions using both CV and amperometry techniques. In this way, the EFK8-SWNT hybrid layer shows promise as a biocompatible layer for simple non-covalent enzyme immobilization and the basis of a mediatorless biosensor.

6.1 Introduction

Since the 1970s, direct electron transfer between redox proteins and electrode surfaces and its application for mediatorless electrochemical biosensors have been extensively studied. The most efficient method to make a redox protein-based electrochemical biosensor is to establish direct electron transfer between the protein and electrode. The use of a mediator facilitates not only the electron transfer between the electrode and enzyme but also various interfering reactions. Mediatorless biosensors can offer better selectivity since they are able to operate in a potential range closer to the redox potential of the protein itself and thus make interfering reactions less likely to occur [155156]. In addition, most *in-vivo* devices are mediatorless to prevent the potential leaching and toxicity of the mediator. Mediated systems also tend to be less stable during extended continuous operation [157]. Normally direct adsorption of proteins on the electrode surface leads to their denaturation and loss of their catalytic and electrochemical activity [158]. Thus, an important first step in designing a mediatorless biosensor is to immobilize the protein without denaturation.

Hemoglobin (Hb) is an important protein in red blood cells as a reversible oxygen carrier in the body through its four polypeptide chains which contain electroactive heme groups. It has been reported that Hb also can catalyze the reduction of hydrogen peroxide [159]. The ability to rapidly and accurately determine hydrogen peroxide concentration is very important since it is the product of many enzymatic reactions and is also commonly found in food, clinical, pharmaceutical, industrial and environmental systems [159–161156]. A number of techniques such as HPLC [161], titrimetry [162], spectrometry [163], chemiluminescence [164] and electrochemical methods [165] are currently available for hydrogen peroxide determination.

Electrochemical methods for hydrogen peroxide analysis have attracted extensive interest because they are fast, less prone to interferences and relatively inexpensive [161]. Basically, two types of amperometric enzyme-based H_2O_2 probes can be used − mediated biosensors and mediatorless biosensors. Although the mediated H_2O_2 biosensors can detect very low concentrations by use of electron transfer mediators such as ferrocene derivatives [166], hexacyanoferrates [167], tetrathiafulvalene [168] or phenazine methosulphate [169], the danger exists that mediator molecules can contaminate the sample or electrode system or can diffuse out of the

enzyme layer [170]. Mediatorless biosensors which operate through the direct electron transfer between redox proteins and electrode, have gained increasing attention because they do not suffer from this leakage problem and have potentially simpler design without the need for a chemical mediator.

In addition to its ability to electrocatalyze H_2O_2 reduction, Hb is an ideal model protein for the study of the direct electron transfer of heme molecules due to its commercial availability, reasonable cost and well-known structure. However, the direct electrochemical reaction of Hb on an electrode is very difficult for a number of reasons. Since the heme group resides inside the Hb structure and is surrounded by the protein polypeptide chains, the electrons being transferred must travel a large distance to the electrode surface and a mediator is often required to help transport them. Once adsorbed, Hb on the surface frequently denatures and loses its electrochemical activity and bioactivity. Hb becomes a barrier to electron transfer on the electrode surface once it becomes denatured [171]. Finally, Hb located at the electrode surface may not have a favorable orientation for electron transfer. To date, different methods and nanomaterials including Au, Pt and CdTe nanoparticles as well as graphene, CNTs and TiO_2 nanorods have been employed to overcome the above obstacles and facilitate direct electron transfer from Hb to the electrode [159,161,172–183]. These methods mainly operate by providing a strong electronically conducting environment for Hb molecules on the surface. Although promising results have been observed using these nanomaterials, the biosensor efficiency of Hb–based H_2O_2 biosensors is still lower than other ones using different types of heme proteins such as HRP and CAT [156].

Recently, the potential of using ionic-complementary peptides in biocompatible electrodes to immobilize glucose oxidase covalently and fabricate glucose biosensors was demonstrated [4849213]. These peptides can self-assemble on surfaces as β-sheet layers that have considerable biological and physiological stability [5450] and good *in vitro* and *in vivo* biocompatibility [55186]. This is crucial for *in vivo* biosensors. However, at the same time, these results showed that the peptides on the surface act as barriers to electron transfer from the enzyme to the electrode and thereby hinder the electrode response and biosensor sensitivity. Previously, we have shown the ability of the same self-assembling peptides to disperse multi-walled and single-walled carbon nanotubes in

water [191,209]. The surfaces modified with the peptide-CNT dispersions also have enough biocompatibility for cell attachment and growth [191]. Consequently, we propose that the combination of the peptides and carbon nanotubes in the form of a hybrid dispersion on the surface should provide a biocompatible electrode for protein immobilization and *in vivo* biosensing with an enhanced electrochemical response. This combination can provide a basis for designing a mediatorless biosensor.

In the current study, we report a novel simple method to modify and increase the electrochemical response of glassy carbon electrode using a self-assembling peptide-SWNT coating. Then we show that this coating can adsorb Hb physically, remain biocompatible enough for Hb to retain its redox activity and thereby enable direct electron transfer from the Hb to the electrode and improve its catalytic activity toward H_2O_2 reduction.

6.2 Materials and Methods

6.2.1 Materials

The ionic complementary peptide EFK8 with a sequence of FEFEFKFK where F corresponds to phenylalanine, E to glutamic acid and K to lysine was used in this study. This peptide was synthesized in our laboratory using an Aapptec Apex 396 peptide synthesizer (Aapptec LLC, USA). At neutral pH, F is a neutral hydrophobic residue, while E and K are negatively and positively charged, respectively. The peptide was protected by acetyl and amino groups at the N terminus and C-terminus, respectively, to prevent end-to-end electrostatic interactions between peptides. EFK8 was dissolved in pure water (18.2 MΩ; Millipore Milli-Q system) at a concentration of 0.5 mg/ml to prepare the peptide stock solution and then stored at 4°C before use. The metallic SWNTs (carbon > 90%, carbon as SWNT > 77%) were purchased from Sigma-Aldrich Co (catalog# 727777, lot# MKBH7136V). Hemoglobin (from bovine blood), potassium ferrocyanide ($K_3Fe(CN)_6$) and H_2O_2 (30%) were obtained from Sigma-Aldrich. Phosphate buffer saline (PBS) solution was made using Na_2HPO_4 and NaH_2PO_4 both at analytical grade (EMD).

6.2.2 Methods

6.2.2.1 Peptide synthesis

All amino acids (Fmoc protected), activator 2-(6-chloro-1H-benzotriazole-1-yl)-1,1,3,3-tetramethylaminium hexafluorophosphate (HCTU) and Rink Amide-AM resin were obtained from Aapptec LLC (USA). All other solutions were purchased from Acros Organics (USA). The EFK8 peptide with a molecular weight of 1162.60 g/mol was synthesized in our laboratory using the solid-phase peptide synthesis (SPPS) method using an Aapptec Apex 396 peptide synthesizer before being purified by repeated precipitation in cold ether. Then it was freeze-dried and the final powder stored in a refrigerator. Matrix-assisted laser desorption ionization time-of-flight mass spectroscopy (Q-TOF Ultima Global, Waters, Milford, MA, USA) was used to measure the molar mass of the synthesized peptide.

6.2.2.2 SWNT dispersion preparation

The stock suspensions were prepared by combining EFK8 and as-received SWNT (carbon > 90%, carbon as SWNT > 77%) together at a 1:1 mass ratio in pure water (18.2 MΩ; Millipore Milli-Q system) to yield concentrations of 2 mg/ml of both the peptide and SWNTs. The concentration of 2 mg/ml SWNT is based on the mass of as-received material and so may include components that are not actual SWNT. The suspensions were then mixed for 1 hour using a Qsonica XL-2000 probe sonicator at a power of 10W and centrifuged at a speed of 2,000×g for 1h to produce a supernatant that was decanted for later use in electrode modification.

6.2.2.3 Electrochemical analysis

Electrochemical measurements were done using a VMP3 potentiostat/ galvanostat (Bio-Logic instruments) using a three-electrode electrochemical cell at room temperature. Glassy carbon electrode (GCE, diameter: 5mm) was used as the working electrode, platinum wire as the counter and saturated calomel electrode (SCE) as the reference electrode. Electrolytes were deoxygenated with pure nitrogen before each experiment. Cyclic voltammetry was done at a scan rate of 100 mV s^{-1} over the potential range from 0.6 V to −0.2 V in 10 mM $K_3Fe(CN)_6$ dissolved in 1M KCl electrolyte, from 0.2 V to −0.8 V in 0.1 M PBS and from 0 V to −0.8 V in 0.1M PBS (pH 7.0).

Electrochemical impedance spectroscopy (EIS) was performed potentiostatically with 10 mV amplitude sinusoidal waves superimposed on a constant potential of 0.29 V over a frequency range of 1 mHz − 100 kHz in 10 mM $K_3Fe(CN)_6$ dissolved in 1M KCl electrolyte. Amperometric experiments were done in 0.1M PBS (pH 7.0) containing different concentrations of hydrogen peroxide.

6.2.2.4 Scanning electron microscopy

The coating was removed from the GCE surface and examined with SEM. The SEM images were obtained using an FE-SEM (LEO 1530).

6.2.2.5 Electrode modification

Before modification, the electrode was polished successively with 1.0, 0.3 and 0.05 μm alumina slurry on a woolen cloth to obtain a mirror-like surface followed by bath sonication in ethanol and water. Then the electrode was washed with acetone and air-dried. Electrode modification was done by casting 35 μl of the peptide or hybrid dispersion on the GCE surface and then left to air-dry. For hemoglobin immobilization, Hb was dissolved in water and then mixed with an EFK8-SWNT dispersion at a 1:1 (v/v) ratio. Then the mixture was casted on the GCE surface as mentioned above and left overnight to dry at 4°C.

6.3 Results and Discussion

6.3.1 Electrode modification using EFK8 and EFK8-SWNT hybrid dispersion

As the first step, we investigate the effects of the following two modifications of the GCE – first with a coating formed from an EFK8 peptide solution and the second with an EFK8-SWNT dispersion coating. Cyclic voltammetry was conducted on these modified electrodes in a 1M KCl solution containing 10 mM $K_3Fe(CN)_6$. The resulting current associated with the $[Fe(CN)_6]^{3-}/[Fe(CN)_6]^{4-}$ couple is used as a measure of the electrochemical response of the electrodes. A comparison of the scans obtained on the bare GCE and EFK8-modified GCE shows that the presence of the peptide alone on the surface diminishes the cathodic and anodic peak currents associated with the $Fe(CN)_6^{3-}/Fe(CN)_6^{4-}$ couple (Figure 6.1). This is presumably due to the peptide layer blocking the electron transfer pathway from the solution to the electrode. On the

other hand, when the GCE is coated with EFK8-SWNT, the electrochemical response is improved and the current associated with the $[Fe(CN)_6]^{3-}/[Fe(CN)_6]^{4-}$ couple increases significantly. This increase can be attributed to the presence of highly conductive SWNTs on the surface that facilitate electron transfer to the electrode. The separation between the anodic and cathodic peaks ($E_{Pa} - E_{Pc}$) obtained on the EFK8-SWNT-modified GCE is measured to be 59.2/n mV (where n = 1 in this case), which is reflective of a reversible reaction.

To further characterize the electrochemical response of the electrodes, electrochemical impedance spectroscopy was conducted. In Nyquist plots, the diameter of the semicircle obtained at higher frequencies corresponds to the polarization resistance, which is a reflection of the electron transfer kinetics of the redox reaction at the electrode surface. A comparison of the responses in Figure 6.2 shows that the impedance of the EFK8 film is always larger than that of the EFK8-SWNT coating at the same frequency, consistent with expectations if EFK8 alone is a greater barrier for electron transfer at the electrode surface. Again, this observation is another indicator of the positive role of SWNTs in tunneling electrons to the surface.

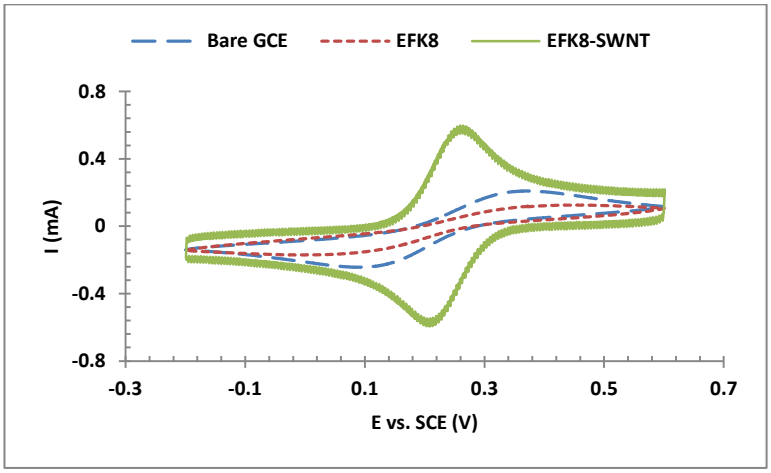

Figure 6.1 CVs obtained on bare GCE, GCE modified with EFK8 and GCE modified with EFK8-SWNT in 1M KCl containing 10 mM $K_3Fe(CN)_6$ at a scan rate of 100 mV/s.

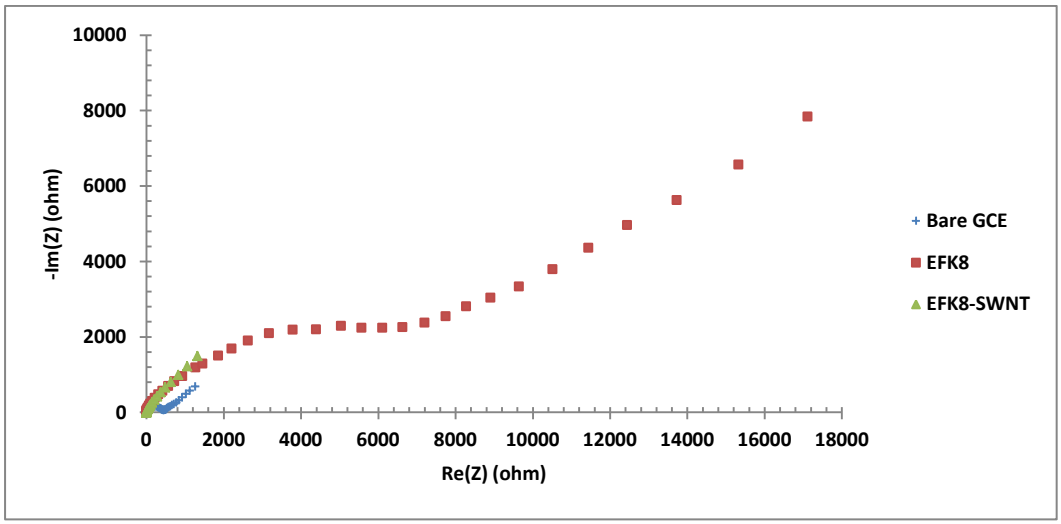

(a)

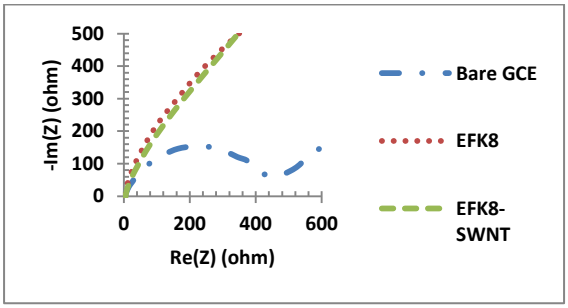

(b)

Figure 6.2 (a) Nyquist plots obtained on bare GCE, EFK8-modified GCE and EFK8-SWNT-modified GCE over a frequency range of 1 mHz − 100 kHz in 10 mM $K_3Fe(CN)_6$ dissolved in 1M KCl electrolyte. (b) Nyquist plot at higher frequencies.

Cyclic voltammetry of the EFK8-SWNT-modified GCE has also been conducted over a range of scan rates between 25 and 200 rpm. Analysis of these CVs reveals that the peak currents for the $[Fe(CN)_6]^{3-}/[Fe(CN)_6]^{4-}$ couple rise linearly as the scan rate increases, while the peak separation remains constant and the cathodic and anodic peak potentials change by less than 1% (Figure 6.3a). Also, the peak currents and potentials do not change over 50 consecutive scan cycles, indicating that the hybrid coatings remain stable (Figure 6.3b).

In order to investigate the effect of the thickness of EFK8-SWNT coating, additional layers (each of which is introduced as a 35 μl dispersion) were applied to the GCE surface after drying the previous coating. Although the addition of more layers might be expected to impede electron transfer, the opposite is actually observed. As can be seen in Figure 6.3c, the presence of more layers increases the peak current probably due to an increase in surface area and increased SWNT population on the surface. The SEM image in Figure 6.4a presents a top view of the EFK8-SWNT coating showing that it consists of fibers laid over each other. When this coating was removed from the GCE electrode, a crack in the coating developed. This turned out to be fortuitous since it reveals some of the EFK8-SWNT structure that would not otherwise be evident. As shown in Figure 6.4b and at higher magnification in Figure 6.4c, the EFK8-SWNT coating has a fibrous structure, consistent with that observed in Fig. 6.4a. The SWNTs cannot be distinguished from the peptide fibers due to similarities in their size and composition and the fact that the SWNTs are normally wrapped with peptides in the dispersion. Nevertheless, such a fibrous structure should significantly increase the surface area of the hybrid layer for electrochemical reactions and could be the explanation for the improved electrochemical response for the $[Fe(CN)_6]^{3-}/[Fe(CN)_6]^{4-}$ couple observed previously in this study.

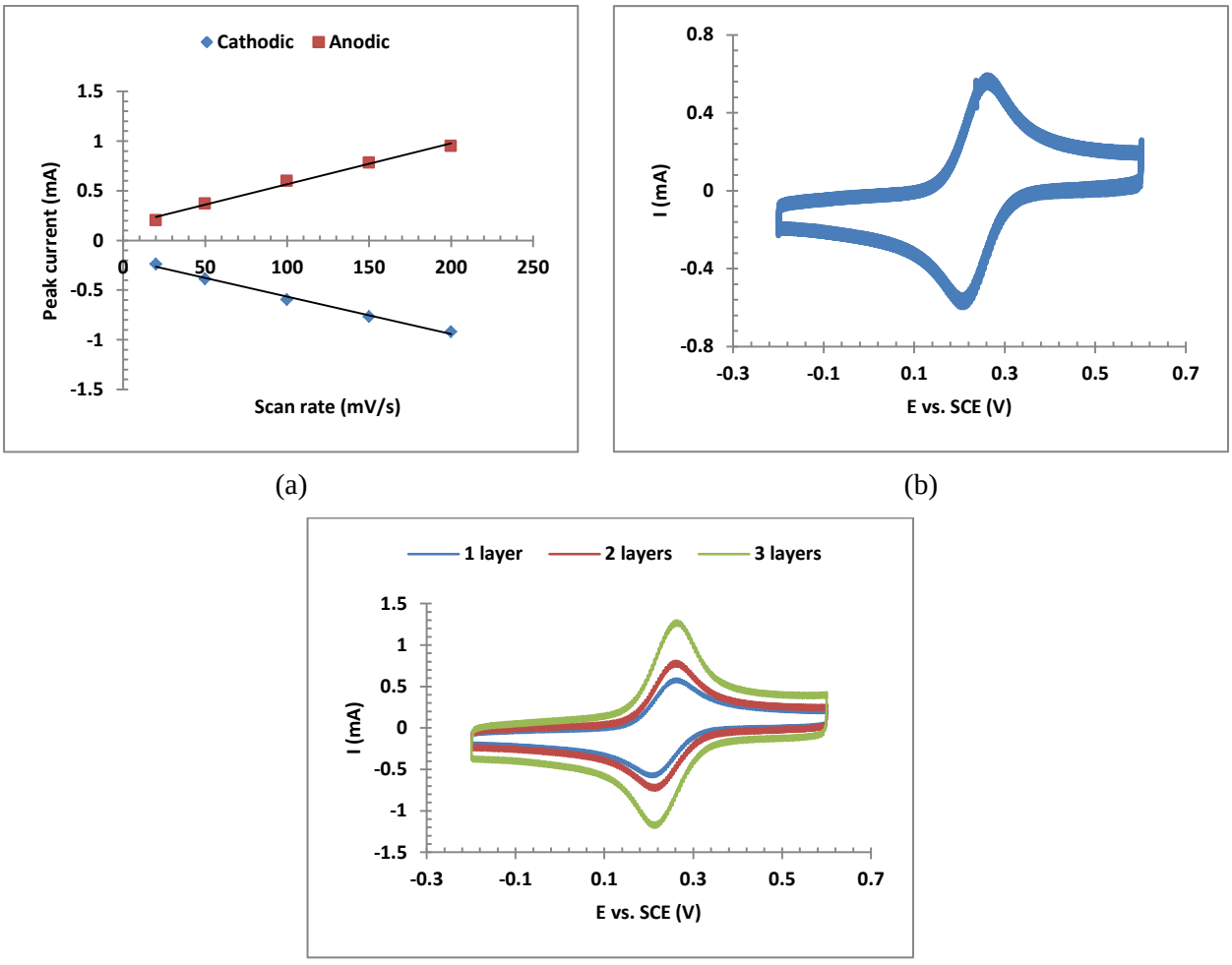

Figure 6.3 (a) Effect of scan rate on the cathodic and anodic peak currents of $Fe(CN)_6^{3-}/Fe(CN)_6^{4-}$ couple on an EFK8-SWNT modified electrode. (b) Traces of the CV responses over 50 cycles. (c) Effect of the number of EFK8-SWNT hybrid layers on the CVs obtained at a scan rate of 100 mV/s in 1M KCl containing 10 mM $K_3Fe(CN)_6$.

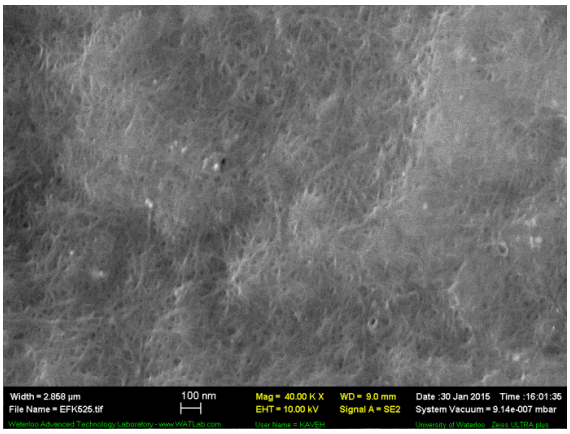

(a)

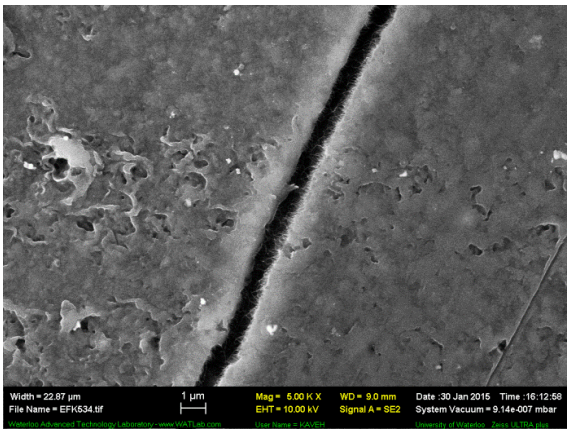

(b)

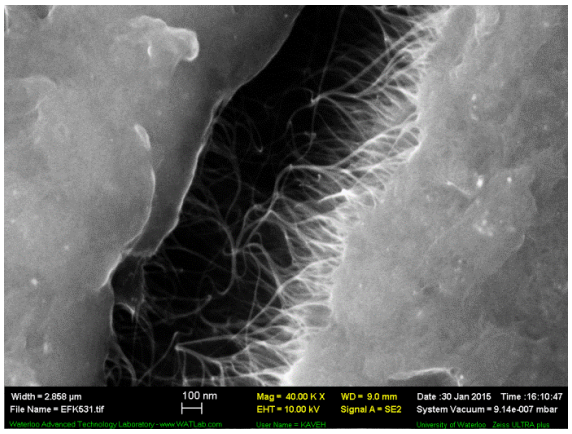

(c)

Figure 6.4 (a) Top view of EFK8-SWNT coating. (b) Top view of coating after removal from the GCE surface, showing the crack that had developed. (c) Higher magnification of (b) showing the fibrous structure of the coating**.**

6.3.2 Immobilization of hemoglobin

Given these promising results in using the EFK8-SWNT-modified GCE electrode, a solution containing 5 mg ml^{-1} Hb was mixed with EFK8-SWNT dispersion and applied to the GCE. To obtain evidence that Hb had been immobilized on the surface, a CV obtained using the modified EFK8-SWNT-Hb-GCE electrode was compared to those obtained using electrodes that had not been contacted with Hb (i.e., EFK8-SWNT-modified GCE and bare GCE electrodes). In each

case, the electrode was immersed in a 1M KCl solution containing 10mM $K_3Fe(CN)_6$. As shown in Figure 6.5a, the inclusion of Hb in the hybrid layer leads to a drop in the peak currents for the $Fe(CN)_6^{3-}/Fe(CN)_6^{4-}$ couple. Such an effect would be expected if Hb were successfully immobilized on the surface since this should lead to some inhibition of electron transfer. It is interesting to note that the current due to the $Fe(CN)_6^{3-}/Fe(CN)_6^{4-}$ couple rises more steeply and the peak separation is narrower on the EFK8-SWNT-Hb-GCE than on the bare GCE. This trend indicates faster electrode kinetics on the modified electrode than on the unmodified GCE although it remains considerably slower than on the EFK8-SWNT-GCE. EIS experiments were also conducted to check the consistency with the trends observed in the CVs. The data shown in Figure 6.5b reveal that the mixing of Hb with an EFK8-SWNT dispersion in preparing the coating for the GCE has a significant effect on the resulting Nyquist plots. The diameter of the high frequency semi-circle corresponding to the polarization resistance is larger than that obtained on the EFK8-SWNT- modified GCE. At the same time, it is still lower than that of the bare GCE which reflects the effect of SWNTs in facilitating electron transfer. The trends are perfectly in accord with those observed in the CVs in Figure 6.5a.

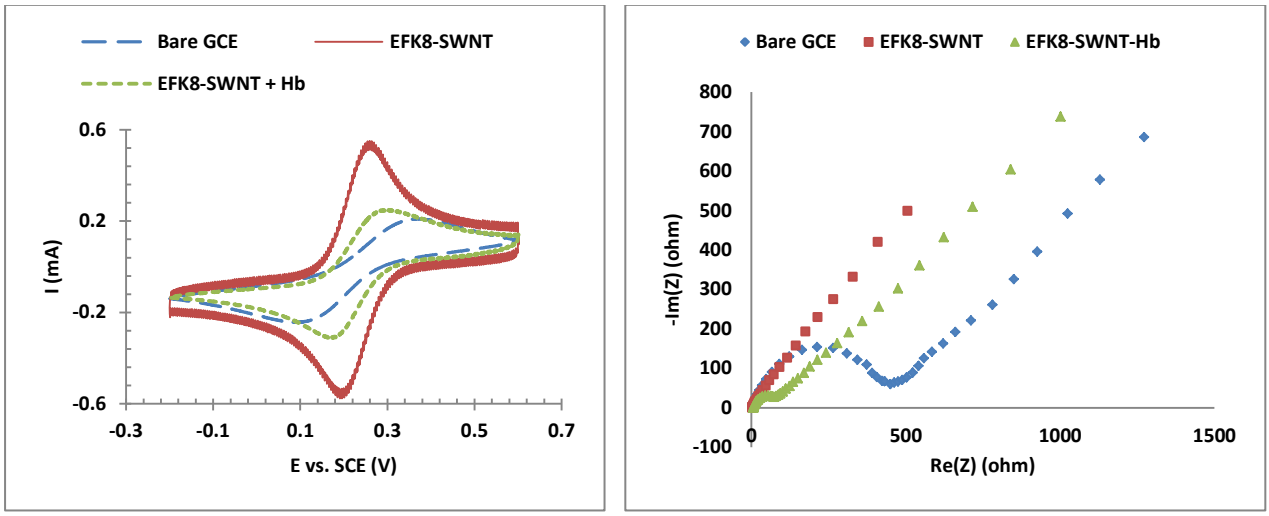

(a) (b)

Figure 6.5 (a) CV and (b) Nyquist plots obtained on bare GCE, EFK8-SWNT and EFK8-SWNT-Hb-modified GCE immersed in 1M KCl containing 10mM $K_3Fe(CN)_6$.

6.3.3 Direct electrochemistry of hemoglobin on the electrode

To explore the electrochemical behavior of immobilized Hb on the surface, CVs were obtained on the modified GCEs in 0.1M PBS. Figure 6.6a shows that the presence of Hb on the modified GCE surface leads to higher cathodic current during the cathodic scan in which Fe^{3+} is reduced to Fe^{2+}. This again supports the conclusion that Hb has not only been successfully immobilized on the surface but has also maintained electrochemical functionality, suggesting that it has not denatured and has retained its structure. In addition, it shows that the EFK8-SWNT modification layer provides a platform to utilize Hb in the direct electron transfer and mediatorless electron transfer on an electrode surface. As shown in Figure 6.6b, the current obtained on an EFK8-SWNT-Hb modified GCE is found to rise as the scan rate is increased from 20 to 200 mV/s.

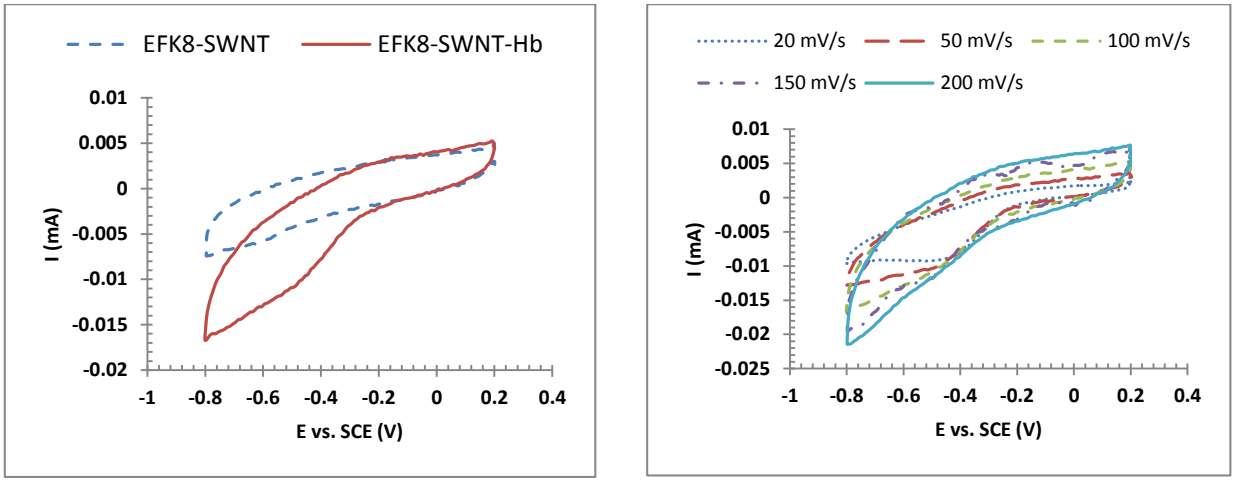

(a) (b)

Figure 6.6 (a) CVs obtained on mediatorless EFK8-SWNT and EFK8-SWNT-Hb modified GCE in 0.1M PBS. (b) Effect of scan rate on CVs obtained on mediatorless EFK8-SWNT-Hb modified GCE in 0.1M PBS.

6.3.4 Biocatalytic activity of Hb within EFK8-SWNT

The bioelectrocatalytic activity of Hb for hydrogen peroxide reduction was investigated using CV and chronoamperometry. Only 1 EFK8-SWNT hybrid layer was applied to the GCE in this series of experiments. Figure 6.7 shows that the addition of 2.4×10^{-4} M H_2O_2 to PBS leads to a change in the voltammogram and the appearance of cathodic and anodic peaks. This shows that a GCE modified with EFK8-SWNT-Hb is sensitive to H_2O_2 and the immobilized Hb can catalyze

reduction and oxidation of H_2O_2 without using any mediator. Furthermore, the current at a potential of −0.4 V (SCE) where H_2O_2 reduction occurs [183] increases as the H_2O_2 concentration rises. This sensitivity of the current to the H_2O_2 concentration makes EFK8-SWNT a promising platform to immobilize Hb and serve as a mediatorless biosensor to measure H_2O_2 concentrations.

To investigate this question more closely and quantitatively, a series of chronoamperometry experiments were conducted on an EFK8-SWNT-Hb-modified GCE to obtain a calibration curve of the current measured at −1.0V as a function of H_2O_2 concentration. Again, the GCEs were coated with only 1 EFK8-SWNT hybrid layer. In all cases, the current was found to reach steady state within 10 s. The calibration curve over the relatively wide range from 0 to 0.002 M H_2O_2 is presented in Figure 6.8a. The relationship between current and concentration is linear up to a concentration of 0.001 M before deviating above this level. Fig. 6.8b shows the calibration curve over the linear portion from 0 to 0.001 M. The high r^2 value for this correlation and the relatively high sensitivity of 1.06 mA mM^{-1} cm^{-2} compared with that reported in previous work [156] shows that the EFK8-SWNT-Hb-modified GCE shows promise as a biosensor. The calibration curve at very low concentrations between 0 and 0.0001 M is shown in the right inset (Figure 6.8c). Although the sensitivity of 0.639 mA mM^{-1} cm^{-2} is not as good as in Figure 6.8b, the calibration curve is still linear. Given that the cytotoxic level of H_2O_2 in the body is more than 50 μM [214], the results here demonstrate the effectiveness of this electrode as a H_2O_2 biosensor for clinical applications.

Finally, the stability of the modified electrode was evaluated by measuring the current at a potential of −1.0V while being immersed in PBS (pH 7.0) at 4°C over a 14-day period. Although not shown here, the electrode retained 90.2% of its initial response to H_2O_2 during these amperometric measurements.

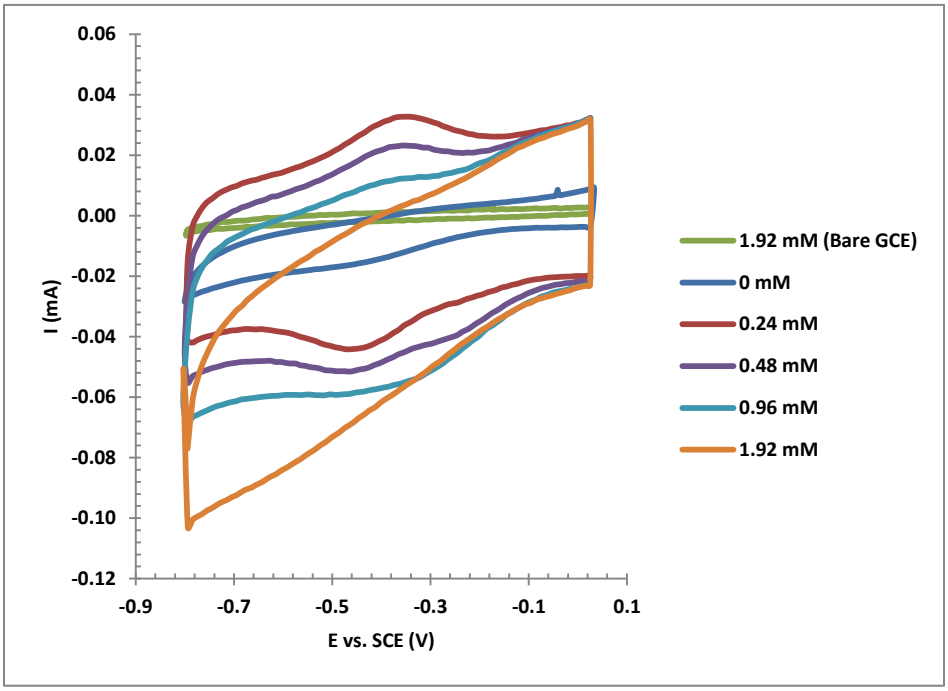

Figure 6.7 CVs of EFK8-SWNT-Hb-modified GCE in 0.1M PBS (pH:7.0) obtained at different H_2O_2 concentrations.

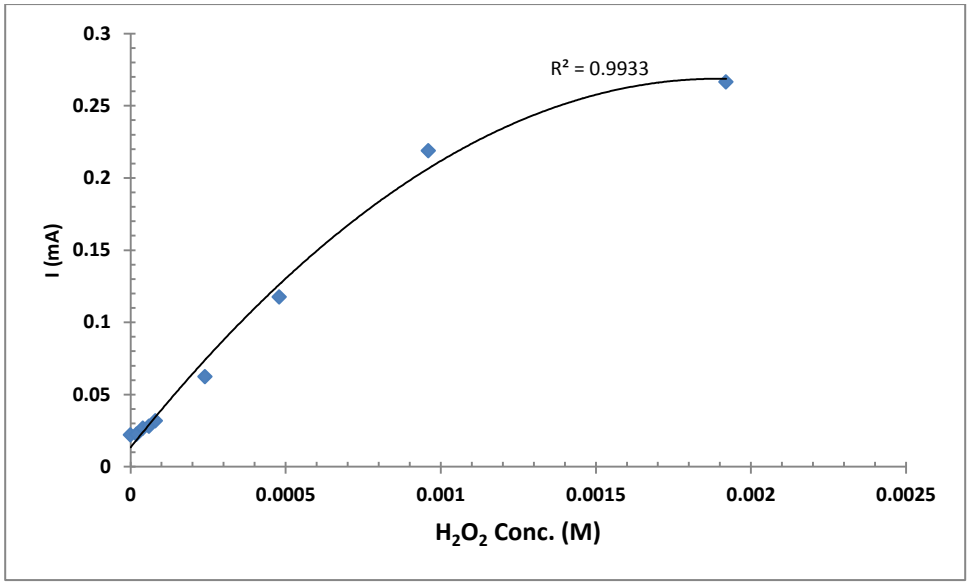

(a)

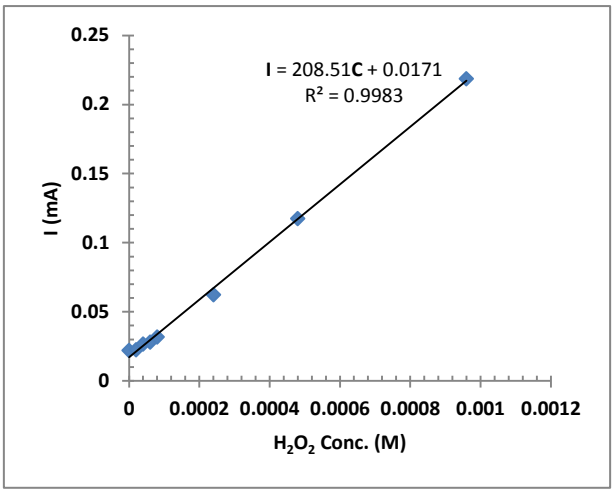

(b)

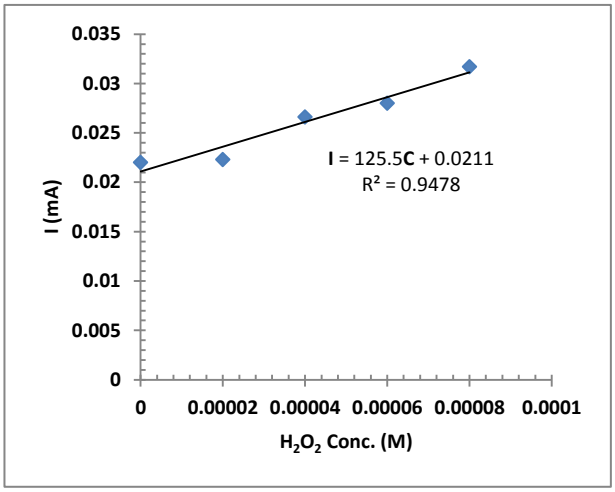

(c)

Figure 6.8 (a) Amperometric calibration curve of EFK8-SWNT-Hb-modified GCE at different H_2O_2 concentrations acquired at −1.0V after 10s. (b) Linear part of the graph. (c) Lower concentrations of the linear part.

6.4 Conclusions

This study showed for the first time the use of dispersions of peptide and single-walled carbon nanotubes to modify GCEs to enhance their electrochemical response. It was shown that a peptide-only layer hinders the electrode response for the $[Fe(CN)_6]^{3-}/[Fe(CN)_6]^{4-}$ redox couple, whereas the inclusion of SWNTs in the same coating increases the electrode response significantly. This is attributed to the effect of the SWNTs in conducting electrons at the surface. We showed that hemoglobin could be easily immobilized on the electrode surface by mixing with the EFK8-SWNT dispersion and applying to the electrode. The immobilized Hb did not denature and was found to participate in direct electron transfer from heme group to the electrode in a PBS solution without the need for a mediator. This was again possible due to the role of SWNTs in tunneling electrons to the electrode surface. Furthermore, the modified electrode was shown to be sensitive to hydrogen peroxide dissolved in PBS and a promising mediatorless biosensor to measure its concentration. Based on these results, this modification provides a suitable platform for electrochemical mediatorless biosensors with redox proteins.

Chapter 7
Conclusions and Recommendations

7.1 Original contributions to research

Due to problems such as reduced performance and biocompatibility of CNTs after dispersing via covalent modification or the addition of most surfactants, the use of biocompatible nanomaterials for this purpose is of great interest. Therefore, the possibility of dispersing CNTs using a particular sequence of self-assembling peptide has been investigated in this study. This thesis focuses on hybrid dispersions of ionic-complementary self-assembling peptides and carbon nanotubes, investigates the interaction between these peptides and CNTs, uses these hybrid dispersions to form a composite hydrogel and exploits their properties for tissue engineering and biosensor applications. In the following, the most important outcomes of this research are summarized:

Dispersion of MWNTs using EFK16-II peptide

EFK16-II appears to self-assemble on the sidewalls of MWNTs and disperse them in water through a non-covalent functionalizing mechanism involving hydrophobic and π-π interactions. The stability of suspensions containing EFK16-II-modified MWNTs in water depends very strongly on pH. They remain stable for long periods of time at pH below about 5 and above about 8 where the modified particles are highly charged. On the other hand, at pHs close to the isoelectric point of EFK16-II (pH ~6.7), MWNTs agglomerate and their suspensions become unstable. Furthermore, experiments using tissue culture plates modified with EFK16-II-modified MWNTs show that they provide a biocompatible surface for attachment and growth of normal and cancer cells.

Dispersion of SWNTs using EFK8 peptide and formation of hybrid hydrogel

By applying scanning probe microscopy (SPM), this study provides new evidence that the EFK8 peptide can wrap around the nanotubes, thereby rendering them hydrophilic and enabling their

dispersion in aqueous media. For the first time, nano-mechanical measurements as well as electric force microscopy (EFM) technique have been successfully used to distinguish peptide fibers from SWNTs on the surface, something which was not possible using regular AFM imaging. Also, by adding salt to EFK8-SWNT dispersions, we have shown that dispersed SWNTs remain entrapped and incorporated in hybrid EFK8-SWNT hydrogels that form.

Application of hybrid EFK8-SWNT hydrogel for tissue engineering and 3D cancer spheroid formation

It has been shown that the presence of SWNTs in the EFK8 hydrogel promotes NIH-3T3 cell attachment and leads to a spindle-like morphology, an indication of healthy cells. Also, cells grow faster on the SWNT-containing hydrogel. Also, cells are observed to spread evenly and migrate more rapidly on the hybrid hydrogel than on an EFK8 hydrogel in both 2D and 3D cultures. Furthermore, EFK8-SWNT is able to encapsulate the cells for use in delivery applications, while the presence of SWNTs in the hydrogel did not hinder the cell behavior observed in 2D cultures. Microindentation tests reveal that the compressive modulus of the resulting hydrogels is increased by raising the peptide concentration. On the other hand, the presence of the SWNT in the EFK8 hydrogel does not alter its compressive modulus. Also, culturing NIH-3T3 cells on a stiffer hydrogel has no significant apparent effect on their subsequent behavior. This implies that the improvement in the cell attachment, growth, spreading and migration on the hybrid hydrogel are not strongly related to the change in stiffness and instead is probably related to the enhanced cell-scaffold attachment. EFK8 hydrogels have also been used as 3D cell culture scaffolds for cancer cells and found to promote spheroid formation of A549 cancer cell colonies which grow by time. This effect makes these hydrogels useful for 3D drug screening. An increase in the compressive modulus of the hydrogel leads to cells with a more stretched morphology and more able to migrate over the surface. On the other hand, the addition of SWNTs to the EFK8 hydrogel (while keeping its modulus unchanged) results in cells with mobility similar to that observed on stiffer hydrogels, signifying the importance of cell-scaffold interactions for metastasis.

Application of hybrid EFK8-SWNT dispersion for Hb immobilization, direct electrochemistry and H2O2 sensing

This study shows for the first time the use of dispersions of peptide and single-walled carbon nanotubes to modify GCEs to enhance their electrochemical response. It has been shown that a peptide-only layer hinders the electrode response for the $[Fe(CN)_6]^{3-}/[Fe(CN)_6]^{4-}$ redox couple, whereas the inclusion of SWNTs in the same coating increases the electrode response significantly. This is attributed to the effect of the SWNTs in conducting electrons at the surface. We showed that hemoglobin can be easily immobilized on the electrode surface by mixing with the EFK8-SWNT dispersion and applying onto the electrode. The immobilized Hb does not denature and is found to participate in direct electron transfer between its heme group and the electrode in a PBS solution without the need for a mediator. This behavior is again possible due to the role that SWNTs play in tunneling electrons to the electrode surface. Furthermore, the modified electrode is sensitive enough to hydrogen peroxide dissolved in PBS in order for it to be a promising mediatorless biosensor to measure its concentration. Based on these results, this modification provides a suitable platform for electrochemical mediatorless biosensors with redox proteins.

7.2 Recommendations

Based on the thesis outcomes, future research on the following topics is recommended:

1. Application of new SPM techniques (i.e. nano-mechanical measurements and EFM) to more closely investigate peptide-MWNT interactions
2. Dispersion of semiconducting SWNTs using peptides to benefit from the fluorescing properties of this type of SWNT as a tool to gain greater insight into this interaction
3. Introduction of an RGD motif into the EFK8 peptide sequence to further enhance cell attachment
4. Improvement of the EFK8 sequence in order to load more SWNT and better manipulate hydrogel electrical and mechanical properties

5. Investigation of the mechanism of cell attachment to the EFK8-SWNT hydrogel to gain a better understanding of the role that SWNTs play
6. Use of several layers of the EFK8-SWNT dispersion for Hb immobilization and investigation of its effect on the sensitivity of the resulting H_2O_2 biosensor

Bibliography

1. Wagner, V., Dullaart, A., Bock, A. & Zweck, A. The emerging nanomedicine landscape. *Nat. Biotechnol.* **24,** 1211–1217 (2006).

2. Freitas, R. A. What is nanomedicine? *Nanomedicine* **1,** 2–9 (2005).

3. Sapsford, K. E. *et al.* Functionalizing Nanoparticles with Biological Molecules: Developing Chemistries that Facilitate Nanotechnology. *Chem. Rev.* **113,** 1904–2074 (2013).

4. Ijima, S. Helical microtubules of graphitic carbon. *Nature* **354,** 56–58 (1991).

5. De Volder, M. F. L., Tawfick, S. H., Baughman, R. H. & Hart, A. J. Carbon Nanotubes: Present and Future Commercial Applications. *Science (80-.).* **339,** 535–539 (2013).

6. Yu, M. *et al.* Strength and Breaking Mechanism of Multiwalled Carbon Nanotubes Under Tensile Load. *Science (80-.).* **287,** 637–641 (2000).

7. Popov, M., Kyotani, M., Nemanich, R. & Koga, Y. Superhard phase composed of single-wall carbon nanotubes. *Phys. Rev. B* **65,** 033408 (2002).

8. Hong, S. & Myung, S. Nanotube Electronics: A flexible approach to mobility. *Nat. Nanotechnol.* **2,** 207 – 208 (2007).

9. Pop, E., Mann, D., Wang, Q., Goodson, K. & Dai, H. Thermal Conductance of an Individual Single-Wall Carbon Nanotube above Room Temperature. *Nano Lett.* **6,** 96–100 (2006).

10. *Carbon Nanotubes and Related Structures Synthesis, Characterization, Functionalization, and Applications*. 103–198 (WILEY-VCH Verlag GmbH & Co, 2010).

11. Feng, M., Hanb, H., Zhang, J. & Tachikawa, H. in *Electrochem. Sensors, Biosens. their Biomed. Appl.* (Zhang, X., Ju, H. & Wang, J.) 459–501 (Elsevier Inc., 2008).

12. Pantarotto, D. *et al.* Synthesis , Structural Characterization , and Immunological Properties of Carbon Nanotubes Functionalized with Peptides. *J. Am. Chem. Soc* **125,** 6160–6164 (2003).

13. Wang, S. *et al.* Peptides with selective affinity for carbon nanotubes. *Nat. Mater.* **2,** 196–200 (2003).

14. Su, Z., Mui, K., Daub, E., Leung, T. & Honek, J. Single-walled carbon nanotube binding peptides: probing tryptophan's importance by unnatural amino acid substitution. *J. Phys. Chem. B* **111,** 14411–7 (2007).

15. Dieckmann, G. R. *et al.* Controlled assembly of carbon nanotubes by designed amphiphilic Peptide helices. *J. Am. Chem. Soc.* **125,** 1770–7 (2003).

16. Zorbas, V. *et al.* Preparation and characterization of individual peptide-wrapped single-walled carbon nanotubes. *J. Am. Chem. Soc.* **126,** 7222–7 (2004).

17. Arnold, M. S., Guler, M. O., Hersam, M. C. & Stupp, S. I. Encapsulation of carbon nanotubes by self-assembling peptide amphiphiles. *Langmuir* **21,** 4705–9 (2005).

18. Lim, Y., Moon, K.-S. & Lee, M. Recent advances in functional supramolecular nanostructures assembled from bioactive building blocks. *Chem. Soc. Rev.* **38,** 925–34 (2009).

19. Yanlian, Y. *et al.* Designer self-assembling peptide nanomaterials. *Nano Today* **4,** 193–210 (2009).

20. Loo, Y., Zhang, S. & Hauser, C. A. E. From short peptides to nanofibers to macromolecular assemblies in biomedicine. *Biotechnol. Adv.* **30,** 593–603 (2012).

21. Yang, Z. & Zhao, X. A 3D model of ovarian cancer cell lines on peptide nanofiber scaffold to explore the cell-scaffold interaction and chemotherapeutic resistance of anticancer drugs. *Int. J. Nanomedicine* **6,** 303–10 (2011).

22. Fung, S. Y. *et al.* Self-Assembling Peptide as a Potential Carrier for Hydrophobic Anticancer Drug Ellipticine: Complexation, Release and In Vitro Delivery. *Adv. Funct. Mater.* **19,** 74–83 (2009).

23. Wu, E. C., Zhang, S. & Hauser, C. A. E. Self-Assembling Peptides as Cell-Interactive Scaffolds. *Adv. Funct. Mater.* **22,** 456–468 (2012).

24. Lakshmanan, A., Zhang, S. & Hauser, C. A. E. Short self-assembling peptides as building blocks for modern nanodevices. *Trends Biotechnol.* **30,** 155–65 (2012).

25. Wang, J. Carbon-Nanotube Based Electrochemical Biosensors: A Review. *Electroanalysis* **17,** 7–14 (2005).

26. Rivas, G. A. *et al.* Carbon nanotubes for electrochemical biosensing. *Talanta* **74,** 291–307 (2007).

27. Harrison, B. S. & Atala, A. Carbon nanotube applications for tissue engineering. *Biomaterials* **28,** 344–53 (2007).

28. Voge, C. M. & Stegemann, J. P. Carbon nanotubes in neural interfacing applications. *J. Neural Eng.* **8,** 011001 (2011).

29. Li, J., Cassell, A., Delzeit, L., Han, J. & Meyyappan, M. Novel Three-Dimensional Electrodes: Electrochemical Properties of Carbon Nanotube Ensembles. *J. Phys. Chem. B* **106,** 9299–9305 (2002).

30. Britto, P. J., Santhanam, K. S. V., Rubio, A., Alonso, J. a. & Ajayan, P. M. Improved Charge Transfer at Carbon Nanotube Electrodes. *Adv. Mater.* **11,** 154–157 (1999).

31. Kang, Y. & Taton, T. A. Micelle-encapsulated carbon nanotubes: a route to nanotube composites. *J. Am. Chem. Soc.* **125,** 5650–1 (2003).

32. Shi, J. *et al.* Actuator based on MWNT/PVA hydrogels. *J. Phys. Chem. B* **109,** 14789–91 (2005).

33. Ogoshi, T., Takashima, Y., Yamaguchi, H. & Harada, A. Chemically-responsive sol-gel transition of supramolecular single-walled carbon nanotubes (SWNTs) hydrogel made by hybrids of SWNTs and cyclodextrins. *J. Am. Chem. Soc.* **129,** 4878–9 (2007).

34. Tong, X., Zheng, J., Lu, Y., Zhang, Z. & Cheng, H. Swelling and mechanical behaviors of carbon nanotube/poly(vinyl alcohol) hybrid hydrogels. *Mater. Lett.* **61,** 1704–1706 (2007).

35. Thompson, B. C. *et al.* Carbon nanotube biogels. *Carbon N. Y.* **47,** 1282–1291 (2009).

36. Gavalas, V. G., Andrews, R., Bhattacharyya, D. & Bachas, L. G. Carbon Nanotube Sol−Gel Composite Materials. *Nano Lett.* **1,** 719–721 (2001).

37. Yildirim, E. D., Yin, X., Nair, K. & Sun, W. Fabrication, characterization, and biocompatibility of single-walled carbon nanotube-reinforced alginate composite scaffolds manufactured using freeform fabrication technique. *J. Biomed. Mater. Res. B. Appl. Biomater.* **87,** 406–14 (2008).

38. Abarrategi, A. *et al.* Multiwall carbon nanotube scaffolds for tissue engineering purposes. *Biomaterials* **29,** 94–102 (2008).

39. Firkowska, I. Carbon Nanotube Substrates for Tissue Engineering Applications. (2008).

40. Lewitus, D. Y. *et al.* Biohybrid Carbon Nanotube/Agarose Fibers for Neural Tissue Engineering. *Adv. Funct. Mater.* **21,** 2624–2632 (2011).

41. Haniu, H. *et al.* Basic Potential of Carbon Nanotubes in Tissue Engineering Applications. *J. Nanomater.* **2012,** 1–10 (2012).

42. Yang, S. & Zang, R. Perspectives on Carbon Nanotube-Based Scaffolds in Nerve Tissue Engineering. *J. Tissue. Sci. Eng.* **3,** 1–2 (2012).

43. Zhang, M. *et al.* Electrostatic layer-by-layer assembled carbon nanotube multilayer film and its electrocatalytic activity for O2 reduction. *Langmuir* **20,** 8781–5 (2004).

44. Moore, V. C. *et al.* Individually Suspended Single-Walled Carbon Nanotubes in Various Surfactants. *Nano Lett.* **3,** 1379–1382 (2003).

45. Zhang, S. Emerging biological materials through molecular. *Biotechnol. Adv.* **20,** 321–339 (2002).

46. Ellis-Behnke, R. G. *et al.* Nano hemostat solution: immediate hemostasis at the nanoscale. *Nanomedicine* **2,** 207–15 (2006).

47. Fung, S.-Y. *et al.* Amino Acid Pairing for De Novo Design of Self-Assembling Peptides and Their Drug Delivery Potential. *Adv. Funct. Mater.* **21,** 2456–2464 (2011).

48. Yang, H. *et al.* Ionic-Complementary Peptide-Modified Highly Ordered Pyrolytic Graphite Electrode for Biosensor Application. *Biotechnol. Prog.* **24,** 964–971 (2008).

49. Yang, H., Fung, S.-Y., Pritzker, M. & Chen, P. Ionic-complementary peptide matrix for enzyme immobilization and biomolecular sensing. *Langmuir* **25,** 7773–7 (2009).

50. Zhang, S., Holmes, T., Lockshin, C. & Rich, A. Spontaneous assembly of a self-complementary oligopeptide to form a stable macroscopic membrane. *Proc. Natl. Acad. Sci. U. S. A.* **90,** 3334–8 (1993).

51. Zhang, S. *et al.* Self-complementary oligopeptide matrices support mammalian cell attachment. *Biomaterials* **16,** 1385–93 (1995).

52. Mujeeb, A., Miller, A. F., Saiani, A. & Gough, J. E. Self-assembled octapeptide scaffolds for in vitro chondrocyte culture. *Acta Biomater.* **9,** 4609–17 (2013).

53. Fung, S. Y., Keyes, C., Duhamel, J. & Chen, P. Concentration effect on the aggregation of a self-assembling oligopeptide. *Biophys. J.* **85,** 537–48 (2003).

54. Zhang, S., Lockshin, C., Cook, R. & Rich, A. Unusually Stable β-Sheet Formation in an Ionic Self-Complementary Oligopeptide Stability of the Structure in Dilute Solution. *Biopolymers* **34,** 663–672 (1994).

55. Zhang, S. *et al.* Self-complementary oligopeptide matrices support mammalian cell attachment. *Biomaterials* **16,** 1385–93 (1995).

56. Fung, S. Y., Yang, H. & Chen, P. Formation of colloidal suspension of hydrophobic compounds with an amphiphilic self-assembling peptide. *Colloids Surf. B. Biointerfaces* **55,** 200–11 (2007).

57. Gelain, F., Horii, A. & Zhang, S. Designer self-assembling peptide scaffolds for 3-d tissue cell cultures and regenerative medicine. *Macromol. Biosci.* **7,** 544–51 (2007).

58. Horii, A., Wang, X., Gelain, F. & Zhang, S. Biological designer self-assembling peptide nanofiber scaffolds significantly enhance osteoblast proliferation, differentiation and 3-D migration. *PLoS One* **2,** e190 (2007).

59. Kumada, Y. & Zhang, S. Significant type I and type III collagen production from human periodontal ligament fibroblasts in 3D peptide scaffolds without extra growth factors. *PLoS One* **5,** e10305 (2010).

60. Gelain, F., Bottai, D., Vescovi, A. & Zhang, S. Designer self-assembling peptide nanofiber scaffolds for adult mouse neural stem cell 3-dimensional cultures. *PLoS One* **1,** e119 (2006).

61. Kumada, Y., Hammond, N. A. & Zhang, S. Functionalized scaffolds of shorter self-assembling peptides containing MMP-2 cleavable motif promote fibroblast proliferation and significantly accelerate 3-D cell migration independent of scaffold stiffness. *Soft Matter* **6,** 5073 (2010).

62. Galler, K. M., Aulisa, L., Regan, K. R., Souza, R. N. D. & Hartgerink, J. D. Self-Assembling Multidomain Peptide Hydrogels: Designed Susceptibility to Enzymatic Cleavage Allows Enhanced Cell Migration and Spreading. *J. Am. Chem. Soc* **132,** 3217–3223 (2010).

63. Giano, M. C., Pochan, D. J. & Schneider, J. P. Controlled biodegradation of self-assembling β-hairpin peptide hydrogels by proteolysis with matrix metalloproteinase-13. *Biomaterials* **32,** 6471–7 (2011).

64. Caplan, M. R., Schwartzfarb, E. M., Zhang, S., Kamm, R. D. & Lauffenburger, D. A. Control of self-assembling oligopeptide matrix formation through systematic variation of amino acid sequence. *Biomaterials* **23,** 219–27 (2002).

65. Ulijn, R. V & Smith, A. M. Designing peptide based nanomaterials. *Chem. Soc. Rev.* **37,** 664–75 (2008).

66. Schneider, J. P. *et al.* Responsive Hydrogels from the Intramolecular Folding and Self-Assembly of a Designed Peptide. *J. Am. Chem. Soc* **124,** 15030–15037 (2002).

67. Pochan, D. J. *et al.* Thermally Reversible Hydrogels via Intramolecular Folding and Consequent Self-Assembly of a de Novo Designed Peptide. *J. Am. Chem. Soc* **125,** 11802–11803 (2003).

68. Haines-Butterick, L. A., Salick, D. A., Pochan, D. J. & Schneider, J. P. In vitro assessment of the pro-inflammatory potential of beta-hairpin peptide hydrogels. *Biomaterials* **29,** 4164–9 (2008).

69. Haines-butterick, L. *et al.* Controlling hydrogelation kinetics by peptide design for three-dimensional encapsulation and injectable delivery of cells. *PNAS* **104,** 7791–7796 (2007).

70. Yan, C. *et al.* Injectable solid hydrogel: mechanism of shear-thinning and immediate recovery of injectable β-hairpin peptide hydrogels. *Soft Matter* **6,** 5143–5156 (2010).

71. Ryadnov, M. G. & Woolfson, D. N. Engineering the morphology of a self-assembling protein fibre. *Nat. Mater.* **2,** 329–332 (2003).

72. Papapostolou, D. *et al.* Engineering nanoscale order into a designed protein fiber. *PNAS* **104,** 10853–10858 (2007).

73. Bromley, E. H. C., Sessions, R. B., Thomson, A. R. & Woolfson, D. N. Designed α-Helical Tectons for Constructing Multicomponent Synthetic Biological Systems. *J. Am. Chem. Soc* **131,** 928–930 (2009).

74. Banwell, E. F. *et al.* Rational design and application of responsive alpha-helical peptide hydrogels. *Nat. Mater.* **8,** 596–600 (2009).

75. Woolfson, D. N. & Mahmoud, Z. N. More than just bare scaffolds: towards multi-component and decorated fibrous biomaterials. *Chem. Soc. Rev.* **39,** 3464–79 (2010).

76. Zhou, M. *et al.* Self-assembled peptide-based hydrogels as scaffolds for anchorage-dependent cells. *Biomaterials* **30,** 2523–30 (2009).

77. Hauser, C. A. E. *et al.* Natural tri- to hexapeptides self-assemble in water to amyloid beta-type fiber aggregates by unexpected alpha-helical intermediate structures. *Proc. Natl. Acad. Sci. U. S. A.* **108,** 1361–6 (2011).

78. Mishra, A. *et al.* Ultrasmall natural peptides self-assemble to strong temperature-resistant helical fibers in scaffolds suitable for tissue engineering. *Nano Today* **6,** 232–239 (2011).

79. Mitchison, T. J. *et al.* Self-Assembly and Mineralization of Peptide-Amphiphile Nanofibers. *Science (80-.).* **294,** 1684–1688 (2001).

80. Hosseinkhani, H., Hosseinkhani, M., Tian, F., Kobayashi, H. & Tabata, Y. Osteogenic differentiation of mesenchymal stem cells in self-assembled peptide-amphiphile nanofibers. *Biomaterials* **27,** 4079–86 (2006).

81. Zhang, S. *et al.* A self-assembly pathway to aligned monodomain gels. *Nat. Mater.* **9,** 594–601 (2010).

82. Matson, J. B. & Stupp, S. I. Self-assembling peptide scaffolds for regenerative medicine. *Chem. Commun. (Camb).* **48,** 26–33 (2012).

83. Lee, K. Y. & Mooney, D. J. Hydrogels for Tissue Engineering. *Chem. Rev.* **101,** 1869–1880 (2001).

84. Drury, J. L. & Mooney, D. J. Hydrogels for tissue engineering: scaffold design variables and applications. *Biomaterials* **24,** 4337–4351 (2003).

85. Li, Y., Rodrigues, J. & Tomás, H. Injectable and biodegradable hydrogels: gelation, biodegradation and biomedical applications. *Chem. Soc. Rev.* **41,** 2193–221 (2012).

86. Gurski, L. A., Petrelli, N. J., Jia, X. & Farach-Carson, M. C. 3D Matrices for Anti-Cancer Drug Testing and Development. *Oncol. Issues* 20–25 (2010).

87. Breslin, S. & Driscoll, L. O. Three-dimensional cell culture: the missing link in drug discovery. *Drug Discov. Today* **18,** 240–249 (2013).

88. Brandl, F., Sommer, F. & Goepferich, A. Rational design of hydrogels for tissue engineering: impact of physical factors on cell behavior. *Biomaterials* **28,** 134–46 (2007).

89. Barrera, D. A., Zylstra, E., Lansbury, P. T. & Langer, R. Synthesis and RGD peptide modification of a new biodegradable copolymer: poly(lactic acid-co-lysine). *J. Am. Chem. Soc* **115,** 11010–11011 (1993).

90. Lasprilla, A. J. R., Martinez, G. a R., Lunelli, B. H., Jardini, A. L. & Filho, R. M. Poly-lactic acid synthesis for application in biomedical devices - a review. *Biotechnol. Adv.* **30,** 321–8 (2012).

91. Elisseeff, J. *et al.* Photoencapsulation of chondrocytes in poly (ethylene oxide)-based semi-interpenetrating networks. *J Biomed Mater Res* **51,** 164–171 (2000).

92. Mooney, D. J. *et al.* Stabilized polyglycolic acid fibre-based tubes for tissue engineering. *Biomaterials* **17,** 115–124 (1996).

93. Schmedlen, R. H., Masters, K. S. & West, J. L. Photocrosslinkable polyvinyl alcohol hydrogels that can be modified with cell adhesion peptides for use in tissue engineering. *Biomaterials* **23,** 4325–4332 (2002).

94. Baker, M. I., Walsh, S. P., Schwartz, Z. & Boyan, B. D. A review of polyvinyl alcohol and its uses in cartilage and orthopedic applications. *J. Biomed. Mater. Res. B. Appl. Biomater.* **100,** 1451–7 (2012).

95. Zhu, J. Bioactive modification of poly(ethylene glycol) hydrogels for tissue engineering. *Biomaterials* **31,** 4639–56 (2010).

96. Collins, M. N. & Birkinshaw, C. Hyaluronic acid based scaffolds for tissue engineering--a review. *Carbohydr. Polym.* **92,** 1262–79 (2013).

97. Croisier, F. & Jérôme, C. Chitosan-based biomaterials for tissue engineering. *Eur. Polym. J.* **49,** 780–792 (2013).

98. Gros, T., Sakamoto, J. S., Blesch, A., Havton, L. A. & Tuszynski, M. H. Regeneration of long-tract axons through sites of spinal cord injury using templated agarose scaffolds. *Biomaterials* **31,** 6719–29 (2010).

99. Lee, K. Y. & Mooney, D. J. Alginate: properties and biomedical applications. *Prog. Polym. Sci.* **37,** 106–126 (2012).

100. Zhang, S., Zhao, X. & Spirio, L. in *Scaffolding tissue Eng.* (Ma, P. X. . & Elisseeff, J.) 217–238 (CRC Press, 2005). at <http://www.3d-matrix.co.jp/dl_file/PuraMatrix_Introduction.pdf>

101. Glowacki, J. & Mizuno, S. Collagen scaffolds for tissue engineering. *Biopolymers* **89,** 338–44 (2008).

102. Lien, S.-M., Ko, L.-Y. & Huang, T.-J. Effect of pore size on ECM secretion and cell growth in gelatin scaffold for articular cartilage tissue engineering. *Acta Biomater.* **5,** 670–9 (2009).

103. Ahmed, T. A. E., Dare, E. V & Hincke, M. Fibrin: a versatile scaffold for tissue engineering applications. *Tissue Eng. Part B. Rev.* **14,** 199–215 (2008).

104. Daamen, W., Veerkamp, J., Vanhest, J. & Vankuppevelt, T. Elastin as a biomaterial for tissue engineering. *Biomaterials* **28,** 4378–4398 (2007).

105. Vepari, C. & Kaplan, D. L. Silk as a Biomaterial. *Prog. Polym. Sci.* **32,** 991–1007 (2007).

106. Loo, Y., Zhang, S. & Hauser, C. A. E. From short peptides to nanofibers to macromolecular assemblies in biomedicine. *Biotechnol. Adv.* **30,** 593–603 (2012).

107. Nagai, Y., Yokoi, H., Kaihara, K. & Naruse, K. The mechanical stimulation of cells in 3D culture within a self-assembling peptide hydrogel. *Biomaterials* **33,** 1044–51 (2012).

108. Fischbach, C. *et al.* Engineering tumors with 3D scaffolds. *Nat. Methods* **4,** 855–860 (2007).

109. Gurski, L. A., Jha, A. K., Zhang, C., Jia, X. & Farach-Carson, M. C. Hyaluronic acid-based hydrogels as 3D matrices for in vitro evaluation of chemotherapeutic drugs using poorly adherent prostate cancer cells. *Biomaterials* **30,** 6076–85 (2009).

110. Feder-Mengus, C., Ghosh, S., Reschner, A., Martin, I. & Spagnoli, G. C. New dimensions in tumor immunology: what does 3D culture reveal? *Trends Mol. Med.* **14,** 333–40 (2008).

111. David, L. *et al.* Hyaluronan hydrogel: an appropriate three-dimensional model for evaluation of anticancer drug sensitivity. *Acta Biomater.* **4,** 256–63 (2008).

112. Horning, J. L. *et al.* 3-D Tumor Model for In Vitro Evaluation of Anticancer Drugs. *Mol. Pharm.* **5,** 849–862 (2008).

113. Bizzarri, M., Cucina, A. & Proietti, S. The tumor microenvironment as a target for anticancer treatment. *Oncobiology and Targets* **1,** 3–11 (2014).

114. Soto, A. M. & Sonnenschein, C. The tissue organization field theory of cancer: a testable replacement for the somatic mutation theory. *Bioessays* **33,** 332–40 (2011).

115. Kenny, P. A. & Bissell, M. J. Tumor reversion: correction of malignant behavior by microenvironmental cues. *Int. J. Cancer* **107,** 688–95 (2003).

116. Hendrix, M. J. C. *et al.* Reprogramming metastatic tumour cells with embryonic microenvironments. *Nat. Rev. Cancer* **7,** 246–55 (2007).

117. Albini, A. & Sporn, M. B. The tumour microenvironment as a target for chemoprevention. *Nat. Rev. Cancer* **7,** 139–147 (2007).

118. Hanna, E., Quick, J. & Libutti, S. K. The tumour microenvironment: a novel target for cancer therapy. *Oral Dis.* **15,** 8–17 (2009).

119. Kraning-Rush, C. M., Califano, J. P. & Reinhart-King, C. A. Cellular traction stresses increase with increasing metastatic potential. *PLoS One* **7,** e32572 (2012).

120. Leach, J. B., Brown, X. Q., Jacot, J. G., Dimilla, P. A. & Wong, J. Y. Neurite outgrowth and branching of PC12 cells on very soft substrates sharply decreases below a threshold of substrate rigidity. *J. Neural Eng.* **4,** 26–34 (2007).

121. Saha, K. *et al.* Substrate modulus directs neural stem cell behavior. *Biophys. J.* **95,** 4426–38 (2008).

122. Leipzig, N. D. & Shoichet, M. S. The effect of substrate stiffness on adult neural stem cell behavior. *Biomaterials* **30,** 6867–78 (2009).

123. Frey, M. T. & Wang, Y.-L. A photo-modulatable material for probing cellular responses to substrate rigidity. *Soft Matter* **5,** 1918–1924 (2009).

124. Galie, P. A., Westfall, M. V & Stegemann, J. P. Reduced serum content and increased matrix stiffness promote the cardiac myofibroblast transition in 3D collagen matrices. *Cardiovasc. Pathol.* **20,** 325–33 (2011).

125. Mason, B. N., Califano, J. P. & Reinhart-king, C. A. in *Eng. Biomater. Regen. Med.* (Bhatia, S. K.) 19–38 (Springer New York, 2012). doi:10.1007/978-1-4614-1080-5

126. Paszek, M. J. *et al.* Tensional homeostasis and the malignant phenotype. *Cancer Cell* **8,** 241–54 (2005).

127. Kumar, S. & Weaver, V. M. Mechanics, malignancy, and metastasis: the force journey of a tumor cell. *Cancer Metastasis Rev.* **28,** 113–27 (2009).

128. Mouw, J. K. *et al.* Tissue mechanics modulate microRNA-dependent PTEN expression to regulate malignant progression. *Nat. Med.* **20,** 360–7 (2014).

129. Tilghman, R. W. *et al.* Matrix rigidity regulates cancer cell growth and cellular phenotype. *PLoS One* **5,** e12905 (2010).

130. Tilghman, R. W. *et al.* Matrix rigidity regulates cancer cell growth by modulating cellular metabolism and protein synthesis. *PLoS One* **7,** e37231 (2012).

131. Gill, B. J. *et al.* A synthetic matrix with independently tunable biochemistry and mechanical properties to study epithelial morphogenesis and EMT in a lung adenocarcinoma model. *Cancer Res.* **72,** 6013–23 (2012).

132. Mi, K. *et al.* Influence of a self-assembling peptide, RADA16, compared with collagen I and Matrigel on the malignant phenotype of human breast-cancer cells in 3D cultures and in vivo. *Macromol. Biosci.* **9,** 437–43 (2009).

133. Liang, Y. *et al.* A cell-instructive hydrogel to regulate malignancy of 3D tumor spheroids with matrix rigidity. *Biomaterials* **32,** 9308–15 (2011).

134. Yip, D. & Cho, C. H. A multicellular 3D heterospheroid model of liver tumor and stromal cells in collagen gel for anti-cancer drug testing. *Biochem. Biophys. Res. Commun.* **433,** 327–332 (2013).

135. Girard, Y. K. *et al.* A 3D fibrous scaffold inducing tumoroids: a platform for anticancer drug development. *PLoS One* **8,** e75345 (2013).

136. Beck, J. N., Singh, A., Rothenberg, A. R., Elisseeff, J. H. & Ewald, A. J. The independent roles of mechanical, structural and adhesion characteristics of 3D hydrogels on the regulation of cancer invasion and dissemination. *Biomaterials* **34,** 9486–95 (2013).

137. Satarkar, N. S. *et al.* Hydrogel-MWCNT Nanocomposites : Synthesis , Characterization , and Heating with Radiofrequency Fields. *J. ofAppliedPolymer Sci.* **117,** 1813–1819 (2010).

138. Adhikari, B. & Banerjee, A. Short peptide based hydrogels: incorporation of graphene into the hydrogel. *Soft Matter* **7,** 9259 (2011).

139. Meng, X. *et al.* Novel injectable biomimetic hydrogels with carbon nanofibers and self assembled rosette nanotubes for myocardial applications. *J. Biomed. Mater. Res. A* 1–8 (2012). doi:10.1002/jbm.a.34400

140. Shin, S. R. *et al.* Carbon nanotube reinforced hybrid microgels as scaffold materials for cell encapsulation. *ACS Nano* **6,** 362–72 (2012).

141. Marks, W. H., Yang, S. C., Dombi, G. W. & Bhatia, S. K. Translational potential for hydrogel composites containing carbon nanobrushes. in *38th Annu. Northeast Bioeng. Conf.* 392–393 (IEEE, 2012). doi:10.1109/NEBC.2012.6207129

142. Soliman, E., Yang, S. C., Dombi, G. W. & Bhatia, S. K. Electrically Conductive , Biocompatible Composite Containing Carbon Nanobrushes for Applications in Neuroregeneration. in *38th Annu. Northeast Bioeng. Conf.* 343–344 (IEEE, 2012). doi:10.1002/jbm.a.32841.Nicola

143. Shin, S. R. *et al.* Carbon-Nanotube-Embedded Hydrogel Sheets for Engineering Cardiac Constructs and Bioactuators. *ACS Nano* **7,** 2369–2380 (2013).

144. Cheng, E., Li, Y., Yang, Z., Deng, Z. & Liu, D. DNA-SWNT hybrid hydrogel. *Chem. Commun. (Camb).* **47,** 5545–7 (2011).

145. MacDonald, R. A., Laurenzi, B. F., Viswanathan, G., Ajayan, P. M. & Stegemann, J. P. Collagen-carbon nanotube composite materials as scaffolds in tissue engineering. *J. Biomed. Mater. Res. A* **74,** 489–96 (2005).

146. MacDonald, R. A., Voge, C. M., Kariolis, M. & Stegemann, J. P. Carbon nanotubes increase the electrical conductivity of fibroblast-seeded collagen hydrogels. *Acta Biomater.* **4,** 1583–92 (2008).

147. Homenick, C. M., Sheardown, H. & Adronov, A. Reinforcement of collagen with covalently-functionalized single-walled carbon nanotube crosslinkers. *J. Mater. Chem.* **20,** 2887 (2010).

148. Tosun, Z. & McFetridge, P. S. A composite SWNT-collagen matrix: characterization and preliminary assessment as a conductive peripheral nerve regeneration matrix. *J. Neural Eng.* **7,** 066002 (2010).

149. Cho, Y. & Borgens, R. Ben. The effect of an electrically conductive carbon nanotube/collagen composite on neurite outgrowth of PC12 cells. *J. Biomed. Mater. Res. A* **95,** 510–7 (2010).

150. Tan, W., Twomey, J., Guo, D., Madhavan, K. & Li, M. Evaluation of nanostructural, mechanical, and biological properties of collagen-nanotube composites. *IEEE Trans. Nanobioscience* **9,** 111–20 (2010).

151. Behan, B. L. *et al.* Single-walled carbon nanotubes alter Schwann cell behavior differentially within 2D and 3D environments. *J. Biomed. Mater. Res. A* **96,** 46–57 (2011).

152. Voge, C. M., Johns, J., Raghavan, M., Morris, M. D. & Stegemann, J. P. Wrapping and dispersion of multiwalled carbon nanotubes improves electrical conductivity of protein-nanotube composite biomaterials. *J. Biomed. Mater. Res. A* 1–8 (2012). doi:10.1002/jbm.a.34310

153. Lee, J. Y. *et al.* Nerve growth factor-immobilized electrically conducting fibrous scaffolds for potential use in neural engineering applications. *IEEE Trans. Nanobioscience* **11,** 15–21 (2012).

154. Saha, K. *et al.* Substrate modulus directs neural stem cell behavior. *Biophys. J.* **95,** 4426–38 (2008).

155. Gorton, L. *et al.* Direct electron transfer between heme-containing enzymes and electrodes as basis for third generation biosensors. *Anal. Chim. Acta* **400,** 91–108 (1999).

156. Chen, W., Cai, S., Ren, Q.-Q., Wen, W. & Zhao, Y.-D. Recent advances in electrochemical sensing for hydrogen peroxide: a review. *Analyst* **137,** 49–58 (2012).

157. Wang, J. Electrochemical Glucose Biosensors. *Chem. Rev.* **108,** 814–825 (2008).

158. Liu, Y. *et al.* Direct electrochemistry of horseradish peroxidase immobilized on gold colloid/cysteine/nafion-modified platinum disk electrode. *Sensors Actuators B Chem.* **115,** 109–115 (2006).

159. Yu, J. & Ju, H. Amperometric biosensor for hydrogen peroxide based on hemoglobin entrapped in titania sol–gel film. *Anal. Chim. Acta* **486,** 209–216 (2003).

160. Wang, J., Lin, Y. & Chen, L. Organic-phase Biosensors for Monitoring Phenol and Hydrogen Peroxide in Pharmaceutical Antibacterial Products. *Analyst* **118,** 277–280 (1993).

161. Chen, S. *et al.* Amperometric third-generation hydrogen peroxide biosensor based on the immobilization of hemoglobin on multiwall carbon nanotubes and gold colloidal nanoparticles. *Biosens. Bioelectron.* **22,** 1268–74 (2007).

162. Hurdis, E. C. & Romeyn, H. Accuracy of Determination of Hydrogen Peroxide by Cerate Oxidimetry. *Anal. Chem.* **26,** 320–325 (1954).

163. Matsubara, C., Kawamoto, N. & Takamura, K. Oxo[5, 10, 15, 20-tetra(4-pyridyl)porphyrinato]titanium(IV): an ultra-high sensitivity spectrophotometric reagent for hydrogen peroxide. *Analyst* **117,** 1781–1784 (1992).

164. Li, J. ., Tan, S. N. . & Ge, H. . Silica sol-gel immobilized amperometric biosensor for hydrogen peroxide. *Anal. Chim. Acta* **335,** 137–145 (1996).

165. Garguilo, M. G., Huynh, N., Proctor, A. & Michael, A. C. Amperometric Sensors for Peroxide, Choline, and Acetylcholine Based on Electron Transfer between Horseradish Peroxidase and a Redox Polymer. *Anal. Chem.* **65,** 523–528 (1993).

166. Tatsuma, T., Okawa, Y. & Watanabe, T. Enzyme Monolayer- and Bilayer-Modified Tin Oxide Electrodes for the Determination of Hydrogen Peroxide and Glucose. *Anal. Chem.* **61,** 2352–2355 (1989).

167. Schubert, F., Saini, S. & Turner, A. P. F. Mediated amperometric enzyme electrode incorporating peroxidase for the determination of hydrogen peroxide in organic solvents. *Anal. Chim. Acta* **245,** 133–138 (1991).

168. Wendzinski, F., Griindig, B. & Spenepb, F. Highly sensitive determination of hydrogen peroxide and peroxidase with tetrathiafulvalene-based electrodes and the application in immunosensing. *Biosens. Bioelectron.* **12,** 43–52 (1997).

169. Qian, J., Liu, Y., Liu, H., Yu, T. & Deng, J. Characterization of regenerated silk fibroin membrane for immobilizing peroxidase and construction of an amperometric hydrogen peroxide sensor employing pnenazme methosulphate as electron shuttle. *J. Electroanal. Chem.* **397,** 157–162 (1995).

170. Wang, B. & Dong, S. Sol – gel-derived amperometric biosensor for hydrogen peroxide based on methylene green incorporated in Nafion film. *Talanta* **51,** 565–572 (2000).

171. Armstrong, F. A., Hill, H. A. & Walton, N. J. Direct Electrochemistry of Redox Proteins. *Acc. Chem. Res.* **21,** 407–413 (1988).

172. Gu, H.-Y., Yu, A.-M. & Chen, H.-Y. Direct electron transfer and characterization of hemoglobin immobilized on a Au colloid–cysteamine-modified gold electrode. *J. Electroanal. Chem.* **516,** 119–126 (2001).

173. Han, X., Cheng, W., Zhang, Z., Dong, S. & Wang, E. Direct electron transfer between hemoglobin and a glassy carbon electrode facilitated by lipid-protected gold nanoparticles. *Biochim. Biophys. Acta* **1556,** 273–7 (2002).

174. Lei, C., Wollenberger, U., Bistolas, N., Guiseppi-Elie, A. & Scheller, F. W. Electron transfer of hemoglobin at electrodes modified with colloidal clay nanoparticles. *Anal. Bioanal. Chem.* **372,** 235–9 (2002).

175. Cai, C. & Chen, J. Direct electron transfer and bioelectrocatalysis of hemoglobin at a carbon nanotube electrode. *Anal. Biochem.* **325,** 285–292 (2004).

176. Lu, X., Hu, J., Yao, X., Wang, Z. & Li, J. Composite system based on chitosan and room-temperature ionic liquid: direct electrochemistry and electrocatalysis of hemoglobin. *Biomacromolecules* **7,** 975–80 (2006).

177. Gao, F. *et al.* Amperometric third-generation hydrogen peroxide biosensor based on immobilization of Hb on gold nanoparticles/cysteine/poly(p-aminobenzene sulfonic acid)-modified platinum disk electrode. *Colloids Surfaces A Physicochem. Eng. Asp.* **295,** 223–227 (2007).

178. Ma, G.-X., Lu, T.-H. & Xia, Y.-Y. Direct electrochemistry and bioelectrocatalysis of hemoglobin immobilized on carbon black. *Bioelectrochemistry* **71,** 180–5 (2007).

179. Zheng, W., Li, J. & Zheng, Y. F. An amperometric biosensor based on hemoglobin immobilized in poly(epsilon-caprolactone) film and its application. *Biosens. Bioelectron.* **23,** 1562–6 (2008).

180. Tan, X.-C. *et al.* Amperometric hydrogen peroxide biosensor based on immobilization of hemoglobin on a glassy carbon electrode modified with fe(3)o(4)/chitosan core-shell microspheres. *Sensors (Basel).* **9,** 6185–99 (2009).

181. Xu, H., Dai, H. & Chen, G. Direct electrochemistry and electrocatalysis of hemoglobin protein entrapped in graphene and chitosan composite film. *Talanta* **81,** 334–8 (2010).

182. Norouzi, P., Larijani, B., Faridbod, F. & Ganjali, M. R. Hydrogen Peroxide Biosensor Based on Hemoglobin Immobilization on Gold Nanoparticle in FFT Continuous Cyclic Voltammetry Flow Injection System. *Int. J. Electrochem. Sci.* **5,** 1550–1562 (2010).

183. Yu, C., Zhou, X. & Gu, H. Immobilization, direct electrochemistry and electrocatalysis of hemoglobin on colloidal silver nanoparticles-chitosan film. *Electrochim. Acta* **55,** 8738–8743 (2010).

184. Cai, C. & Chen, J. Direct electron transfer of glucose oxidase promoted by carbon nanotubes. *Anal. Biochem.* **332,** 75–83 (2004).

185. Zhao, G.-C., Zhang, L., Wei, X.-W. & Yang, Z.-S. Myoglobin on multi-walled carbon nanotubes modified electrode: direct electrochemistry and electrocatalysis. *Electrochem. commun.* **5,** 825–829 (2003).

186. Davis, M. E. *et al.* Injectable self-assembling peptide nanofibers create intramyocardial microenvironments for endothelial cells. *Circulation* **111,** 442–50 (2005).

187. Yang, H., Fung, S., Pritzker, M. & Chen, P. Surface-Assisted Assembly of an Ionic-Complementary Peptide: Controllable Growth of Nanofibers. *J. Am. Chem. Soc* **129,** 12200–12210 (2007).

188. Yang, H. Assembly of an Ionic-Complementary Peptide on Surfaces and its Potential Applications. 180 (2007).

189. Hong, Y., Legge, R. L., Zhang, S. & Chen, P. Effect of Amino Acid Sequence and pH on Nanofiber Formation of Self-Assembling Peptides EAK16-II and EAK16-IV. *Biomacromolecules* **4,** 1433–1442 (2003).

190. Zhang, S., Zhao, X. & Spirio, L. in *Scaffolding tissue Eng.* (Ma, P. X. & Elisseeff, J. H.) 217–238 (CRC Press, 2006). at <http://www.3d-matrix.co.jp/dl_file/PuraMatrix_Introduction.pdf>

191. Sheikholeslam, M., Pritzker, M. & Chen, P. Dispersion of multiwalled carbon nanotubes in water using ionic-complementary peptides. *Langmuir* **28,** 12550–6 (2012).

192. Pittenger, B., Erina, N. & Su, C. *Bruker Application Note # 128 Quantitative Mechanical Property Mapping at the Nanoscale with PeakForce QNM*. **im,** 1–12 (2012).

193. Marini, D. M., Hwang, W., Lauffenburger, D. A., Zhang, S. & Kamm, R. D. Left-Handed Helical Ribbon Intermediates in the Self-Assembly of a -Sheet Peptide. *Nano Lett.* **2,** 295–299 (2002).

194. Young, T. J. *et al.* The use of the PeakForce TM quantitative nanomechanical mapping AFM-based method for high-resolution Young's modulus measurement of polymers. *Meas. Sci. Technol.* **22,** 125703 (2011).

195. Adamcik, J. *et al.* Measurement of intrinsic properties of amyloid fibrils by the peak force QNM method. *Nanoscale* **4,** 4426–9 (2012).

196. Adamcik, J. & Mezzenga, R. Study of amyloid fibrils via atomic force microscopy. *Curr. Opin. Colloid Interface Sci.* **17,** 369–376 (2012).

197. Dokukin, M. E. & Sokolov, I. Quantitative mapping of the elastic modulus of soft materials with HarmoniX and PeakForce QNM AFM modes. *Langmuir* **28,** 16060–71 (2012).

198. Landoulsi, J. & Dupres, V. Direct AFM force mapping of surface nanoscale organization and protein adsorption on an aluminum substrate. *Phys. Chem. Chem. Phys.* **15,** 8429–40 (2013).

199. Clausen, C. H., Jensen, J., Castillo, J., Dimaki, M. & Svendsen, W. E. Qualitative mapping of structurally different dipeptide nanotubes. *Nano Lett.* **8,** 4066–9 (2008).

200. Clausen, C. H. *et al.* Electrostatic force microscopy of self-assembled peptide structures. *Scanning* **33,** 201–7 (2011).

201. Bockrath, M. *et al.* Scanned Conductance Microscopy of Carbon Nanotubes and λ-DNA. *Nano Lett.* **2,** 187–190 (2002).

202. Zheng, M. *et al.* Structure-based carbon nanotube sorting by sequence-dependent DNA assembly. *Science* **302,** 1545–8 (2003).

203. Yarotski, D. A. *et al.* Scanning tunneling microscopy of DNA-wrapped carbon nanotubes. *Nano Lett.* **9,** 12–7 (2009).

204. Wan, Y., Liu, G., Zhu, X. & Su, Y. pH induced reversible assembly of DNA wrapped carbon nanotubes. *Chem. Cent. J.* **7,** 14 (2013).

205. Johnson, R. R., Johnson, A. T. C. & Klein, M. L. Probing the structure of DNA-carbon nanotube hybrids with molecular dynamics. *Nano Lett.* **8,** 69–75 (2008).

206. Karachevtsev, M. V & Karachevtsev, V. a. Peculiarities of homooligonucleotides wrapping around carbon nanotubes: molecular dynamics modeling. *J. Phys. Chem. B* **115,** 9271–9 (2011).

207. Roxbury, D., Jagota, A. & Mittal, J. Sequence-Specific Self-Stitching Motif of Short Single-Stranded DNA on a Single-Walled Carbon Nanotube. *J. Am. Chem. Soc.* **133,** 13545–13550 (2011).

208. Roxbury, D., Mittal, J. & Jagota, A. Molecular-basis of single-walled carbon nanotube recognition by single-stranded DNA. *Nano Lett.* **12,** 1464–9 (2012).

209. Sheikholeslam, M., Pritzker, M. & Chen, P. Hybrid peptide–carbon nanotube dispersions and hydrogels. *Carbon N. Y.* **71,** 284–293 (2014).

210. Shin, S. R. *et al.* Cell-laden microengineered and mechanically tunable hybrid hydrogels of gelatin and graphene oxide. *Adv. Mater.* **25,** 6385–91 (2013).

211. Wang, Y. *et al.* Fluorinated graphene for promoting neuro-induction of stem cells. *Adv. Mater.* **24,** 4285–90 (2012).

212. Liu, F. & Tschumperlin, D. J. Micro-mechanical characterization of lung tissue using atomic force microscopy. *J. Vis. Exp.* 1–7 (2011). doi:10.3791/2911

213. Qian, Z., Khan, M. A., Mikkelsen, S. & Chen, P. Improved enzyme immobilization on an ionic-complementary peptide-modified electrode for biomolecular sensing. *Langmuir* **26,** 2176–80 (2010).

214. Y, B. H., Veronique, M. & Hua, L. Hydrogen peroxide in the human body. *FEBS Lett.* **486,** 10–13 (2000).